Endocytosis against the high turgor of guard cells

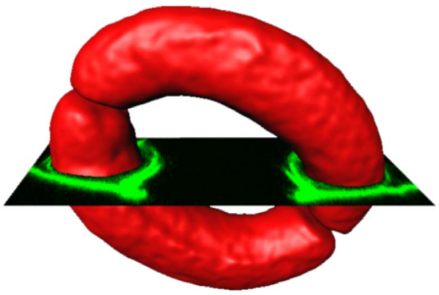

Vom Fachbereich Biologie der Technischen Universität Darmstadt
zur Erlangung des akademischen Grades
Doctor rerum naturalium
genehmigte Dissertation

von

Tobias Meckel

aus Stuttgart

Berichterstatter:	Prof. Dr. Gerhard Thiel
Mitberichterstatter:	Prof. Dr. Thomas W. Holstein
Tag der Einreichung:	6. September 2004
Tag der mündlichen Prüfung:	29. Oktober 2004

Darmstadt 2004

D17

”Einfälle sind Läuse der Vernunft”
Friedrich Hebbel

”I bet the human brain is a kludge”
Marvin Minsky

Eidesstattliche Erklärung

Ich erkläre hiermit an Eides statt, dass ich die vorliegende Dissertation selbständig und nur mit den angegebenen Hilfsmitteln angefertigt habe.

Ich habe noch keinen Promotionsversuch unternommen.

Darmstadt, den 6. September 2005

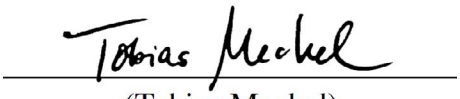

(Tobias Meckel)

Die vorliegende Arbeit wurde unter Leitung von Prof. Dr. Gerhard Thiel und PD Dr. Ulrike Homannn am Institut für Botanik der Technischen Universität Darmstadt durchgeführt und unter dem Geschäftszeichen TH 558/6-1 sowie HO 2046/5-2 von der Deutschen Forschungsgemeinschaft (DFG) gefördert.

publications / talks

Teile der vorliegenden Arbeit sowie anderer Projekte während der Promotionszeit wurden bisher wie folgt publiziert bzw. auf Konferenzen präsentiert:

Meckel T, Hurst AC, Thiel G, Homann U (2004) Endocytosis against high turgor: Guard cells of *Vicia faba* constitutively endocytose fluorescently labelled plasma membrane and GFP tagged K^+-channel KAT1. *Plant J.* 39(2):182-193

Meckel T (2004) Endocytosis against high tugor - detection limit of CLSM allows for subresolution measurements. *Focus On Microscopy*, Philadelphia, PA, USA (Poster)

Epimashko S, **Meckel T**, Fischer-Schliebs E, Lüttge U, Thiel G (2004) Two functionally different vacuoles for static and dynamic purposes in one plant mesophyll leaf cell. *Plant J.* 37(2):294-300

Hurst AC, **Meckel T**, Tayefeh S, Thiel G, Homann U. (2004) Trafficking of the plant potassium inward rectifier KAT1 in guard cell protoplasts of *Vicia faba*. *Plant J.* 37(3):391-397

Meckel T, Hurst AC, Homann U, Thiel G (2003) Cycling of K^+-channels and membrane tunover in guard cells. *European Plant Endomembrane Meeting*, Glasgow, GB (Talk)

Mehmel M, Rothermel M, **Meckel T**, Van Etten JL, Moroni A, Thiel G. (2003) Possible function for virus encoded K^+-channel Kcv in the replication of chlorella virus PBCV-1. *FEBS Lett.* 552(1):7-11.

Hurst AC, **Meckel T**, Homann U, Thiel G (2003) Unerwartet viel Dynamik: Exo- und Endocytose in Pflanzenzellen. *Zellbiologie aktuell*, 29. Jahrgang, Ausgabe 2:21-25

Meckel T, (2003) Single vesicles internalize either no or few K^+-channels during endocytosis in turgid guard cells. *Single Molecule Detection in Living Cells*, Altleinigen, Germany (Talk)

Meckel T, Hurst AC, Thiel G, Homann U (2002) 3D reconstruction of stomatal movement. *European Plant Endomembrane Meeting*, Varenna, Italy (Talk)

Moroni A, Viscomi C, Sangiorgio V, Pagliuca C, **Meckel T**, Horvath F, Gazzarrini S, Valbuzzi P, Van Etten JL, DiFrancesco D, Thiel G (2002) The short N-terminus is required for functional expression of the virus-encoded miniature K(+) channel Kcv. *FEBS Lett.* 530(1-3):65-69

Meckel T, Homann U, Thiel G (2001) Exo- and endocytosis in intact, turgid plant cells. *Plant Membrane Biology*, 12th International Workshop, Madison, WI, USA (Poster)

Contents

Zusammenfassung

Stomata, befinden sich in der Epidermis photosynthetisch aktiver Pflanzenorgane. Sie bestehen aus zwei Schließzellen, die eine Pore bilden, welche den Austausch von CO_2 und Wasser mit der Umwelt gestattet. Dieser Austausch wird reguliert, indem die Schließzellen aktiv ihr Vo-lumen und damit unweigerlich auch ihre Oberfläche ändern, um die Appertur der Pore zu variieren. Die Änderungen erfolgen durch die Aufnahme oder Abgabe von K^+ über K^+-selektive Kanäle, was den Ein- bzw. Ausstrom von Wasser zur Folge hat. Die Quantifizierung dieser osmotisch angetriebenen Änderung anhand der 3D Rekonstruktion der Schließzellen von *Vicia faba* L. ergab bei einer Apperturdifferenz von 50 % eine Änderung des Volumens um 25 % und der Oberfläche um 15 %.

Da die Dehnbarkeit von biologischen Membranen auf etwa 2 % beschränkt ist, erfordern die Oberflächenänderungen während der Bewegung der Stomata einen Ein- bzw. Ausbau von Membran an der Plasmamembran (PM). Allerdings wurde Endocytose in Pflanzen aufgrund energetischer Überlegungen oft in Frage gestellt, da ein hoher Turgor die Vesikelbildung an der PM erschwert. Um diesen Prozess in den extrem turgeszenten Schließzellen zu untersuchen, wurde die Dynamik der PM mit Hilfe der Konfokalmikroskopie analysiert. Dabei wurde der Verbleib von membran-affinen Styryl-Farbstoffen (FM4-64, FM2-10, FM1-43), sowie der fluid-affine Farbbstoff Alexa 488 Hydrazid unter natürlichen und konstanten osmotischen Verhältnissen verfolgt. Als weitere Markierung der Membran diente die fluoreszierende Chimäre des einwärts gleichrichtenden Kaliumkanals KAT1 (KAT1::GFP), einem für die stomatäre Funktion wichtigen Protein.

Wenige Minuten nach Inkubation in FM-Farbstoffen wurden endozytische Strukturen im kortikalen Zytoplasma direkt unterhalb der PM angefärbt. Die Identifikation dieser Strukturen basiert auf dem Befund, dass ihre Größenverteilung mit der von endozytischen Vesikeln, die mit Patch-clamp Kapazitätsmessungen erhalten wurden, nahezu übereinstimmt. Alle endozytischen Markierungen, ob membran-affin (FM-Farbstoffe, KAT1::GFP) oder fluid-affin (Alexa 488 hydrazide), machten Strukturen mit beugungsbegrenztem Durchmesser und ähnlicher Lokalisation im kortikalen Zytoplasma sichtbar. Berechnungen zum mittleren Durchmesser der mit Alexa 488 Hydrazid markierten Strukturen ergaben Werte von 60 - 80 nm. Dies stimmt gut mit Durchmessern überein, die für Clathrin-umhüllte Vesikel in Pflanzen gefunden wurden. Darüber hinaus wurde ein Teil der Vesikel sowohl mit dem extrazellulär angebotenen Membranfarbstoff FM4-64 als auch mit dem intrazellulär produzierten KAT1::GFP markiert. Dies lässt den Schluss zu, dass diese Vesikel K^+-Kanäle enthalten, die bereits zur PM transportiert und nun per Endozytose internalisiert wurden. Insgesamt zeigen die Befunde, dass turgeszente Schließzellen eine hohe konstitutive endocytische Aktivität aufweisen und neben Membran auch Proteine wie den K^+-Kanal KAT1 endozytieren.

Summary

Stomata are found in the epidermis of photosynthetic active plant organs. They are formed by pairs of guard cells which create a pore to facilitate CO_2 and water exchange with the environment. In order to control this gas exchange, guard cells actively change their volume and, consequently, surface area to alter the aperture of the stomatal pore. These changes are achieved by an uptake or release of K^+ through K^+-selective channels followed by the respective osmotic water fluxes. The quantification of such osmotically driven changes on 3D reconstructions revealed that guard cells of open and closed stomata of *Vicia faba* L., which show a 50 % change in aperture, differ in volume and surface area by 25 % and 15 %, respectively.

Since biological membranes only have a limited elasticity of about 2 %, such excursions in surface area during stomatal movement require an addition or retrieval of membrane to or from the plasma membrane (PM). However, the relevance of endocytosis in plants has frequently been questioned on the basis of energetic considerations, because high turgor poses a barrier on the budding of the PM into vesicles. To investigate this process in highly turgescent guard cells, the dynamics of the PM were examined by monitoring with confocal microscopy the fate of membrane-affine styryl dyes (FM4-64, FM2-10, FM1-43) and the fluid-affine dye Alexa 488 hydrazide under natural and constant osmotic conditions. As a third marker, a relevant transporter for stomatal function was observed by following the retrieval of a fluorescent chimera of the K^+-channel KAT1 (KAT1::GFP).

Over some minutes of incubation in FM-dyes, endocytic vesicles in the cortical cytoplasm beneath the PM were fluorescently labelled. The identification was based on the observation that the size distribution of these structures is very similar to that of endocytic vesicles obtained from patch-clamp capacitance recordings. All markers, whether membrane- (FM-dyes, KAT1::GFP) or fluid-phase-affine (Alexa 488 hydrazide), are taken up into structures of diffraction-limited size and similar localisation in the cortical cytoplasm. The calculated size of Alexa 488 hydrazide labelled structures was 60 - 80 nm. This is well in accordance with sizes reported for clathrin-coated vesicles in plants. Moreover, a subset of single vesicles was labelled with the externally supplied membrane marker FM4-64 and the intracellular produced KAT1::GFP. Consequently these vesicles carry K^+-channels, which had already been delivered to the PM and are now retrieved via endocytosis. To summarize, the data provide strong evidence that turgid guard cells undergo vigorous constitutive endocytosis and retrieve membrane including the K^+-channel KAT1 from the PM via endocytic vesicles.

Abbreviations

1P, 2P	one photon, two photon
2D , 3D	two dimensional, three dimensional
ABA	abscisic acid
BY-2	*Nicotiana tabaccum* cv. bright yellow-2
CFP	cyan fluorescent protein
CHAPS	3-[(3-cholamidopropyl)-dimethylammonio]-1-propanesulfonate
CLSM	confocal laser scanning microscopy
DIC	differential interference contrast
DNA	deoxyribonucleic acid
ER	endoplasmatic reticulum
ERC	endocytic recycling compartment
FRET	fluorescence resonance energy transfer
FWHM	full width at half maximum (peak height)
GFP	green fluorescent protein
KAT1	inward rectifying potassium channel from *Arabidopsis thaliana*
LAMP1	human lysosomal associated membrane protein
MPLSM	multiphoton laser scanning microscopy
MVB	multi vesicular body
NA	numerical aperture
PAR	photosynthetic active radiation
PCR	polymerase chain reaction or partly coated reticulum
PVC	pre-vacuolar compartment
PM	plasma membrane
POPC	1-palmitoyl-2-oleoyl-*sn*-glycero-3-phosphocholine
PSF	point spread function
ROI	region of interest
ROS	reactive oxygen species
SE	sorting endosome
SD	standard deviation
SNR	signal-to-noise ratio
TGN	trans golgi network
TM23	23 amino acid long transmembrane domain from LAMP1
YFP	yellow fluorescent protein

Chapter 1

Introduction

When plants left their aquatic environment about 400 million years ago and invaded land, water became a limiting factor. In order to survive, plants developed stomata which prevent excessive water loss while allowing CO_2 to enter the plant for photosynthesis. Thus, together with the cuticle and the vascular tissue, these cells were key elements to the emergence and development of large terrestrial plants (Chaloner 1970).

1.1 Stomata

Stomata are formed by a pair of specialized cells, the guard cells, which are found in the epidermis of aerial parts of most higher plants (Fig. 1.1). The pore can be opened and closed actively to control the gas exchange between the plant and its environment. Thus, stomata act as the portals for entry of CO_2 and as an exit for water vapour. The former is required for photosynthesis while the latter generates a continuous flux of water, the so called transpiration stream, which aids uptake of nutrients and facilitates long range transport from the root to the shoot, e.g. for salts and hormones. In addition, evaporation of water is important in lowering leaf temperature. The major function of stomata is to allow sufficient CO_2 to enter the leaf in order to optimize photosynthesis under prevailing conditions, while conserving as much water as possible.

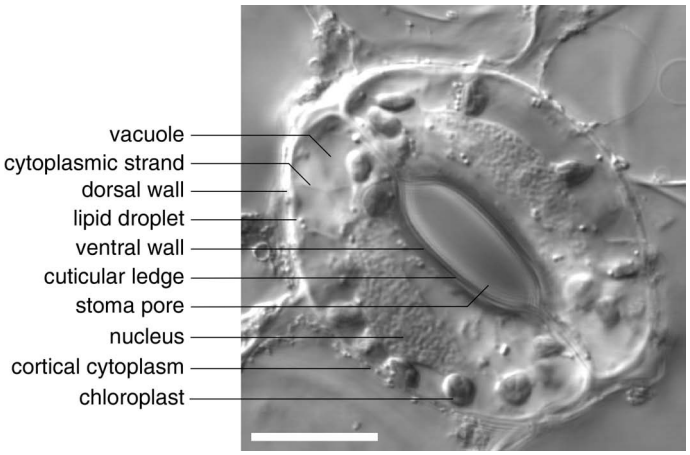

Figure 1.1: Differential interference contrast (DIC) image of a guard cell of *Vicia faba* L. Numerous organelles become visible by DIC imaging of a guard cell.

Stoma, plural stomata, which is Greek for mouth, is used as a term for the pore including the surrounding pair of guard cells, much as lips are considered part of the mouth. The discovery of these ”breathing pores” in the surface of leaves by Nehemiah Grew (1641-1712) coincided with the invention of the compound microscope and the first observation of ”cells” by Robert Hooke (1635-1703). Grew, who used Hook’s microscope for his studies, describes in his publication *The Anatomy of Plants* (1682): ”[T]he skins of at least many plants are formed with several orifices or passports, either for the better alveolation [evaporation] of superfluous sap, or the admission of air.” Thus, the microscopic investigation of stomata stands at the beginning of both, research on stomata and microscopy in general.

Stomatal guard cells have ever provided one of the best studied experimental systems to study fundamental aspects of plant physiology. Without doubt they are currently the best characterized model system for ion transport and signal transduction. Moreover, this cell type has a fundamental role in control of two of the most important plant processes, i.e. photosynthesis and transpiration. Detailed understanding of stomata is thus a key element for an understanding of plants and their communication with the environment.

1.2 Endocytosis

Endocytosis is a collective term which is used to describe the mechanisms by which cells ingest selected regions of their plasma membrane (PM). Typically, endocytosis begins with an invagination of a closed vesicle that becomes detached from the parent membrane. In the cytoplasm, the endocytic vesicle fuses with the first compartment of a complex membrane system that makes up the endocytic pathway. This pathway of membrane traffic serves as a communication between the extracellular environment and intracellular organelles (Oparka at al. 1991). It is a a conserved process for all eukaryotic cells and required for diverse cellular functions. These include turnover and degradation of PM proteins and receptors, transduction and dispersal of signals within the cell and between cells of an organized tissue, spread of morphogens, cell-to-cell communication, elimination of pathogenic microorganisms, establishment of symbiosis with microorganisms, and nutrient uptake.

Several basic forms of endocytosis have been defined for the processes observed in animal cells according to the type of cargo and molecular machinery driving its internalization. The endocytic pathways include clathrin-mediated, caveolae/lipid raft-mediated, clathrin-, and caveolae-independent endocytosis, fluid-phase endocytosis, and phagocytosis (Conner and Schmidt 2003, Mousavi et al. 2004). But besides this diversity endocytotic vesicles always consist of membrane components (protein and lipid) which are derived from excised regions of the PM as well as material which binds (specifically or non-specifically) to the apoplasmic face of the PM. In addition to these molecules, solutes dispersed in the fluid phase of the apoplastic medium are inevitably trapped in the lumen of the vesicle during the process of engulfment. This fluid entrapment and internalization is known as fluid-phase endocytosis or pinocytosis.

1.3 The relevance of endocytosis during stomatal movement

Opening and closing of stomata is an osmotic driven process. Following the accumulation or discharge of K^+ salts, water enters or leaves the cells, respectively. As a consequence of these water fluxes guard cells undergo large changes in turgor pressure and volume (Franks et al. 2001), which finally results in opening or closing of the stomatal pore.

1.3.1 The membrane traffic problem

The considerable and repetitive changes in cell volume during stomatal movement are associated also with repetitive, variation in the surface area of the guard cell's PM. Based on the fact that the elasticity of a biomembrane, i.e. the amount it can be stretched before rupture occurs, is limited to only about 2 % (Wolfe and Steponkus 1983), the issue of membrane turnover is brought into particular focus with this cell type. Despite the fact that no other higher plant cell has been investigated more intensively in terms of transport events at the membrane (Willmer and Fricker 1996), research on the transport of the membrane itself has been largely ignored.

Investigations using the patch-clamp technique were among the first to address this topic. Measurements on guard cell protoplasts (i.e. guard cells whose membrane was digested enzymatically) have shown that these cells accomplish an increase in surface area by incorporating exocytic vesicles into the PM. Vesicles of about the same size are retrieved in an endocytic process to achieve a reduction of the surface area when cells shrink (Homann 1998). Furthermore, vesicular traffic has been demonstrated to be additionally involved in the incorporation and removal of PM potassium channels during surface area variations (Hurst et. al 2004).

These investigations have all been carried out on protoplasts which have no cell wall and consequently no turgor. However, it is questionable, whether it is possible to a priori extrapolate the data on the endocytic activity in guard cell protoplasts to intact guard cells. To understand membrane traffic during stomatal functioning it is therefore essential to investigate this process in turgid, walled cells.

1.3.2 Endocytosis against high turgor

It has been a matter of debate whether intact plant cells are able to perform endocytosis against their generally high turgor pressure (Cram 1980, Gradmann and Robinson 1989, Robinson et al. 1991, Saxton and Breidenbach 1988). With pressure values of up to 4.5 MPa guard cell develop one of the highest turgor known in the plant kingdom. Since an overpressure is known to impose a barrier on the budding of membrane into vesicles (Rauch and Farge 2000), the possible hurdle of turgor pressure for endocytosis in guard cells would be even more pronounced than in other plant cells which generally have a turgor below 1 MPa. In accordance to these considerations, uptake of extra cellular markers has so far only been shown in intact plant cells with a relatively low turgor pressure such as cells of *Nicotiana tabaccum* cv. bright yellow-2 (BY-2; Emans et

al. 2002), root apices of *Zea mays* (Baluska et al. 2002) and pollen tubes of *Lilium longiflorum* (Parton et al. 2001).

In contrast, uptake of the fluid phase marker Lucifer Yellow could never be detected in intact guard cells (Hillmer et al. 1990, Diekmann et al. 1993). Also electron micrographs of closed stomata showed no occurrence of vesicles, which would point to an endocytic activity (Diekmann et al. 1993). In a recent publication Shope et al. (2003) were able to show a general uptake of the endocytic marker FM4-64 in guard cells, which were closed by hyperosmotic treatment. However, no direct evidence for the formation of endocytic vesicles was found. Thus, any attempts to demonstrate endocytosis in living, intact, and highly turgid plant cells have so far failed which casts doubt on the relevance of endocytosis in turgid guard cells.

Despite the lack of any functional relevance, the molecular machinery for endocytosis is present in plant cells. Clathrin-coated vesicles have been found in EM studies on plant tissue long ago (Low and Chandra 1994). Recently clathrin mediated endocytosis in plant cells, has been proven even on the molecular level (Holstein 2002). The dissection of counterparts to the numerous proteins of animal and yeast cells, which are also part of the endocytic machinery, is also at the beginning (Barth and Holstein 2004).

This poses the question, as to whether endocytosis is absent from plant cells with a high turgor or whether it has been failed to be detected. It was the aim of this work to readress the question on the general existence of endocytosis in turgid plant cells.

1.4 The approach of this work

The cell wall of intact plant cell hampers the use of several techniques generally applied in endocytic research. Neither patch-clamp capacitance measurements nor the use of membrane impermeable high molecular weight markers (e.g transferrin, cationized ferritin, fluorescent dextrans or styrol beads) can be used. While a cell wall in general prevents the use of the first technique, its porosity imposes a limit on the diffusion of particles with Stokes' radii above 3 nm (Baron-Epel et al. 1988).

The approach of the present work was therefore based on the use of autofluorescent proteins and extracellular fluorescent markers with low molecular weights to ensure that the markers freely diffuse through the cell wall and reach the PM. Fluorescence is then detected with sensitive laser scanning microscopy techniques.

1.4.1 Fluorescent markers

To monitor the membrane during endocytosis the fate of the PM was traced by membrane-affine (FM-dyes) and a fluid-phase-affine (Alexa 488 hydrazide) fluorescent chemical dyes. Complementary, an important membrane protein for stomatal function, the inward rectifying

potassium channel from *Arabidopsis thaliana* (KAT1), was traced by engineering a fluorescent chimera with the green fluorescent protein (GFP; Fig. 1.2). After particle bombardment, the channel was transiently expressed in intact guard cells of *V. faba*.

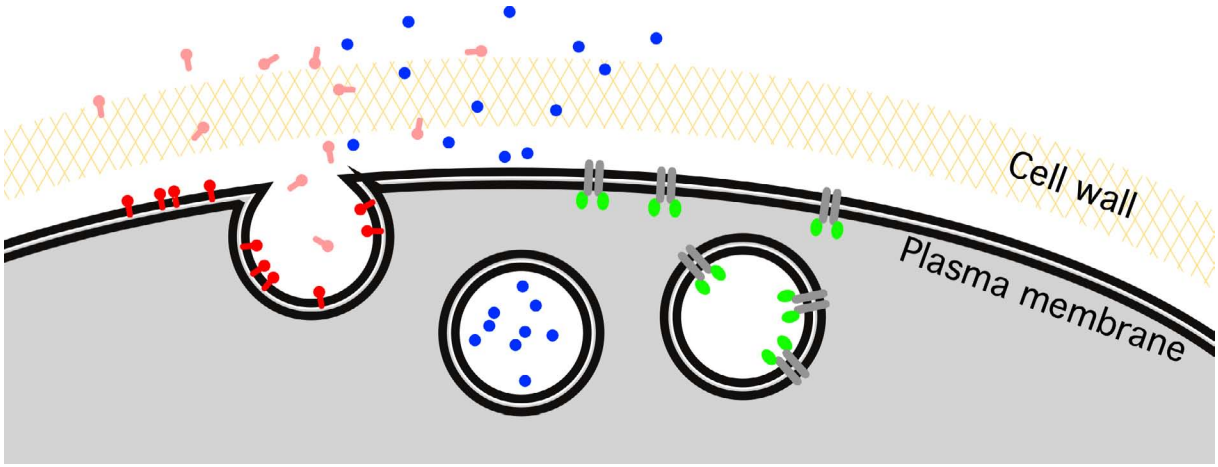

Figure 1.2: Endocytic markers. Endocytic vesicles can be fluorescently labelled in three ways. First, by marking the extracellular fluid with fluid-phase-affine dyes (blue, e.g. Alexa 488 hydrazide). Second, by labelling the extracytoplasmic leaflet of the PM with impermeable membrane-affine dyes (red, e.g. FM-dyes), and third, by expressing a fluorescent chimera of a membrane protein fused to GFP (green, e.g. KAT1::GFP).

FM-dyes

The membrane-selective FM-dyes (i.e. FM1-43, FM2-10 and FM4-64), belong to a class of amphiphilic styryl dyes developed by Betz and co-workers (Betz et al. 1992, 1996). The abbreviation ”FM” stands for the chemist’s name, Fei Mao, who developed the FM-dyes from the related probe, dimethyl-aminostyryl-methylpyridiniumiodine (DASPMI), a membrane-potential probe used to study mitochondria (Bereiter-Hahn 1976; Betz et al. 1992). The numbers designate Fei Mao’s lab books and pages therein (Horobin 2002).

FM-dyes are amphiphilic molecules which consist of a lipophilic dialkylaminophenyl tail group linked to a positively charged pyridinium head group via a double or multi double-bond bridge (Fig. 1.3 and 3.1). The fluorescent properties of the dyes are determined mainly by the double bond bridge between the head and the tail. Dyes with more double bonds between the two aromatic rings have longer excitation and emission wavelengths owing to a higher degree of conjugation between the aromatic rings and double bonds. This leads to a lower transition energy between the ground state and the excited state. FM1-43 and FM2-10 have one double bond and are visible using fluorescein optics, whereas FM4-64 with three double bonds is visible using rhodamine optics (Cochilla et al. 1999).

FM-dyes are soluble in water. Yet, in presence of membrane the hydrophobic tail intercalates between the lipids, which is an entropy driven reaction following the classical hydrophobic effect (Schote and Seelig 1998). The cationic head is believed to maintain the dyes in the outer leaflet and thereby renders these dyes membrane impermeable (Betz et al. 1996). Thus, FM-

dyes are thought to enter the cell primarily by endocytic vesicles which invaginate from the PM and entrap the dye in the inner leaflet of their membrane.

The spectral properties of the dyes change according to their environment (Betz et al. 1992). While they are virtually non fluorescent in water they show a dramatic increase of the quantum yield by more than two orders of magnitude - and consequently a dramatic increase of fluorescence intensity - upon incorporation into a cell membrane or any other hydrophobic environment (e.g. the cuticle).

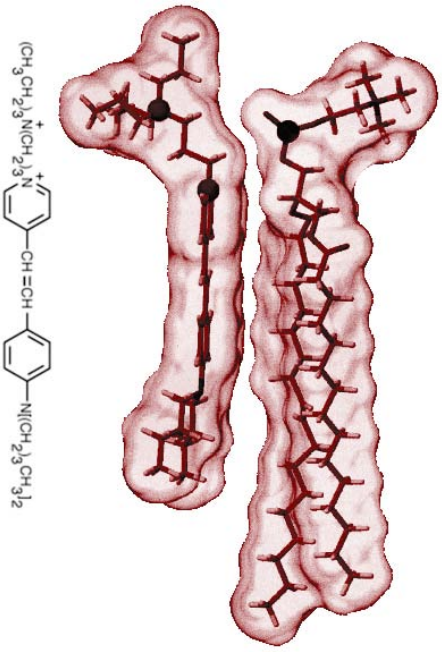

Figure 1.3: Molecular model of FM1-43. Molecular model of the relative position of FM1-43 (left) to a 1-palmitoyl-2-oleoyl-*sn*-glycero-3-phosphocholine (POPC, right) in a bilayer (modified after Schote and Seelig 1998)

Besides an extensive use in studies on animal cells (e.g. Betz et al. 1992, Cochilla et al. 1999), FM-dyes are increasingly used for studying vesicle trafficking and organelle organization in fungal (Vida and Emr 1995, Fischer-Parton et al. 2000) and plant cells. However, with few exceptions (Geldner et al. 2003, Emmans et al. 2002, Shope et al. 2003), these dyes have in the case of plant cells only been applied to single, isolated cells (Caroll et al. 1998, Battey et al. 1999, Kubitscheck et al. 2000, Ueda et al. 2001, Bolte et al. 2004a).

Following a preceding study with guard cell protoplasts (Kubitscheck et al. 2000) the process of endocytosis was examined in the present work on turgid cells. Therefore a thorough investigation was carried out to find, which of the FM-dyes is best to study membrane dynamics in intact guard cells. An important requirement for the amphiphilic dyes is a sufficient hydrophilicity in order to pass the hydrophilic cell wall. At the same time they should be hydrophobic enough to intercalate into the PM with sufficient affinity. Also, in order to report the endocytic pathway correctly, it is of capital importance that the dye must not penetrate a biomembrane, at least in the time window of observation.

The green fluorescent protein (GFP)

GFP acts as an accessory protein to the photoprotein aequorin in the jellyfish *Aeqorea victoria.* It is an autofluorescent protein of 238 amino acids. The extremely stable protein forms a beta-barrel structure with its chromophore located inside the barrel. The latter is formed posttranslationally within the protein upon cyclisation and oxidation of the residues 65 - 67 (Ser-Tyr-Gly). The 27-kDa protein fluoresces bright green when excited by UV or blue light. GFP fluorescence depends on an internal chromophore and so, unlike other biological fluorochromes, it does not need the addition of a cofactor to fluoresce (Tsien 1998).

For the use in plants a cryptic intron, which caused the GFP mRNA to be mis-spliced, had to be removed (Haseloff et al. 1997). The GFP variant used in the present study (mGFP5) is a mutant, which combines the latter mutation with a spectral modification (I165T; Heim et al. 1994). This protein has a dual excitation peak of almost equal amplitude at 400 and 475 nm. This allows the efficient use of techniques that require either UV or blue light excitation of the protein, for example when screening GFP-expressing plants with a UV lamp or when using blue laser light excited confocal microscopy (Haseloff 1999).

The most successful and numerous class of GFP application is as a genetic fusion partner to host proteins to monitor their localisation and fate directly in living cell. The gene encoding GFP is fused in frame with the gene encoding the endogenous protein and the resulting chimera is expressed in the cell or organism of interest. The ideal result is a fusion protein that maintains the normal functions and localisations of the host protein but is now fluorescent. This way GFP has been targeted successfully to practically every major organelle of the cell. Thus the size and shape of GFP and the differing pHs and redox potentials of such organelles do not seem to impose any serious barrier.
In general, fusions can be attempted at either amino or carboxyl terminus of the host protein (Tsien 1998). However, the crystal structures of GFP show that the C- and N-termini of its core domain are not far apart (Ormö et al 1996), so it is also possible to splice GFP into a non critical exterior loop or domain boundary of the host protein. For example, residue 2-233 of GFP have been inserted between the last transmembrane segment and the long cytoplasmic tail of a *Shaker* potassium channel (Siegel and Isacoff 1997).

In the present study GFP has been fused to the C-terminus of KAT1. The construct was transiently expressed in guard cells of *V. faba* and was shown to maintain the normal function and localisation of the KAT1 (Hurst et al. 2004, Meckel et al. 2004). As a membrane protein, it served as an additional and intracellular produced membrane marker.

1.4.2 Microscopy - optical sectioning techniques

In order to follow the fluorescently labelled membrane and fluid phase during endocytosis, laser scanning based microscopy techniques were used. With confocal and multiphoton laser scanning microscopy two techniques are available to locate and follow fluorescence even in living cells with high sensitivity and spatial precision. The principles underlying the techniques are explained briefly.

Confocal Laser Scanning Microscopy (CLSM)

In a conventional wide-field epifluorescence microscope, the entire object in the field of view is bathed in excitatory light, converging and expanding from the focal plane. The fluorescent signal is emitted from all irradiated regions and contributes to the final image. In contrast, in a confocal laser scanning microscope (CLSM) only a single point of excitation light is scanned across the specimen. The principle was developed by Marvin Minsky in 1957.

A laser beam passes a light source pinhole and is focused by an objective lens into a diffraction-limited volume element on a fluorescent specimen (Fig. 1.4). A mixture of emitted fluorescent light as well as reflected laser light from the illuminated spot is then recollected by the objective lens. The dichroic mirror separates the light mixture by reflecting the laser light and allowing only the fluorescent light to pass into the detection region. After passing the detector pinhole aperture the fluorescent light is usually detected by a photomultiplier transforming the light signal into an electrical one which is finally evaluated by a computer to generate an image. The critical feature of the confocal approach is that light emitted from points above (dotted lines) or below the plane of focus (dashed lines) is blocked by the pinhole and so never reaches the detector. The detector pinhole is situated in the **con**jugate **focal** plane to the specimen - giving the technique its name - and thereby only permits fluorescence from the focal plane (solid lines) to be detected. By scanning the laser from point to point over the sample until the entire focal plane is imaged, a single two-dimensional view, i.e. an ”optical section” is obtained (Lichtman 1994). As sectioning is performed using optics rather than the physical sectioning of the sample, living cells can be analyzed (Blancaflor and Gilroy 2000).

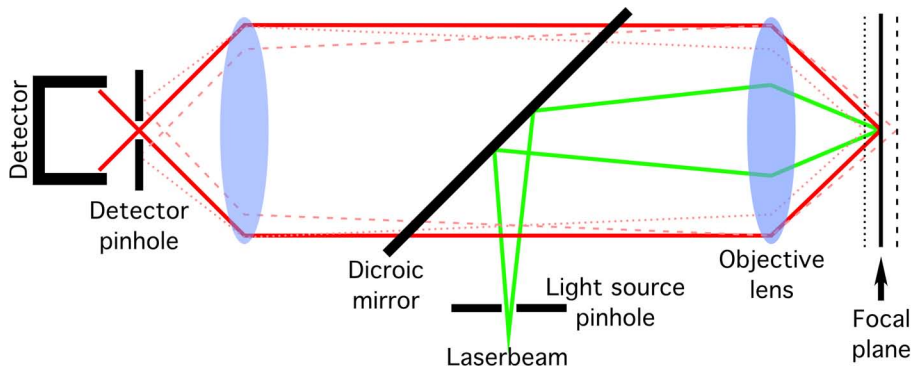

Figure 1.4: The confocal principle. The key feature of confocal microscopy is its ability to produce blur-free images of thick specimens at various depths.

Because only the light at the focal plane of the sample passes through the pinhole onto the detector, the resulting image is almost free from out-of-focus fluorescence. In addition, with only a single point illuminated, the illumination intensity rapidly falls off above and below the plane of focus as the beam converges and diverges. Thereby, the excitation of fluorophores distant to the focus is reduced, which provides further attenuation of out-of focus signals. By collecting a series of optical sections at different focal planes, a 3D-image of the sample can be reconstructed (Webb 1999).

Unfortunately, fluorescence microscopy can all to often have detrimental effects on living tissue. Toxic effects to the specimen under study may arise due to damage caused by absorption of the excitation light by exogenous probes that have been introduced into the tissue. This so called phototoxicity results from the highly reactive and toxic singlet oxygen that is generated through a non-radiative energy transfer between the excited triplet state of the dye and oxygen molecules. Over a limited illumination intensity range, including usual imaging conditions, damage appears roughly proportional to the amount of photobleaching as if the damage was purely accumulative as a function of total number of excitation events. Therefore damage is also directly dependent on the excitation coefficient and quantum yield of the fluorophores used. (Piston 1999).

Thus, the viability of the biological sample while it is being imaged is one of the most important constraints on the usefulness of any microscopy technique. Prolonged investigation of guard cells, e.g. to record stomatal movement, required to limit these detrimental effects as far as possible. This led to the adoption of a familiar laser based fluorescence microscopy technique to investigations on living intact guard cells.

Multiphoton Laser Scanning Microscopy (MPLSM)

Multiphoton laser scanning microscopy is an optical sectioning imaging technique that minimizes bulk fluorophore excitation (Denk et al. 1990). In this technique the sample is illuminated like in the case of CLSM but with a wavelength around twice the wavelength of the absorption peak of the fluorophore being used. Essentially no excitation of the fluorophore will occur at this wavelength. However, a laser is used, which delivers bursts of these low-energy, long-wavelength photons in short pulses, so that the mean power levels are moderate and do not damage the specimen. In the focal spot, in turn, the photon flux density in the pulses is high enough that some of the photons hit a target fluorochrome simultaneously. When the target absorbs two photons at essentially the same time, they produce a similar effect as a single short-wavelength photon with twice the energy, i.e. half the wavelength. Two-photon (2P) excitation as a single quantum event was first predicted by Maria Göppert-Mayer (1931).

The approach has the following advantage. The probability that two photons will arrive at the fluorochrome simultaneously and excite it, drops with the 4^{th} power of distance to the focal plane of the microscope. As a consequence, 80% of the absorption occurs in a volume confined

by the e^{-2} isointensity surface (approx. 300 x 1000 nm for λ_{ex}= 700 nm, Sandison and Webb 1994). Thus fluorescence is only effectively excited at the focal plane (Fig. 1.5), and an optical section analogous to a confocal optical section is generated. Unlike the confocal approach, however, the optical section is produced by the excitation of the fluorophores in a single focal plane. Therefore a spatial filter like a detection pinhole becomes obsolete, since no out of focus fluorescence is generated.

But even more important for live cell imaging is that by limiting the excitation to the focal plane of the sample, photobleaching of the fluorochrome outside the focal plane is minimized. This feature, in addition to the fact that the longer wavelength photons used in multiphoton microscopy have less energy, dramatically reduces phototoxicity to the sample (Denk et al. 1995). Thus, multiphoton microscopy generates confocal-like images while making longer observation times possible. However, systematic evaluation indicated, that bleaching in the focus is elevated with respect to one-photon (1P) excitation (Patterson and Piston 2000).

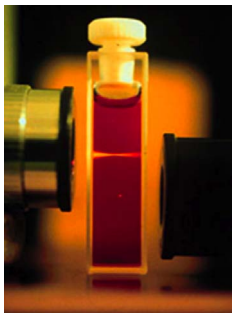

Figure 1.5: 1-Photon vs. 2 Photon. A cuvette of fluorescent dye excited by single photon excitation (fluorescent line) and multiphoton excitation (localized spot of fluorescence) illustrating that two photon excitation is confined to the focus of the excitation beam.

1.5 Imaging Endocytosis - a resolution problem?

The expected small size of endocytic vesicles in the order of 70 - 90 nm (Barth and Holstein 2004, Holstein 2002, Low and Chandra 1994) raises the question whether these small structures can be investigated with a confocal microscope. Concerning microscopy the best-known limit of the technique is resolution. In the common sense, it is defined as the minimum distance two objects are allowed to have in order to be resolvable as two separate entities. Yet, numerous definitions exist, as to what is ”resolvable”.

In order to resolve two (fluorescent) objects from each other, they need to have contrast, which is defined as the difference between the maximum intensity of the two objects and the minimum intensity found between them. Due to the diffraction of light at the edges of a microscopes objective lens (Abbé 1873), point objects produce a blurred image known as ”airy disc” or point spread function (PSF; Fig. 1.6). If two objects are separated by the radius of their airy disc’s center peak, i.e. the Rayleigh criterion, they provide 26.4% contrast. This is generally enough to ”resolve” the objects from each other (Rayleigh 1896). In practice, it is difficult to

measure the radius of the airy disc, since it would require to locate an intensity minimum. It is therefore quite common, to measure the full width at half of the maximum (FWHM) of the airy disc's center peak, as a value for resolution (Jonkman and Stelzer 2002).

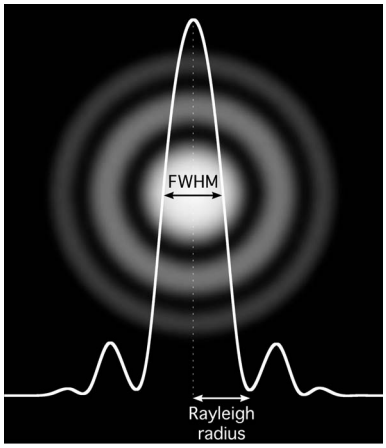

Figure 1.6: Airy disc. Diffraction image of a point object, produced by a microscope objective (circles). The FWHM and the Rayleigh radius of the center peak are shown in the intensity profile of the image (white graph). Under ideal imaging conditions the latter is given by $d \approx 0.61 \frac{\lambda}{NA}$.

In CLSM a fluorescent specimen is excited point by point by the diffraction-limited volume element of a focused laser beam. Consequently, each of these volume elements is associated with a discrete fluorescence intensity. The smaller the excitation volume element, the smaller the volume element which fluoresces and thus, the better the resolution of the image. The size of excitation volume element is determined by the diffraction limit of the optical system which depends on the numerical aperture (NA) of the objective lens as well as on the wavelength of the used laser light. This can be seen as the classical resolution limit of conventional optical microscopes using a so called wide-field illumination (see Eq. in text to Fig. 1.6).

However, with confocal microscopy it is even possible to overcome this resolution limit of wide-field illuminating techniques as only light generated in a small volume element is detected at a time. Here it is very important to note, that the effective volume of light generation, is usually smaller than the volume of illumination i.e. the diffraction pattern of detectable light creation is sharper and smaller than the diffraction pattern of illumination. In other words, the resolution limit in confocal microscopy depends not only on the probability of illumination but also on the probability of creating enough detectable photons. So the actual addressable volume which is associated with a generated light intensity is smaller than the illuminated i.e. solely diffraction-limited volume.

In theory, the resolution in a confocal image can be greater by a factor of $\sqrt{2}$ than with conventional microscopy. This, however, occurs only at great cost of the signal by reducing the diameter of the detector pinhole.

However, spatial resolution does not prevent in the ability to image subresolution objects such as endocytic vesicles. Objects of this size can still cause a recordable signal, if only the signal-to-noise ratio (SNR) is high enough, i.e. enough photons are detected. Even single molecules can in principle give rise to such a signal (Kubitscheck et al. 2000, Wahl et al. 2004). Since

fluorescently labelled vesicles were expected to give a rather low signal, the pinhole in the present study was never closed below one Airy. While this provides only a 10 % resolution gain with respect to conventional fluorescence microscopy it ensures to collect 100 % of the signal from the focal plane.

In conclusion, endocytic vesicles which are expected to have subresolution diameters can be imaged with CLSM, if they are labelled with sufficient fluorophores which emit enough photons during the recording. Resolution, in turn, does not pose a limit on the detection but on the size, which can be attributed to a detected structure.

Applying these techniques enabled to observe a constitutive endocytosis of vesicles with diffraction limited sizes in intact turgid guard cells. This caused an appreciable turnover of the PM including the PM resident potassium channel KAT1.

Chapter 2

Methods

2.1 Guard cells

2.1.1 Plant growth and cell preparation

Plant growth

Seeds of *Vicia faba* L., cv. (Bunyan) Bunyard Exhibition were grown in the green-house at 20 / 18 °C, with 70 / 80 % humidity, in a light / dark regime (14 h / 10 h) and with a photosynthetic active radiation (PAR) of 350-400 μmol m^{-2} s^{-1}. Plants were kept free from water stress at all stages of development. For experiments the two youngest fully expanded leaves from 3 to 4 week-old seedlings were used.

Buffers

All buffers, necessary for cell preparation and investigation are summarized in the following table.

Standard	100 μM $CaCl_2$, 10 mM MES / KOH pH 6.1, 15 mM KCl
Opening	100 μM $CaCl_2$, 10 mM MES / KOH pH 6.1, 45 mM KCl
Closing	100 μM $CaCl_2$, 10 mM MES / KOH pH 6.1, 100 μM abscisic acid (ABA). Osmolarity was adjusted to 580 mosmol/kg by adding sorbitol. Due to titration with KOH the buffer contained approximately 5 mM K^+.
Digestion	2% Cellulase Onozuka RS, 0.025% Pectolyase Y-23 (Yakult Honsha Co., Ltd., Japan), 0.2% Macerocym R10, 0.25% bovine serum albumin, 1 mM $CaCl_2$, 5 mM MES/HCl pH 5.6 Osmolarity was adjusted to 520 mosmol/kg.
Washing	200 μM $CaCl_2$, 10 mM MES / KOH pH 6.1, 10 mM KCl, 2 mM $MgCl_2$ Osmolarity was adjusted to 520 mosmol/kg.

Table 2.1: Buffers for cell preparations and investigation

Abscisic acid (ABA) was purchased from Sigma-Aldrich, Inc., solved in dimethylsulfoxide (DMSO), stored at -20 °C and added immediately prior to use.

Epidermal peels

To get coverslip-bottom-dishes coverslips were glued to the bottom of Teflon® chambers with GE RTV 108 (General Electric Silicones, Wilton, CT, USA), a flexible non-toxic silicon adhesive sealant (Reference CDS4319 "Food Contact Applications", Food and Drug Regulation FDA 21CFR 177.2600).

Approximately 3 x 10 mm strips of abaxial epidermis were carefully placed on *standard* buffer with the cuticle facing the air. A single swimming peel was lifted with a stainless steel grid (kind gift from Beckmann GmbH, Mönchengladbach, Germany) and quickly placed in a coverslip-bottom-dish with the peel facing the coverslip. 250 μl *standard* buffer were added immediately to cover the peel. This approach ensured that the peel was kept flat, close to the coverslip, and in solution without using chemical adhesives. In addition the cuticle was facing the coverslip, thereby exposing the cuticle free site to the solution. This became important when the buffer solution changed in the course of an experiment, to allow hydrophilic buffer components a direct access to the cells. Cells were checked for cytoplasmic streaming as a viability test before, during and after each investigation.

Opening and closing of stomata

Stomata cells were opened either with the fungal toxin fusicoccin (kind gift from Prof. Cornelia Ulrich-Eberius) or by illumination in combination with CO_2 depletion. In the first case, the *standard* buffer was replaced by *opening* buffer with 10 μM fusicoccin for at least 45 min. In the second case, cells were illuminated (PAR = 300 μE) for 2 h in *opening* buffer. The surface of the solution was covered with a round coverslip to avoid any gas exchange with ambient air. The CO_2 in the buffer solution is constantly decreased by the photosynthetic activity of the tissue and thereby creates an additional opening signal for the guard cells on top of the intense light (Willmer and Fricker 1996).

To close stomata the peels were incubated in the dark in *closing* buffer which contained three stimuli for guard cells to close: 100 μM of the plant hormone ABA, low potassium concentration, and elevated osmolarity. Osmolarity was determined with a osmometer (Osmomat 030, Gonotec GmbH, Berlin, Germany). Stomata closed within 30 min and 90% of the guard cells did not show any sign of plasmolysis.

Preparation of guard cell protoplasts

To produce guard cell protoplasts the cell wall of guard cells was enzymatically digested. The buffer below the swimming peels was removed and carefully replaced by *digestion* buffer to ensure that the peels were still swimming after the buffer exchange. Peels from fresh or particle bombarded leaves (Ch. 2.2.4) were incubated in *digestion* buffer for 90 min or 120 min, respectively, at 30 °C under constant gentle agitation. *Digestion* buffer was then replaced by *washing* buffer and the dishes were tapped on the bench for 5 min to release the protoplasts

from the peels. To remove the peels and cell wall fragments, the solution was filtered through a nylon net with 20 μm pores. Finally the protoplast solution was concentrated by low speed centrifugation for 2-3 min with a hand driven centrifuge after which the buffer was removed to 200 μl. Protoplasts were stored in the fridge for at least one hour prior to further use.

2.1.2 Temperature control

In some experiments accurate temperature control of the buffer solution was required during confocal investigation. For this purpose a temperature controller was constructed, which meets the following requirements:·

- lightweight to suffice the lifting forces which can be generated by a piezo-driven z-stepper
- fast to quickly change temperatures in the range of 5 to 65°C
- accurate to enable high resolution imaging during temperature control

The system is based on a programmable process controller (CAL 9500P, CAL Controls, Ltd., Hitchin, Herts, UK). This unit is connected to a thin film platinum temperature sensor (PT100/PTFC101A00, Willow Technologies Ltd., Lingfield, Surrey, UK) which measures the temperature of the bath solution close to the specimen (Fig. 2.1). It is also connected to an array of contactors (SKR 115A 230VAC, ELESTA Elektronik AG, Bad Ragaz, Switzerland) through which a peltier device (RH 1.4-32-06L, Melcor, Trenton, NJ, USA) is powered. Upon a trigger from the controller, the array of contactors change the direction of the current.

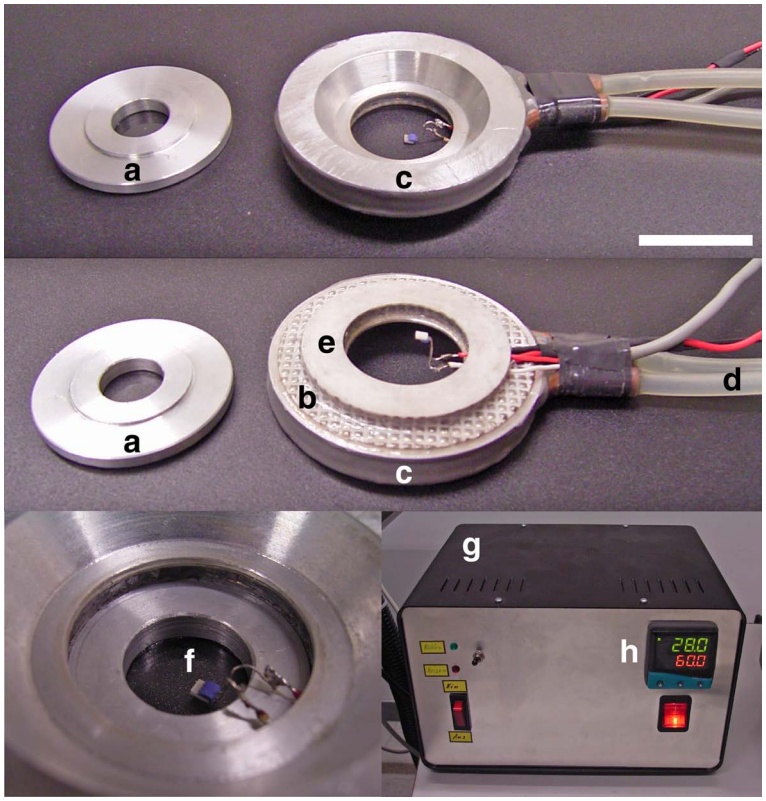

Figure 2.1: Parts of the temperature controller. An aluminium bath chamber with a coverslip bottom (a) is used in place of the normal Teflon® chambers. The large site of a peltier element (b) is attached to an aluminium ring (c), which is constantly cooled by a water circuit (d) to protect the peltier element. The small site of the element (e) is attached to the bath chamber. This brings a thin film platin temperature sensor in place close to the specimen (f). All electric components are connected to the main unit (g), which contains the programmable process controller (h), the power supply and the remaining components illustrated in Fig. 2.2. Scale bar = 2 cm.

In one direction, the small site of the peltier element which is attached to the aluminium chamber becomes cold; on the opposite site which is attached to a water cooled aluminium ring, it becomes hot. This cools the bath chamber and thereby the buffer and the specimen. In the opposite direction the specimen is heated up. The array of contactors can operate in two modes: In the first mode, the peltier element cools the chamber by default unless the controller triggers to heat it. In the other mode, the peltier element is either heating or cooling the chamber or is disconnected from the electrical power.

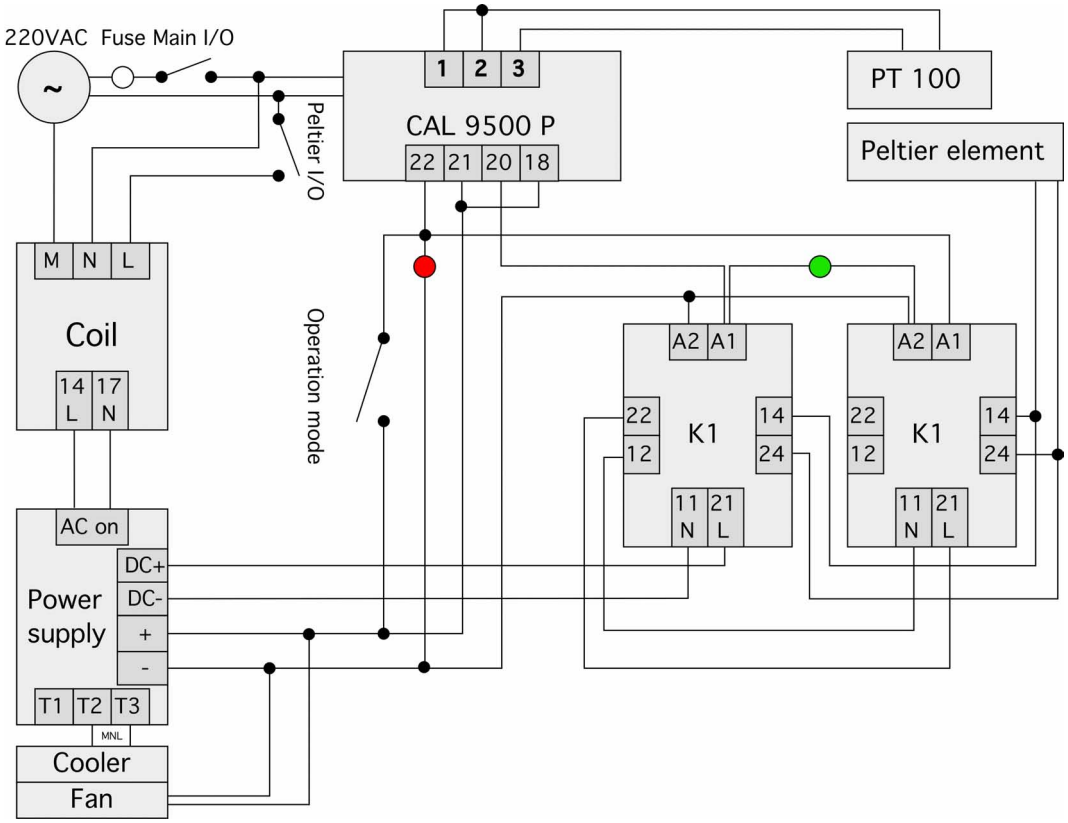

Figure 2.2: Circuit diagram of the temperature controller. The process controller (CAL 9500P) is connected to a temperature sensor (PT100), an array of contactors (K1 and K2), a power supply and the peltier element.

A personal computer, running Calgraphix Software (V. 1.0.1, Melcor, Trenton, NJ, USA) was connected to the controller via a RS232 interface to monitor the set point and the actual value over time. The system achieved temperature changes in the range between 7 and 60 °C with a velocity of around 4 °K min^{-1}.

If the buffer was to cool below room temperature, a water cooled aluminium collar was mounted to the objective in order to cool down the immersion. Otherwise the immersion heats up the buffer in the chamber, especially in the focal area.

2.2 Fluorescent labels

2.2.1 Live cell stains with fluorescent chemical dyes

To label cell structures of interest, fluorescent chemical dyes were applied directly to fresh epidermal peels before microscopic investigation. The fluorescent dyes FM®1-43 (T3163), FM®2-10 (T7508), FM®4-64 (T13320), MitoTracker®Red CMXRos (M7512), Alexa Fluor®488 hydrazide (A10440) (Fig. 2.3) were purchased from Molecular Probes, Inc. (Eugene, OR, USA), stored according to manufacturers instructions, and diluted in buffer solutions immediately prior to use. Since some of the dyes are available in different packagings, the catalog numbers are given in brackets to specify the dyes used.

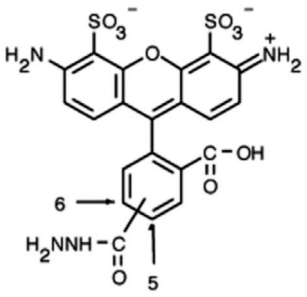

Figure 2.3: Chemical Structure of Alexa 488 hydrazide. The chemical structures of the remaining dyes used are shown in Fig. 3.1.

2.2.2 GFP expression

In order to follow the distribution of proteins in living cells with the CLSM, fluorescent chimera of different proteins fused to auto fluorescent proteins were constructed and inserted into plant expression vectors. Intact guard cells were transiently transfected by particle bombardment to heterologously express these constructs. The following constructs were used:

- **KAT1::mGFP5**
  KAT1 in pYES (kind gift from Sabrina Gazzarini)
  pAVA393 including mGFP5 (kind gift from Dr. Guido Kriete)
- **sGFP6::TM23** in pBIN (kind gift from Jean-Marc Neuhaus)
- **talin::YFP** (kind gift from Benedict Kost)

2.2.3 Construction of the KAT1::GFP fusion vector

The cDNA for KAT1 was amplified by polymerase chain reaction (PCR) from KAT1 in pYES as template deoxyribonucleic acid (DNA) for directed cloning. A BSPLU11I restriction site (in bold) was introduced 5' of the start codon with a forward primer (GGAAAA**CATG**TCTATCTCTTGACTCGAAAT) and a restriction site for isoshizomer *Nco*I (in bold) was introduced 3' with a reverse primer

(TTTCC**CATG**GCATTTGATGAAAAATACAAATGATCACC), depleting the KAT1 stop codon from the cDNA sequence. After digesting the restriction sites, the PCR product was ligated into the plant expression vector pAVA393/*Nco*I restriction site in frame with the mGFP5 (Haseloff et al. 1997) for expression of the fusion protein KAT1::GFP under control of two cauliflower mosaic virus 35S promotors. The plasmid was then cloned in *Escherichia coli/DH5*α, followed by preparation of plasmid DNA (Quiagen high speed Midi-Kit, Quiagen, Germany). The purified vector was used for particle bombardment of intact cells.

Figure 2.4: Schematic diagram of the KAT1::GFP chimeric gene. KAT1 was inserted into pAVA393 plasmid vector which contains two 35S promotors and the mGFP5 coding sequence.

2.2.4 Transfection

Whole leaves of *V. faba* were placed upside down on semi-solid 1.2% agar containing Murashige Skoog medium (Murashige and Skoog 1962) and bombarded with a Bio-Rad BIOLISTIC® PDS-1000/He Particle Delivery System (Bio-Rad, Inc.) with 2 μg gold (1 μm particle diameter, Fig. 2.5) at a pressure of 600 psi, a distance of 6 cm, and a vacuum of 25 inches Hg. The particles were coated with 15 μg plasmid-DNA as described below. This resulted in a transfection efficiency of approximately 30% of intact guard cells in the bombarded area, which were found mainly around the center of the bombardment. At the rim of this area fewer guard cells but more epidermal cells were transfected.

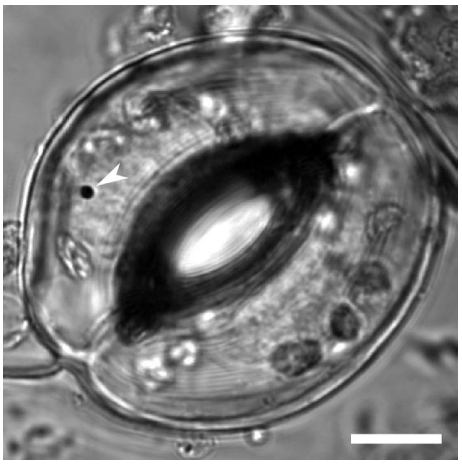

Figure 2.5: Particle bombardment. A gold particle (arrow) in the nucleus of a guard cell. Scale bar = 10 μm.

Bombardments with 900 psi gave comparable results with respect to the efficiency of guard cell transfection but did not result in transfected epidermal cells. The use of wolfram instead of gold particles resulted in a dramatically increased number of dead guard cells.
Bombarded leafs were placed on wet filter paper and kept in the dark at room temperature for approximately 16 h until further use. Transfected protoplasts were obtained by digesting peels of these leafs.

Coating particles

30 mg gold particles were washed according to the manufacturers manual, suspended in 500 μl glycerol (50% v/v) and stored in sealed tubes at -20°C until use. The gold-glycerol mixture was then sonicated and vortexed for 10 min, respectively, to suspend the particles. The mix was then vortexed slowly throughout the remaining coating procedure. Vortexing was stopped shortly, while 33,3 μl suspension (= 2 mg gold) per shot were quickly pipetted from the center of the gold suspension, since unsuspendable gold particles settle to the bottom. The following components were added and mixed with the pipet after each addition:

$\mathrm{V_{Gold}}$	=	33,33 μl per shot (= 2μg Gold)
$\mathrm{V_{DNA}}$	=	15 μg plasmid DNA per shot
$\mathrm{CaCl_2}$	=	50% of total volume ($\mathrm{V_{tot}}$) of a 2,5 mM stock solution
Spermidine	=	16% of total volume ($\mathrm{V_{tot}}$) of a 0,1 mM stock solution
		($\mathrm{CaCl_2}$ and spermidine stocks were stored in aliquots at -20 °C)

$$\mathrm{V_{tot}} = \frac{\mathrm{V_{Gold}} + \mathrm{V_{DNA}}}{0.34} \tag{2.1}$$

The DNA was then allowed to precipitate onto the gold particles on ice for 20 min. The preparations were gently centrifuged at 5000 rpm (Biofuge 13, Heraeus Sepatech GmbH, Osterode, Germany) for 5 s to avoid agglutination but to achieve pelletation. The supernatant was carefully replaced with ethanol (70% v/v, p.a.), thoroughly vortexed, 1-2 s sonicated, and centrifuged. The last steps were repeated twice with pure ethanol (96% v/v, p.a.). Finally the DNA-coated gold particles were suspended in 20 μl ethanol (96% v/v, p.a.) per shot. While vortexing and mixing with the pipette, 20 μl of the suspension were quickly applied onto a macrocarrier which was dried in a vented sterile bench. An even, light brown film of gold with no visible particle agglomeration indicated a successful preparation which is to be used within 2 h.

2.3 Calibration for microscopic imaging

Confocal microscopic analysis was carried out using a Leica TCS SP system (Leica Microsystems GmbH, Heidelberg, Germany) with the following components:

Confocal scanner:	Leica TCS NT/SP
Microscope:	Leica DM-IRBE
Objectives:	HCX PL APO 63x NA 1.20 W CORR UV objective with collar adjustment, to compensate for the relative thickness of layers having higher or lower NA, e.g. the coverslip
1-photon (1P) laser:	25 mW Argon-Krypton continuous wave (cw) wavelengths: 476, 488, 568, 633 nm
2-photon (2P) laser:	Spectra-Physics Millenia V-P 93950-M / Tsunami Ti:Sapphire wavelength ranges: 720-900 nm; pulse repetition rate: 82 MHz laser pulse width: 1.2 ps; coupling to microscope: fiber 1.5 m spectral bandwidth: 1 nm; object pulse width: 1.3 ps

The following software was used for imaging and image analysis:

- Leica Confocal Software 2.00 (Leica Microsystems GmbH, Heidelberg, Germany).
- ImageJ v1.33a (National Institute of Health, USA, http://rsb.info.nih.gov/ij)
- Microsoft® Excel X for Mac® (Microsoft Inc., Redmond, CA, USA)
- IGOR Pro 5.02 (WaveMetrics Inc., Lake Oswego, OR, USA)
- Huygens® 2.0 Professional (SVI, Hilversum, The Netherlands)
- IMARIS® 3.0 (Bitplane AG, Zürich, Swizerland)

To achieve optimal image quality and to ensure the right interpretation of the recorded data, the imaging system, the fluorophores and the biological object were analysed in the spectral, spatial, and signal domain.

2.3.1 Spectral analysis

Fluorescence emission and, in the case of 2P excitation, also excitation spectra were recorded in order to adjust the spectral detection range and beam splitters to:

- maximise the SNR in case of a weak signal to improve spatial resolution.
- minimise excitation intensity in case of recording image stacks to reduce bleaching and, especially at the use of chemical dyes, increase viability of the cells by reducing the production of reactive oxygen species (ROS).
- minimise channel crosstalk in colocalisation experiments.

Spectrometer data

FM 1-43 (10 μM), FM2-10 (20μM) and FM4-64 (10μM) were analysed with a fluorimeter (RF 5001 PC, Shimadzu Co., Kyoto, Japan). They were either solved in H_2O bidest. or in 2 % of the zwitterionic micelle forming detergent 3-[(3-cholamidopropyl)-dimethylammonio]-1-propanesulfonate (CHAPS), to mimic the hydrophobic environment of a phospholipid bilayer. Excitation- and emission spectra (Fig. 2.6) were fitted by Gaussian functions (Eq. 2.4) to extract the peak positions (Tab. 2.2).

All dyes show a dramatic fluorescent increase and a blue shift when solved in a hydrophobic environment with respect to water. The blue shift found for FM1-43 solved in CHAPS (23 nm) is close to the shift observed upon binding of the dye to POPC vesicles (27 nm; (Schote and Seelig 1998). Since the excited state is stabilized only by polar solvents the blue shift provides evidence for the location of the chromophore in a non-polar environment.

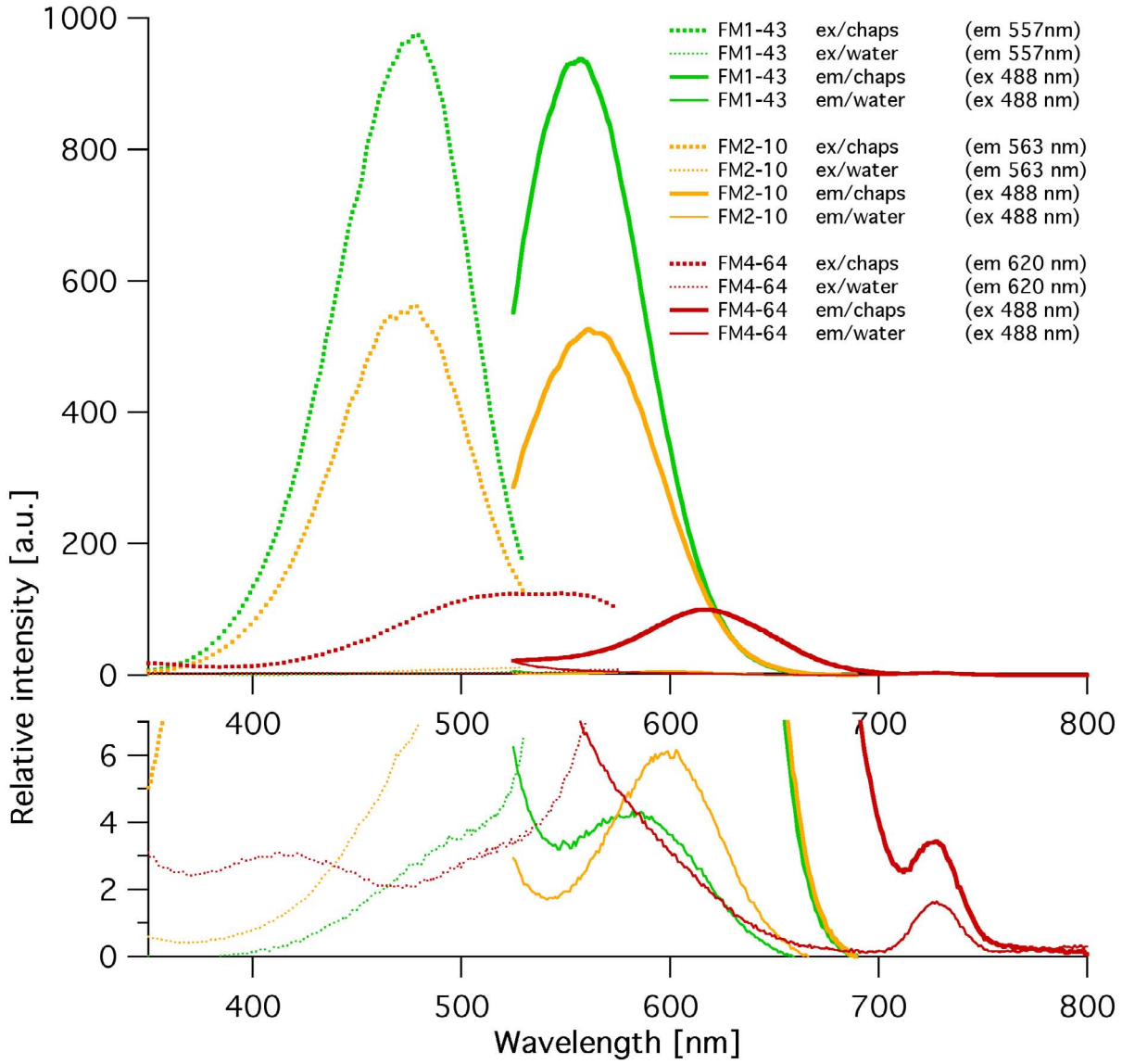

Figure 2.6: Excitation- and emission spectra of FM-dyes. Spectra of FM1-43 (10 μM), FM2-10 (20 μM) and FM4-64 (10 μM) were recorded in H_2O bidest. and 2% CHAPS, respectively. Small values are rescaled in the bottom graph. Spectra were recorded at the respective excitation or emission wavelength as denoted in the legend. Note, that FM4-64 is also excitable with the 568 nm line of an ArKr-Laser.

	FM1-43		**FM2-10**		**FM4-64**	
	r.i. [a.u.]	λ[nm]	r.i. [a.u.]	λ[nm]	r.i. [a.u.]	λ[nm]
Excitation in CHAPS	932.11	472.45	525.98	472.12	59.46	535.43
Emission in CHAPS	937.78	555.98	528.89	561.38	92.49	614.82
Emission in H_2O	5.09	578.59	4.91	596.53	1.59	727.21

Table 2.2: Peaks of excitation and emission spectra of FM-dyes. Spectra of FM1-43 (10 μM), FM2-10 (20 μM) and FM4-64 (50 μM) were fitted to a Gaussian function to extract the position of the peaks. For each peak the relative intensity (r.i.) and the wavelength (λ) are given. Excitation spectra of dyes solved in water have not been fitted due to the lack of local maxima (see Fig. 2.6).

Two-photon excitation spectra

To determine the optimal 2P excitation wavelength for FM2-10, excitation spectra were recorded. As a reference, the 2P excitation spectrum of mGFP5 was also recorded, since it allowed for a comparison with published data (Xu et al. 1996).

The maximum (λ_{max}= 878.07 nm) of the mGFP5 spectrum (Fig. 2.7) is shifted by approximately 30 nm towards shorter wavelengths with respect to the EGFP spectrum determined by Xu et al. (λ_{max}= 900 - 920 nm), probably because output power of the 2P-laser system dropped by approximately 50 % towards longer wavelengths. Consequently, the FM2-10 2P excitation spectrum is not accurate, but still guides for the optimal imaging conditions with the setup used. Note that FM4-64, with a 2P excitation maximum at 1047 nm (Girkin and Wokosin, 2002), was hardly excitable with the Ti:sapphire laser.

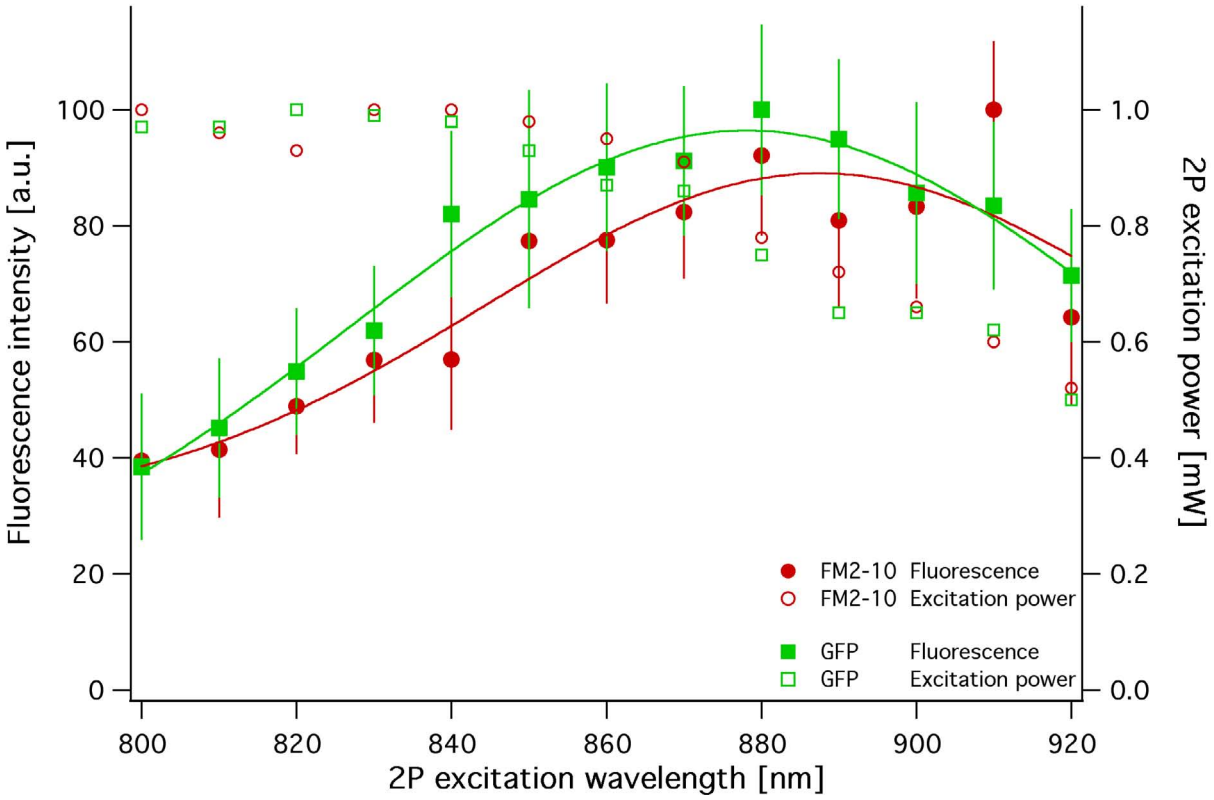

Figure 2.7: Two-photon excitation spectra of GFP and FM 2-10. Relative GFP (green closed squares) and FM 2-10 (red closed circles) emissions versus 2P excitation wavelengths are plotted and fitted with Gaussian functions (Eq. 2.4) to obtain the peak positions. The GFP-spectrum (green graph) peaks at 878.07 ± 1.5 nm, the FM2-10-spectrum (red graph) at 887.53 ± 5.2 nm. The maximum achievable excitation power at which measurements were recorded is also plotted versus 2P excitation wavelength (respective open symbols). Both spectra are means of n = 10 recordings, error bars indicate the standard deviation (SD).

One- and two-photon emission spectra

All spectra were measured on living guard cells by recording λ-stacks. The 1P spectra were measured with a RT30/70, 2P spectra with a SUBSTRATE filter, both of which are spectroscopic neutral. For imaging band- or low-pass filters (DD488/568, RSP500) were used, which are unsuitable to record neutral spectra but are advantageous with respect to sensitivity in a specific range of wavelengths.

Auto fluorescence To determine the auto fluorescent signals of plant material after long-term incubations in buffer and to test the effect of the silicon grease on the cells, epidermal peels were incubated in standard buffer in glass chambers and coverslip-bottom-dishes. Spectral recordings of the same peel were then taken after 1, 2 and 10 h. Epidermal peels show three spatially and spectrally distinguishable autofluorescent signals upon excitation with 488 nm (Fig. 2.8). While the intensities of chlorophyll and cutin autofluorescence did not increase over time, vacuolar autofluorescence did. The intensity of vacuolar autofluorescence emerges to a bright signal within 12 h of incubation in standard buffer. The comparison of long term incubations in glass chambers or coverslip-bottom-dishes revealed no difference with respect to cytoplasmic streaming or intensity of emerging autofluorescence (data not shown). The silicon grease is therefore suitable for long term live cell investigations.

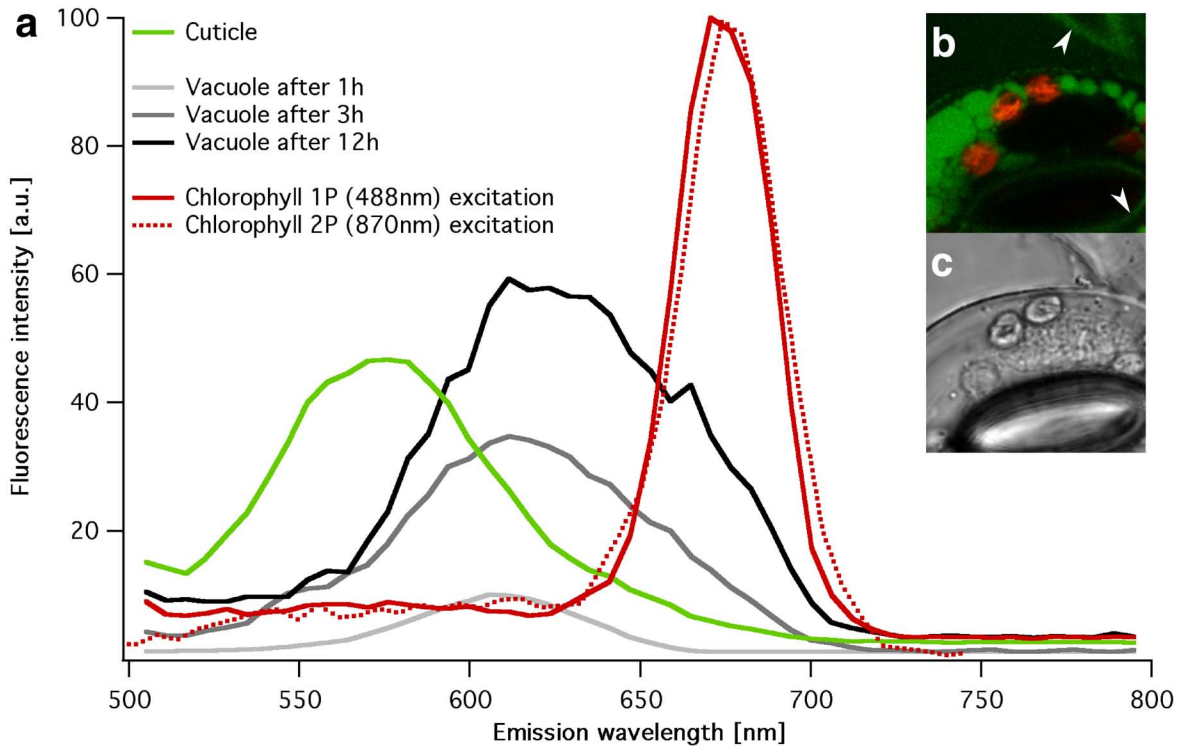

Figure 2.8: Autofluorescence spectra after long term incubation. Autofluorescence of chlorophyll (a, red curve; b, red signal) and the cuticle (a, green curve; b, arrowheads) did not increase over time. In contrast, guard cells showed a strong autofluorescence signal in the vacuole (a, grey curves; b, green signal). The intensity of this autofluorescence is positively correlated with incubation time. (c) DIC image of the cell in (b). λ_{ex}= 488 nm.

Fluorescent dyes Fluorescent emission spectra were measured by recording λ-stacks directly on live cell stains. The spectra of Alexa 488 hydrazide, FM-dyes and the MitoTracker were recorded extracellularly close to the PM, directly at the PM, and at mitochondria, respectively. In addition, spectra for the same dye were recorded at different subcellular positions. For a given dye similar emission spectra were found in different subcellular structures (Fig. 2.9). This provides additional evidence for the subcellular distribution of a dye (Ch. 3.1).

Guided by spectra obtained with the spectroscopic neutral filter RT30/70, the following detection settings were used for confocal imaging:

	Excitation [nm]	**Emission [nm]**	**BeamSplitter**
FM1-43	488	530-630	RSP500
FM2-10	488	530-630	RSP500
FM4-64	488	600-700	DD488/568
Alexa 488	488	505-600	RSP500
MitoTracker	568	590-660	DD488/568

Table 2.3: Detection settings for confocal imaging of chemical fluorescent dyes. Chlorophyll fluorescence (λ_{max} $\sim$670 nm) was allowed to be detected in the FM4-64 channel in order to maximise detection efficiency while minimizing excitation energy.

Colocalisation of FM2-10 and MitoTracker Red CMXRos was performed by sequential scans: First, FM2-10 was excited at 880 nm (2P) and emission was detected between 480 and 550 nm. Then, the MitoTracker was excited at 568 nm (1P) and emission was recorded between 620 and 650 nm to avoid contamination with chlorophyll fluorescence in the images. With this approach both fluorophores could be detected separately without noticeable crosstalk. Signals have not been accumulated in order to get reliable colocalisation during sequential scans in presence of cytoplasmic streaming.

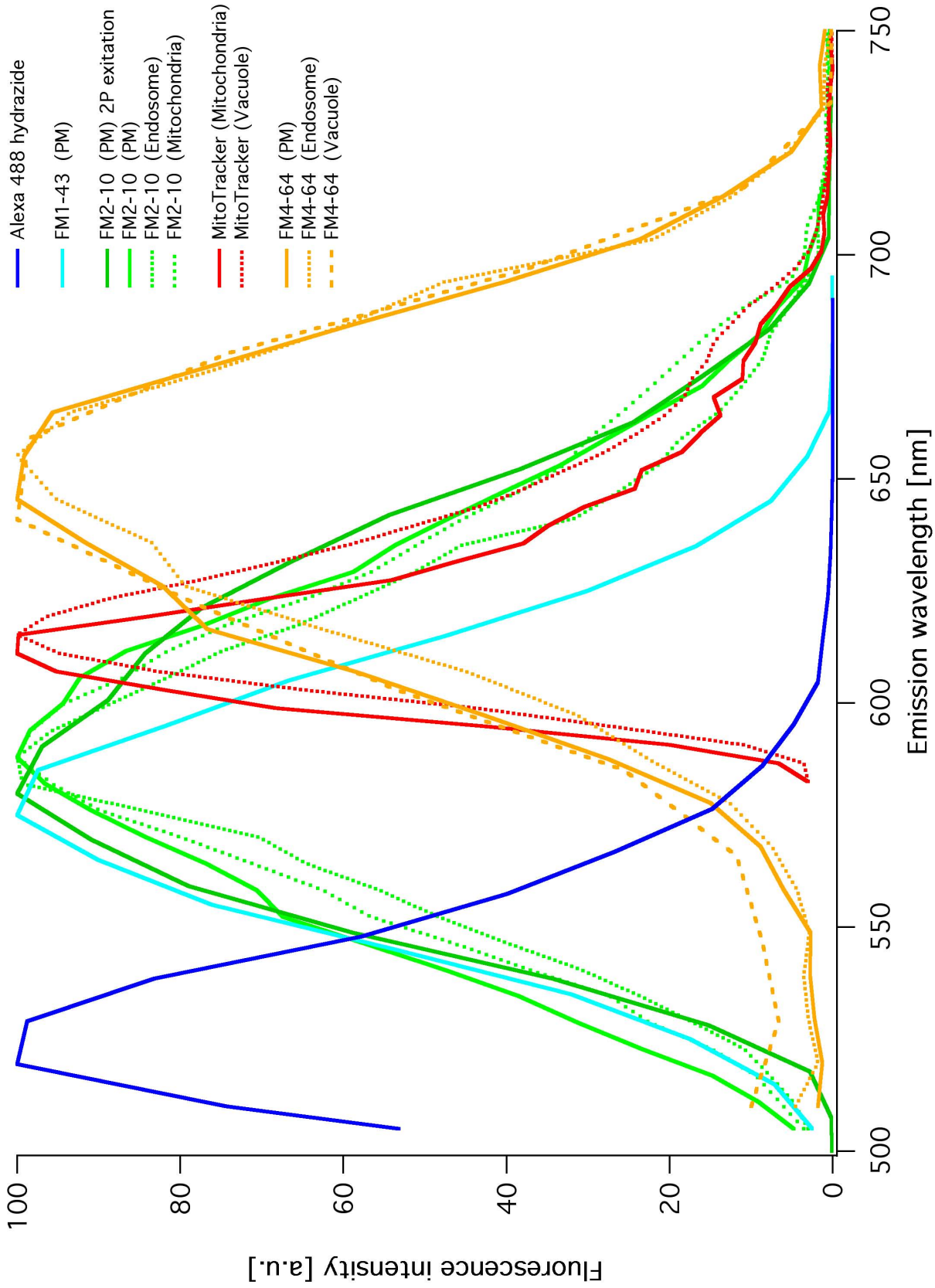

Figure 2.9: Emission spectra of fluorescent dyes. Spectra were measured in λ-stacks at different subcellular locations within a living cell. Alexa 488 hydrazide and all FM-dyes were excited at 488 nm, the MitoTracker at 568 nm. Every spectrum is a mean of measurements on at least 5 recorded λ-stacks.

GFP and variants For colocalisation experiments, precise emission spectra of GFP, the yellow fluorescent protein (YFP) and FM4-64 were determined in combination with the DD488/568 filter. This filter is not spectrally neutral but blocks fluorescence around 488 nm and 568 nm to reach the detector. By using this filter, GFP and FM4-64 could both be excited at 488 nm and simultaneously detected without any crosstalk (Fig. 2.10).

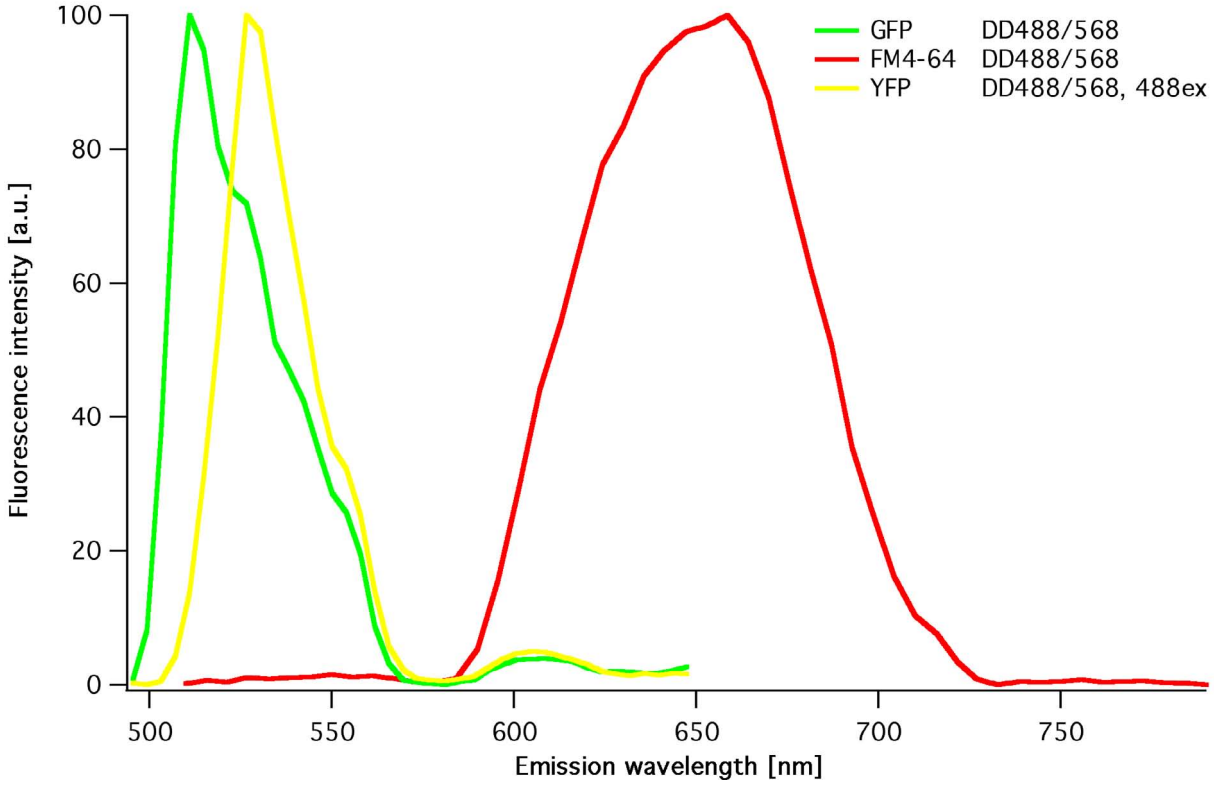

Figure 2.10: Emission spectra of GFP, YFP and FM4-64. The filter DD488/568 allows for co-localisation of GFP or YFP with FM4-64 without any crosstalk. λ_{ex}= 488 nm.

In the final half year of this thesis, lasers and filters of the confocal setup were changed towards the capability of colocalising CFP and YFP and to perform measurements of fluorescence resonance energy transfer (FRET) between the cyan fluorescent protein (CFP) and YFP. New laser lines (456 and 514 nm) and filters (DD456/514 and DD488/643) were added, while the DD488/568 was removed. As a result, the setup has unfortunately become less suitable for the spectral separation of GFP and FM4-64. Lack of the DD488/568 filter hampers to achieve the same spectral separation and detection efficiency. While GFP is not detectable with the DD456/514 filter, the DD488/643 filter only allows FM4-64 to be detected beyond 650 nm. The RSP500 filter, although sold as a low-pass filter, cuts of at 650 nm and thus allows detection of FM4-64 between 600 and 645 nm only.

2.3.2 Spatial analysis

Point spread functions

Utilising lenses in image formation introduces diffraction effects and places a limit on the resolution of the technique (Abbé's diffraction barrier; Abbé 1873). Light cannot be focused into an infinite small point and therefore causes the image to blur. This blur is characterized by the PSF, the output of the imaging system for an input point source.

To measure the resolution limit of a microscope, a light point with preferably no spatial extension should be imaged. To mimic such a light source, fluorescent beads with a diameter of 100 nm were used. This diameter, which is well below the expected resolution limit for conventional fluorescence microscopy, can in this context be treated as an input point source. The lateral and axial intensity profile of such a diffraction-limited bead image is Gaussian distributed. The width at which this profile drops to half the maximal value (FWHM), is frequently used as a value representing the dimensions of the PSF to determine the resolution of the microscope (Jonkman and Stelzer 2002).

To fully characterise the resolution of the setup and to mimic the conditions under which either fluorescent signals in guard cells were recorded, fluorescent beads were placed directly behind the coverslip, behind the cuticle or behind cells (Fig. 2.11). Fluorescence was excited with 1- and 2P processes and recorded in the spectral range also used for GFP and FM2-10 detection.

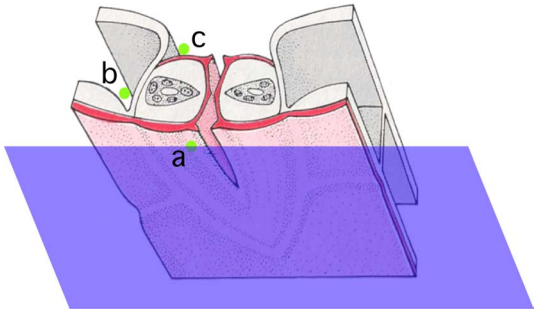

Figure 2.11: Measurements of the PSF at different positions around a guard cell. Fluorescent beads were placed and imaged behind the coverslip (a), the cuticle (b), and stomata (c).

To determine the lateral resolution or sizes of fluorescently labelled structures the intensity values (z) of the 8-bit-image matrix (x,y) of the beads or structures were fitted with a 2D Gaussian function (Eq. 2.2)

$$f(x,y) = z_0 + Ae^{-\frac{1}{2}\left[\left(\frac{x-x_0}{w_x}\right)^2+\left(\frac{y-y_0}{w_y}\right)^2\right]} \tag{2.2}$$

in order to obtain the parameters w_x and w_y (Fig. 2.12). These parameters are proportional to the FWHM (Eq. 2.3) of the 2D-Gaussian curve in x and y direction, respectively.

$$FWHM = 2w\sqrt{ln4} \tag{2.3}$$

In the case of beads, the FWHM specifies the resolution of the microscope (Fig. 2.12a) whereas in the case of measured cellular structures it is used as a value for the quantification of their diameter (Fig. 2.12a). Separate parameters for the diameter of the structures in x and y directions (i.e. w_x and w_y) were chosen in order to identify, whether fluorescently labelled structures are ideal spheres or not.

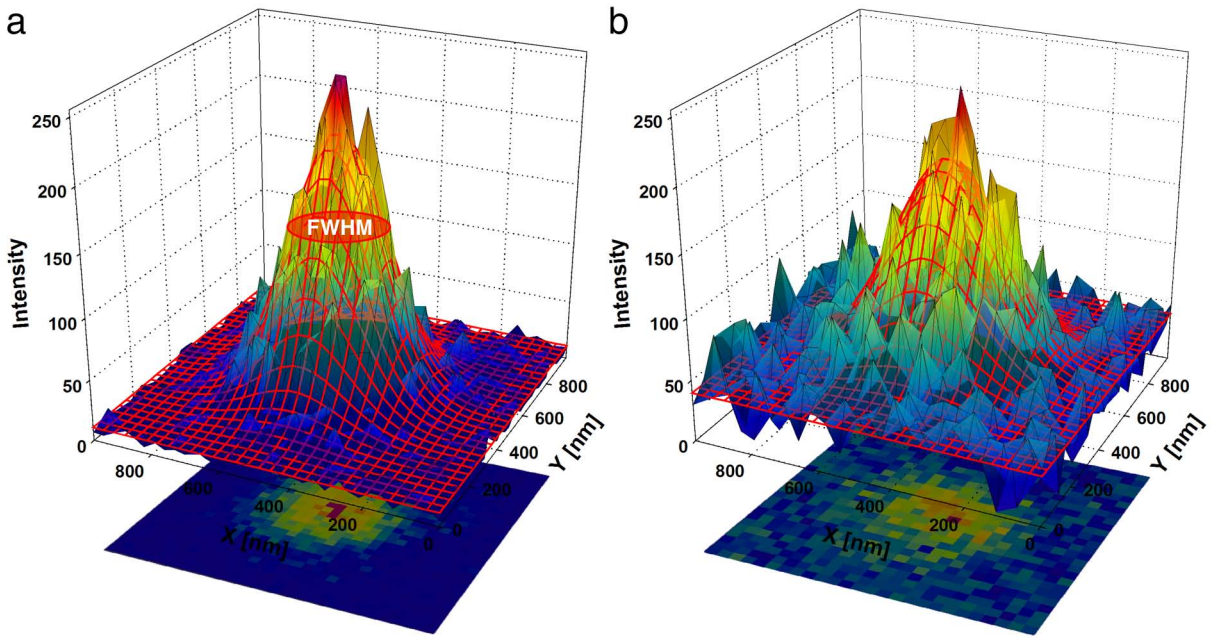

Figure 2.12: Size measurements of fluorescently labelled structures. The distribution of signal intensity against the x and y dimensions of fluorescent images of a bead (a) and of a single vesicle (b) are shown. The bead had a diameter of 100 nm and was imaged through the cuticle to mimic the conditions under which all fluorescent signals in guard cells were recorded. The pseudo surfaces of both distributions were fitted with a 2D-Gaussian function (red net) in order to obtain the FWHM of the signal intensity distribution, which corresponds to the diameter of the structures.

To determine axial resolution a z-profile of an image stack of a bead was generated. Therefore, the equatorial xy-image of a bead was chosen to mark its center as the region of interest (ROI). The mean image intensity values of the ROIs along the z-axis of the image stack yields the z-profile. This z-profile was fit to a 1D-Gaussian function (Eq. 2.4)

$$f(x,y) = z_0 + Ae^{-\frac{1}{2}\left(\frac{x-x_0}{w}\right)^2} \tag{2.4}$$

to obtain w_z and via Eq. 2.3 also $FWHM_z$.

Results of the dimensions of the PSFs measured with beads are summarized in Tab. 2.4. Apparently, resolution decreases most dramatically behind the cuticle but not much further behind the entire guard cell. This is plausible, considering, that the cuticle causes both diffraction and refraction, while the aqueous cell does not. The values are close to those determined for similar measurements on guard cells from *Cammelia communis* (White et al. 1996).

PSF	n	FWHM$_{xy}$[nm]	FWHM$_{xy}$[nm]
1P, generated	1	217.2	589.8
1P, behind coverslip	34	236.9 $\pm$ 5.8	693.9 $\pm$ 27.8
1P, behind cuticle	9	274.4 $\pm$ 24.3	1124.5 $\pm$ 147.8
1P, behind guard cells	14	275.0 $\pm$ 16.7	1137.2 $\pm$ 161.3
2P, generated	3	287.3	773.5
2P, behind coverslip	5	312.41 $\pm$ 33.16	1066.8 $\pm$ 50.26

Table 2.4: Resolution at different positions within the specimen. All FWHMs were determined using beads with a λ_{em}(max) = 510 nm, which were excited with 1P or 2P at 488 or 870 nm, respectively. Emission was recorded between 500 and 520 nm to match parameters for GFP detection. All 1P measurements were recorded or calculated with an Airy disc = 1, which translates into a backprojected pinhole diameter of 294.991182 nm for the setup used. This value is necessary to generate PSFs with Huygens® Professional.

The approximate lateral and axial dimensions of the PSF in the subcellular regions, where most of the fluorescent signals will be recorded, is 275 and 1130 nm respectively. Thus, any fluorescent structure with a size below the diffraction limit, which is bright enough to give a signal will appear to have at least these lateral and axial dimensions in recordings with the confocal setup used.

Size measurements of structures with larger diameters

Structures with diameters beyond the diffraction limit do not produce a completely Gaussian distributed spatial intensity profile. Granted that the fluorescence intensity over the structure is even, the intensity profile has a clear plateau. Only at the rims a sigmoid or ”half-Gaussian” intensity profile is found (Fig. 2.13). These characteristics are again caused by diffraction. To estimate the sizes of such structures, intensity profiles were fit to a Hill-function (Eq. 2.5), which resembles the features of such a profile. In this case the distance between v and w exactly gives the FWHM.

$$f(x) = y_0 + s\frac{v^n}{v^n + x^n}\left(1 - \frac{w^m}{w^m + x^m}\right) \tag{2.5}$$

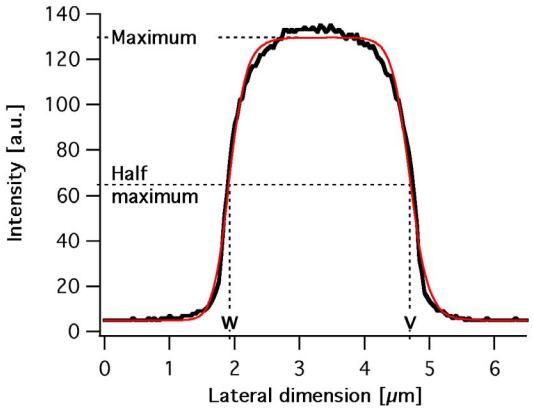

Figure 2.13: Profiles of larger structures. Lateral intensity profile of a fluorescent InSpeck® bead with a diameter of ~2.5 μm. The parameters w and v of the hill function and the maximum, which is given by s + y_0, are marked.

Spatial imaging parameters - the Nyquist-Shannon sampling theorem

According to the Nyquist-Shannon sampling theorem the discrete sequence of a sampled continuous function contains enough information to reproduce the function exactly provided that the sampling rate is at least twice that of the highest frequency contained in the original signal. Since the highest frequencies in a microscopic image are limited by the resolution of the system, a voxel should have at least half the size of the resolution in lateral and axial direction, respectively (Inoué and Spring 1997).

Guard cell pairs were routinely imaged as stacks of paradermal images with voxel sizes of 100 x 100 x 488.44 nm. Only in case of single vesicle or PSF measurements, voxel sizes of 50 x 50 x 200 nm had been used to achieve better Gaussian fits. Considering the resolution behind the cuticle (Tab. 2.4), a voxel size of 100 x 100 x 488.44 corresponds to a lateral and axial sampling rate of 2.7 and 2.3, respectively. The axial sampling rate has been chosen close to the theoretical minimum to obtain 3D stacks with the least possible slices. This maximizes viability while minimizing bleaching.

2.3.3 Signal analysis

FM-dye concentrations

The concentration of styryl dyes was adjusted, to ensure a similar bright signal at the PM of guard cells. Each dye was evenly distributed in the PM of guard cells after about 10 minutes of application. Final concentrations of 5 μM FM1-43, 20 μM FM2-10, and 10 μM FM4-64 yielded stains, which could be recorded with similar SNRs. The MitoTracker was applied in a final concentration of 500 nM.

Alexa 488 self-quenching

Fluorescence intensity does not increase infinitely with dye concentration. In high concentrated solutions, self-quenching limits the maximal fluorescence intensity of a given fluorophore (Hamann et al. 2002).

To test, at which concentration Alexa 488 hydrazide shows self-quenching, the fluorescence intensity of a dilution series was quantified with a fluorimeter. A plot of the relative fluorescence intensity against the concentration of Alexa 488 hydrazide shows an overall linear increase of fluorescence with dye concentration (Fig. 2.14). A linear fit was applied to the data range between 1 and 6 mM. All in all, Alexa 488 does not show any appreciable self-quenching in the concentration range used in this study ($\leq$ 5 mM). The slight deviation from the linear fluorescence increase at concentrations above 8 mM may indicate the beginning of a self-quenching process.

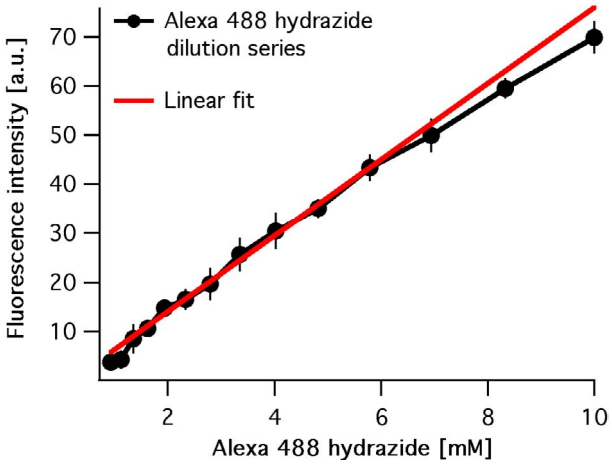

Figure 2.14: Alexa 488 self-quenching. Fluorescence intensity is plotted as a function of Alexa 488 concentration. A 10 mM solution was diluted stepwise with opening buffer. A linear function was fit to the data range between 1 and 6 mM. The slight deviation from the linear fluorescence increase indicates the beginning of a self-quenching process.

Estimated signal demand of the CLSM

Fluorescence intensity does also not increase infinitely with excitation intensity, due to ground state depletion and bleaching processes. In the first process fluorophores become saturated in non-fluorescing electron states by high photon fluxes. The second process describes the interactions of long living excited electron states such as the triplet state with other dye molecules or with oxygen. Both cases lead to non-excitable fluorophores and hence to a limited fluorescence. In addition, the detection of the emitted photons is influenced by the detector and the optical pathway to the detector. The latter is influenced by the specimen and the setup (Stelzer 1998).

Thus, fluorescence intensity and detection efficiency are limited by the properties of the fluorophore, the setup and the settings. For a given fluorophore and confocal setup, a minimum number of excitable dye molecules within the focal spot (PSF) is therefore necessary to produce a recordable signal.

However, it is not possible to indirectly quantify this number by measuring the signal intensity of a dye dilution series with the CLSM. In solution, excitable dye molecules exchange by diffusion with bleached or saturated fluorophores in the detection volume, which is determined by the PSF. This is not possible for molecules, which are immobilized to a confined volume, e.g. in an endocytic vesicle. Hence, the limiting number would be underestimated to an unknown extent.

The signal demand for the setup used in the present study has not been evaluated. It was therefore estimated by a comparison with similar setups.

Kubitscheck et al. (1996) investigated single nuclear pores with a similar confocal setup. The nuclear pores have diffraction-limited diameters (120 nm) and were labelled with $\sim$200 fluorescein fluorophores. This has just been sufficient to produce as recordable signal (Ulrich Kubitscheck, personal communication). In the study of Charpilienne et al. (2001) 120 GFP molecules turned out to be sufficient for detection.

In both studies objectives with a higher NA were used (1.3 and 1.4, respectively). In the

present study a water immersion objective with a NA of 1.2 has been used. In addition, all signals were recorded through the cuticle. It is therefore reasonable to assume that the limiting number for the detection of Alexa or GFP molecules is slightly higher.

In conclusion, at least 200 molecules of either fluorophore are assumed to be necessary for detection in the present study.

2.3.4 Analysis of stomatal movement

For 3D analysis of stomatal movement and analysis of membrane recycling, image stacks of identical stomatal complexes were recorded in both closed and open states. Plants were kept in the dark for 5 h in order to close stomata. The cells were labelled with 20 μM FM2-10 and imaged using 2P excitation. Stomata were then incubated in a dye free buffer and opened by treatment with 10 μM Fusicoccin for 1 h. Open stomata were imaged again in the fusicoccin free but dye containing buffer.

Because illumination is confined to the focal plane, 2P excitation results in a reduced photobleaching outside the focal volume; however, photobleaching in the focal plane is higher than in the case of 1P excitation (Patterson and Piston 2000). Nevertheless, the technique greatly limited the production of ROS, since the major parts of the whole epidermal peel, i.e. the PM and the cuticle, were always thoroughly stained with fluorophores. 2P excitation was found to retain cytoplasmic streaming of guard cells even after 50 scans, while at the same time sufficient signal (SNR > 5) was achieved for subsequent data analysis. 1P excitation produced significantly higher SNR but often had the effect that cytoplasmic streaming stopped after recording a stack of images. To further reduce the harmful effects of prolonged imaging, the temperature of the incubation buffer was kept at 20 °C throughout the measurements to buffer the heat produced by 2P excitation. In addition, 100 μM ascorbate was added to the buffer to quench ROS, which are generated by excited fluorophores.

Stomatal aperture and pore area

Stomatal aperture and pore area were determined from sum-projections of the image stacks (Fig. 2.15). Stomatal aperture was measured as the perpendicular distance between the brightly fluorescent cuticular ledges. The pore area was determined by counting pixels fully enclosed by the ledges.

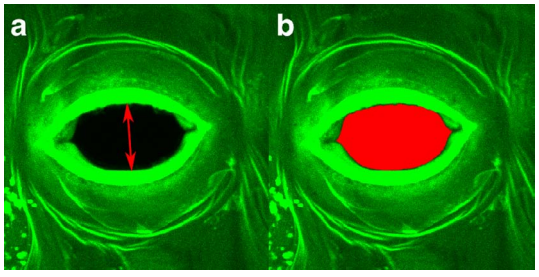

Figure 2.15: Aperture and pore area measurements. Stomatal aperture was determined by measuring the distance between labelled cuticular ledges perpendicular to them (a). Pore area was measured by counting the pixels of the pore (b).

Analysis of 3D image stacks

Since the FM-signal was far too weak to be used for 3D reconstruction directly, all images were pre-processed in the following way: to label the volume of guard cells, a threshold was set for the background at an intensity value of 4. Pixels with a value equivalent to the threshold, which were not located within the guard cell volume were deleted manually (Fig. 2.16).

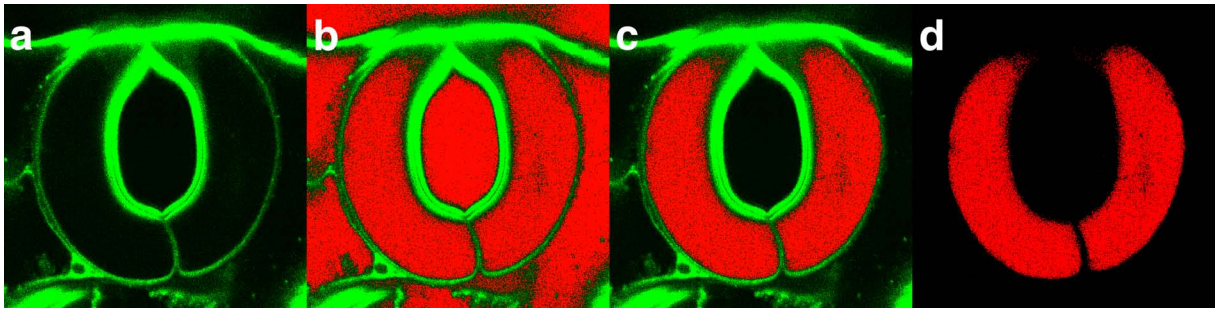

Figure 2.16: Pre-processing of image stacks for 3D analysis. Original data (a), threshold of pixels with intensity values ≤ 4 (b), removal of pixels with a value equivalent to the threshold which were not located within the guard cell volume (c), original data removed (d).

Processed image stacks were further analysed using the software SURPASS which is part of IMARIS® 3.0 (Bitplane AG, Zürich, Switzerland) to reconstruct the isosurfaces and to obtain volume and surface area values.

Before displaying the isosurface SURPASS also processes the data. Two parameters, namely the ”Threshold” and the ”Gaussian filter”, were found to have a strong influence on the calculated volume and surface area values (Fig. 2.17).

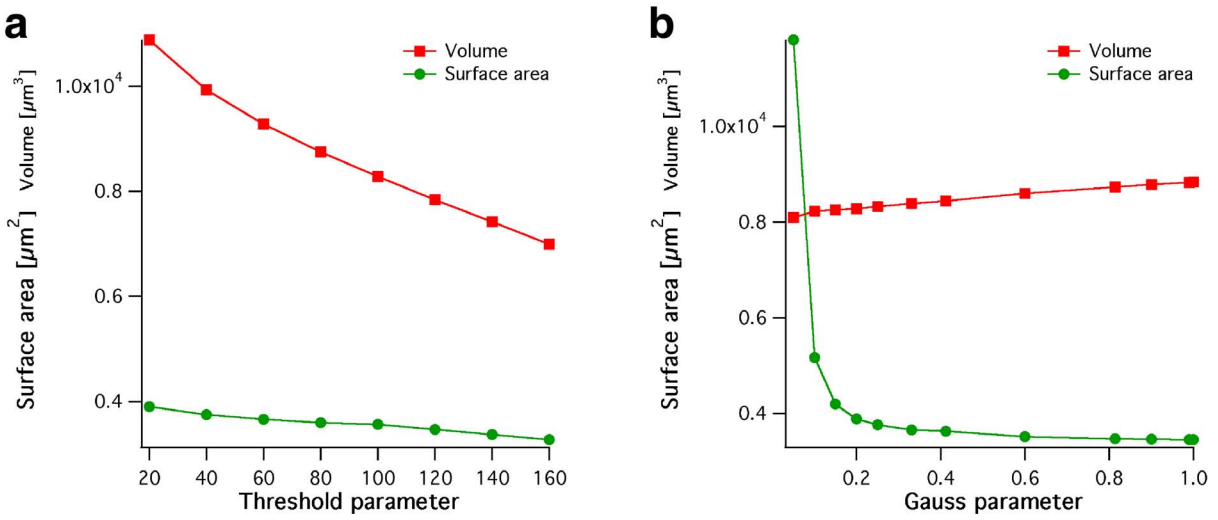

Figure 2.17: Influence of the Surpass Parameters ”Threshold” and ”Gaussian filter” on volume and surface area values. The same guard cell dataset was analysed with different settings for the parameters ”Threshold” (a) and ”Gaussian filter” (b). While the threshold parameter has no substantial influence on the surface area (green curve), the Gaussian filter setting does not change the volume (red curve).

The isosurface encloses all voxels which either have a higher intensity or a higher local density than the specified threshold. By increasing this parameter, progressively decreasing values for surface area and mainly the volume were obtained from a single dataset. (Fig. 2.17a). Consequently, this parameter needs to be adjusted to each dataset individually.
To guide this setting, the threshold parameter was adjusted to yield images with two clearly separated guard cells. The gap between opposing guard cell tips was found to be very constant throughout the datasets (∼600 nm). To further confirm the correct setting, a 2D orthoslice of the original data was displayed to the generated isosurface. Hereby the size of the generated 3D object and the cell in the image stack can be verified (Fig. 2.18).

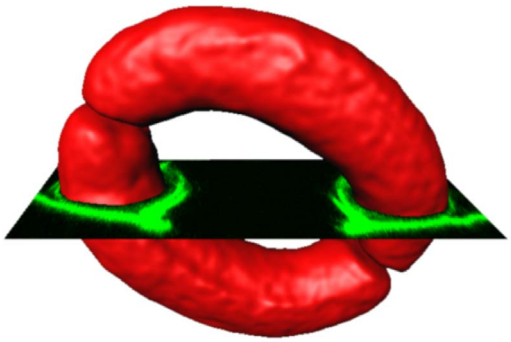

Figure 2.18: Threshold setting. An orthoslice (green) of the original data is used to verify the expansion of the generated isosurface (red) to set the threshold correctly.

Without any further processing, i.e. with the ”Gauss” parameter set to zero, every single threshold voxel now contributes to the isosurface. Since the original dataset is always a cloud of single voxels, this produces an extremely rough surface with a very high value for the surface area (Fig. 2.17b). However, a single voxel is not a single object that was resolved by the imaging system and therefore does not say anything about the true surface. Considering the lateral and axial resolution of the microscope the Gaussian filter was set to 0.5 μm to smooth the dataset before the calculation of the isosurface.

Calibration with beads and protoplasts

To test and calibrate the method for generating 3D reconstructions and the robustness of choosing the required parameters, two geometrically simple structures - large fluorescent beads and guard cell protoplasts - were recorded.

The InSpeck® beads (Molecular Probes, Inc., Eugene, OR, USA) have the same spectral properties as the nanobeads used to record the PSFs but, according to the manufacturer, have diameters of 2.5 μm. This size is far beyond the resolution limit and consequently their intensity profile is not Gaussian distributed (Fig. 2.13). Diameters were therefore estimated as described in Ch. 2.3.2). The mean diameter of three beads measured in the axial and lateral direction was 2.739 μm $\pm$ 0.086 (Tab. 2.5). Thus, the difference to the 2.5 μm specified by the manufacturer is 239 nm, which exactly matches the limit determined for size measurements of diffraction-limited objects directly behind the coverslip (Tab. 2.4).

	bead 1		bead 2		bead 3	
	lateral	axial	lateral	axial	lateral	axial
v-w [μm]	2.775	2.681	2.696	2.589	2.785	2.613

Table 2.5: Diameters of InSpeck®-beads. Results of fits with the Hill function (Eq. 2.5) to lateral and axial intensity profiles of InSpeck®-beads.

Diameters calculated from the values obtained for the surface area and volumes from isosurface reconstructions (Fig. 2.19) are listed in Tab. 2.6.

	bead 1	bead 2	bead 3
volume [μm^3]	11.979	11.695	10.396
surface area [μm^2]	25.338	24.938	23.050
diameter calculated from volume [μm]	2.839	2.816	2.708
diameter calculated from surface area [μm]	2.840	2.817	2.709

Table 2.6: 3D reconstruction of InSpeck®-beads. Volume and surface area values from isosurface generations yielded diameters for the beads.

The mean calculated diameter (2.788 μm $\pm$ 0.063) is overestimated by 1.8% with respect to the diameter determined from the intensity profiles (Tab. 2.5). Since both results were obtained from identical datasets, volume and surface area are also overestimated by 1.8% with this method.

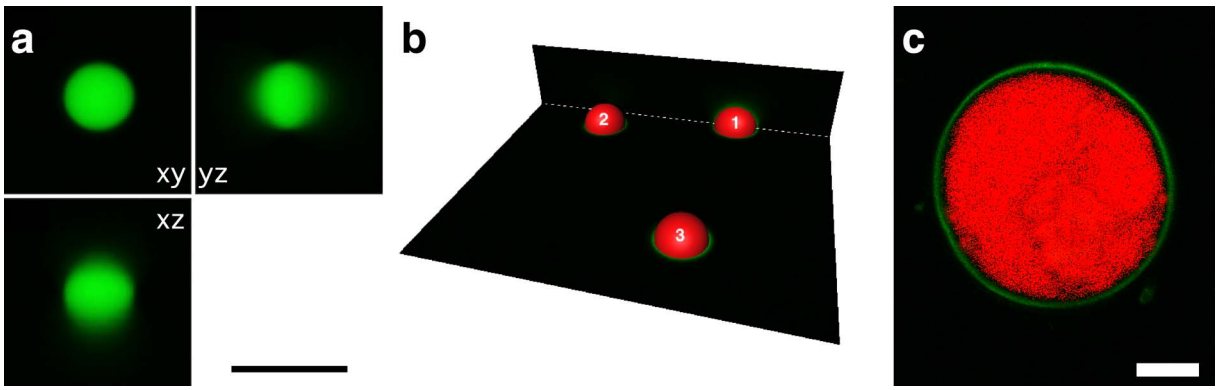

Figure 2.19: Objects for calibration of 3D reconstructions. The method for generating 3D reconstructions was verified on 3D reconstructions of InSpeck®-beads (a, b) and a guard cell protoplast (c). Equatorial slices of an 3D-stack of InSpeck®-beads recorded with the voxel settings of 40.039 x 81.407 nm (a). Orthoslices (green) and isosurfaces (red) of three 3D reconstructed InSpeck® beads (b). FM2-10 labelled guard cell protoplast (c). Red pixels have a value equivalent to the same threshold used in Fig. 2.16. Scale bars = 5 μm.

To evaluate the method on a biological sample, a guard cell protoplast, labelled with the same dye as the intact guard cells, was recorded. The image stack was pre-processed exactly, as were the intact guard cells. The radius determined directly from the raw data is 9.15 μm. The volume and surface area calculated from the isosurface is 3204.9 μm3 and 1061.2 μm2, respectively. These values correspond to spheres with radii of 9.14 and 9.19 μm, respectively. Assuming that 9.15 μm was the true radius of the protoplast, volume and surface area were determined with an accuracy of 0.12 % and 0.86 %, respectively.

Chapter 3

Results

3.1 Membrane uptake

3.1.1 Comparison of staining and toxicity of FM-dyes

Styryl dyes are frequently used for staining the PM and monitoring endocytosis in living cells especially neurons (Betz et al. 1992, 1996). In order to find the appropriate FM-dye for investigating endocytosis in turgid guard cells staining of these cells incubated in FM1-43, FM2-10 and FM4-64 were compared with respect to cytotoxicity.

After 10 minutes of incubation all three dyes were evenly distributed in the PM. Apparently, all dyes needed about the same time to stain the PM, despite their differences in hydrophobicity. However, while it was possible to remove the least hydrophobic dye FM2-10 from the PM and the cuticle by a one-hour washout, this was impossible with the most hydrophobic dye FM4-64 even after washing for more than 6 h. The cuticle remained brightly stained even after removing the dye. Most likely it acted as a dye storage, which also kept the PM stained (data not shown). In continuous presence of dye, staining of cytoplasmic structures was observed also after 10 min for all three styryl dyes (details see below).

While the three dyes exhibited an overall similar staining kinetic, they revealed marked differences in their toxicity. Treatment with FM1-43 for 2 hours resulted in serious damage of more than 50 % of the cells. In damaged cells the cytoplasmic streaming came to a halt. In most of these cells the PM lost its integrity, which was inevitably paralleled by a rapid and intense staining of all intracellular membranous compartments. A visible loss of turgor in many stained cells provided an additional hint for a leaky PM (Fig. 3.1b, right cell). Since FM1-43 was used in a concentration lower than its competitors, it clearly turned out to be the most toxic dye in this study. In contrast, no perceivable damage was visible after treatment with FM2-10 for 2 hours (Fig. 3.1e). Even after 12 hours in FM2-10 and subsequent high exposure to the laser excitation (e.g. during 3D-scans) more than 90 % of the cells were still unaffected in terms of cytoplasmic streaming and cell shape. There was also no sign of unspecific intracellular staining. However,

if the dye was used in a 5-fold higher concentration (100 μM) damage was observed after 6h only. Incubation in FM4-64 gave an intermediate result. The dye caused visible damage in about 20% of the cells after incubation for 2 h and in about 40% after 12 hours. All in all, toxicity was found to be correlated to dye concentration, quantum yield of the dye and duration of incubation.

3.1.2 Intracellular distribution of different styryl dyes

The analysis of cells without any visible damage revealed that the different styryl dyes resulted in labelling of cytoplasmic structures of different size. For analysis the sizes of a large number of fluorescent structures were measured and plotted in a histogram. From each cell, sizes of about 10 structures were analysed in order to give each cell the same statistical weight. The size distribution data were fitted by multiple lognormal distributions (Eq. 3.1), in order to estimate the mean diameters and the relative distributions of the individual structures (Fig. 3.1, Tab. 3.1).

$$y = y_0 + Ae^{-\frac{\left(\ln\frac{x}{x_c}\right)^2}{w^2}} \tag{3.1}$$

FM1-43 In those cases where cells incubated with FM1-43 remained intact, the dye was detected in numerous large cytoplasmic (Fig. 3.1b, left cell) and small cortical (Fig. 3.1c) structures. Because of the toxicity of FM1-43 the number of cells contributing to this size distribution histogram was lower than for the other dyes. Nevertheless, analysis of the size distribution of the stained structures (Fig. 3.1a) revealed three clear peaks. The first peak at $\sim$290 nm corresponds to small cortical and the peaks at $\sim$600 and $\sim$730 nm to large cytoplasmic structures. Close inspection of the distribution also revealed a very small peak at $\sim$470 nm.

FM2-10 As in FM1-43 stained cells, the most prominent cytoplasmic target of FM2-10 were large cytoplasmic structures (Fig. 3.1e) with diameters of $\sim$600 and $\sim$730 nm (Fig. 3.1d). This dye showed the brightest staining of these structures. Close scrutiny of FM2-10 stained cells also shows very small cortical and intermediate structures, which accumulate this dye (Fig. 3.1f, arrowheads and arrows, respectively). The respective histogram (Fig. 3.1d) shows corresponding peaks at $\sim$290 and $\sim$470 nm, respectively. Thus, according to their size, the small structures can clearly be separated into two groups.

FM4-64 Spherical cytoplasmic structures could also be detected after incubation with FM4-64. However, in this case mainly intermediate and small structures are detectable (Fig. 3.1h and k, respectively). The histogram reveals that the structures resemble those of small cortical and intermediate structures stained by FM1-43 and FM2-10 (Fig. 3.1g). The very small cortical structures give a peak at ~310 nm, the intermediate structures at ~470 nm.

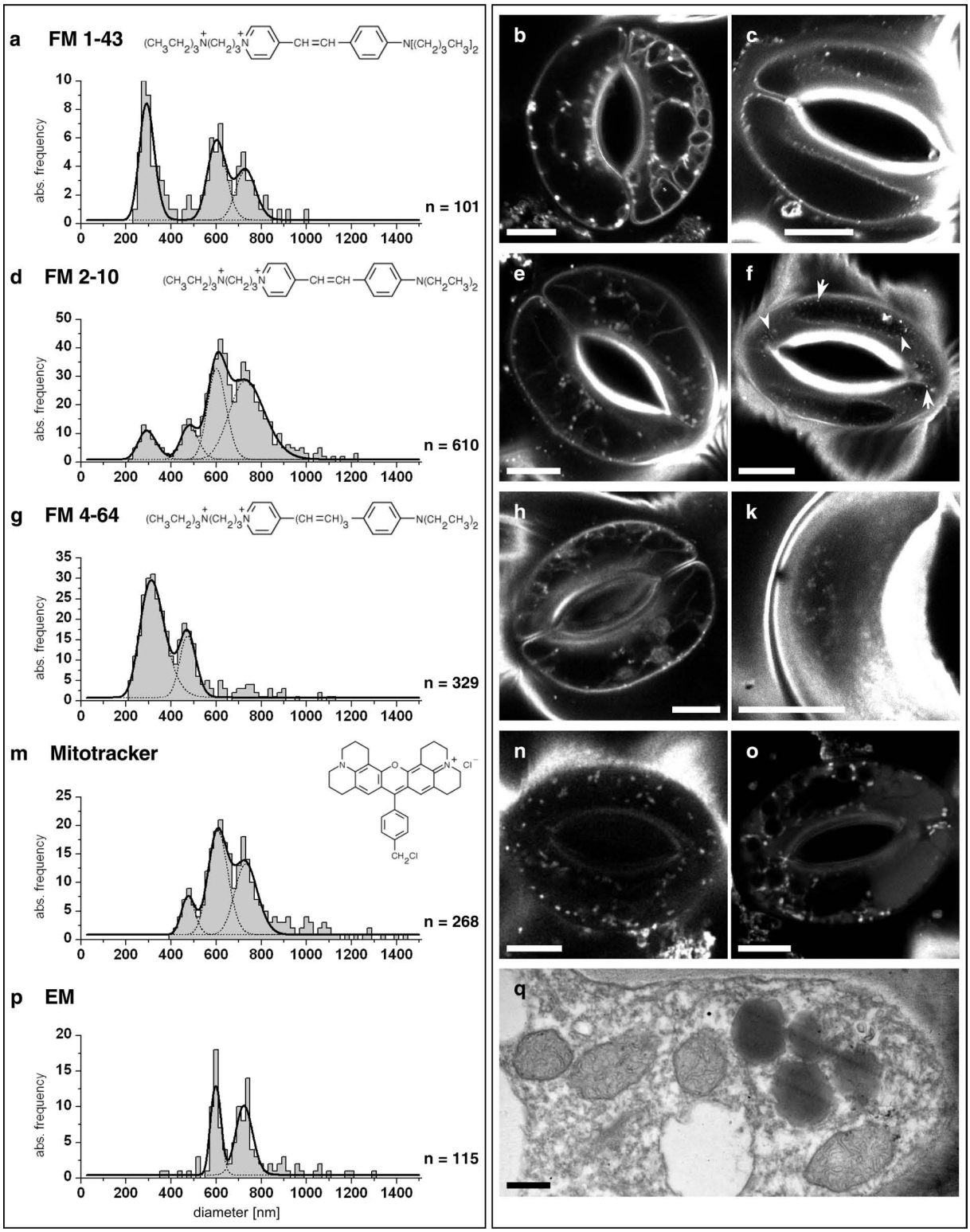

Figure 3.1: Size distributions of fluorescently labelled structures. Size distribution histograms for intracellular structures labelled with FM1-43 (a), FM2-10 (d), FM4-64 (g), MitoTracker Red CMXRos (m) and Mitochondria measured in electron micrographs of guard cells (left column). The histograms were fitted with a multiple lognormal function (solid line). Parameters of these fits are listed in Tab. 3.1. The chemical formula of the respective dye and the number (n) of measured structures is given beneath each histogram. right column: Examples of single optical paradermal confocal sections through the aequatorial (left) or cortical (right) region of guard cells labelled with the respective dyes. In the electron micrograph (q) mitochondria and lipid droplets are visible. Scale bars for confocal images = 10 μm, for the electron micrograph = 500 nm.

	FM1-43	FM2-10	FM4-64	MitoTracker	Mitochondria (EM)
x_c	290.15 ± 2.01	291.29 ± 6.13	311.15 ± 1.91		
w	0.14 ± 0.01	0.18 ± 0.02	0.23 ± 0.01		
A	9.15 ± 0.42	10.82 ± 0.65	29.86 ± 1.78		
		479.58 ± 7.35	472.37 ± 2.48	474.55 ± 4.56	
w		0.10 ± 0.02	0.11 ± 0.01	0.08 ± 0.01	
A		12.82 ± 1.01	16.57 ± 1.43	7.77 ± 0.81	
x_c	601.22 ± 3.98	601.03 ± 4.14		606.01 ± 4.55	597.71 ± 1.14
w	0.09 ± 0.01	0.09 ± 0.01		0.09 ± 0.01	0.04 ± 0.01
a	5.99 ± 0.24	34.10 ± 2.36		19.48 ± 1.36	17.53 ± 1.21
x_c	729.56 ± 5.47	731.81 ± 9.38		730.57 ± 7.04	722.36 ± 2.65
w	0.08 ± 0.01	0.14 ± 0.01		0.09 ± 0.01	0.07 ± 0.01
A	3.72 ± 0.19	27.97 ± 1.67		12.96 ± 0.73	10.58 ± 0.39

Table 3.1: Parameter values of size distribution fits from Fig.3.1. Each size distribution histogram illustrated in Fig. 3.1 was fitted with a multiple lognormal function, yielding these fit parameters. The center (x_c [nm]), width (w [nm]) and amplitude (A [abs. frequency.]) for each peak are given.

After incubation for 4 h in FM4-64 it was also possible to detect labelling of the tonoplast. This was not the case with the two other dyes. Fig. 3.2a shows one optical slice of a FM4-64 stained cell with labelled PM and tonoplast. In three successive optical slices of a different cell the small FM labelled structures can clearly be located in the cytosol i.e. between the brightly stained PM and the less bright tonoplast (Fig. 3.2b-d). In a brightest-point-projection it can further be seen that many structures are distant from the PM in a cytoplasmic strand (Fig. 3.2e) which were found to have an average size of 465 nm ± 27 (n=5). In FM4-64 stained cells only very few large structures were observed after prolonged incubation. In addition, some structures in a very broad size distribution ranging from 600 to 1100 nm (Fig. 3.1g), were observed.

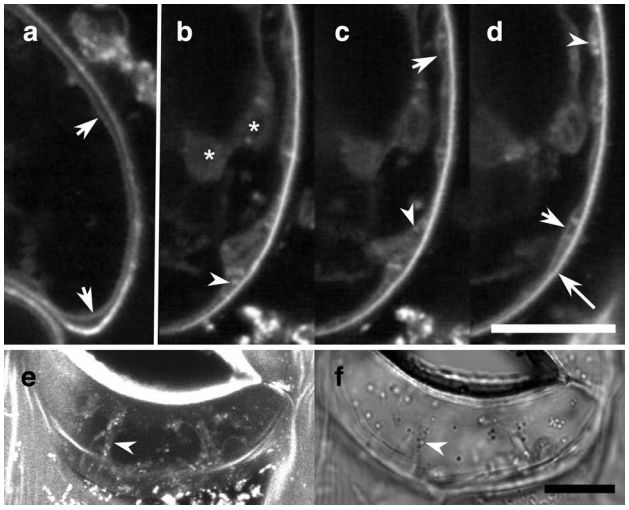

Figure 3.2: Staining of the tonoplast by FM4-64. Paradermal confocal sections of one guard cell (a) and three consecutive sections of a different cell (b-d) labelled with FM4-64 for 4 h (a-d). The brightly stained PM (d, long arrow), vesicles (arrowheads) and the less brightly labelled tonoplast (short arrows) are displayed. Due to the chlorophyll fluorescence in the detection band of FM4-64 chloroplasts (asterisks) are also visible. A cytoplasmic strand (arrowhead) filled with intermediate sized structures can be seen in the fluorescent (e) and transparent (f) channels of a brightest-point-projection of 15 consecutive paradermal sections. The structures have a mean diameter of 465 nm ± 27 (n=5). Scale bars = 10 μm.

3.1.3 Identification of the stained cytoplasmic structures

Lipid droplets

Guard cells contain numerous lipid droplets, which could principally serve as targets for the styryl dyes, because of their hydrophobic nature and size (Willmer and Fricker 1996). These structures can be distinguished from other organelles by their contrast in DIC microscopy (Fig 3.3b, arrows). Inspection of FM2-10 stained guard cells showed that these lipid droplets were never fluorescent (Fig. 3.3a and c). They can therefore be excluded as targets of the styryl dyes.

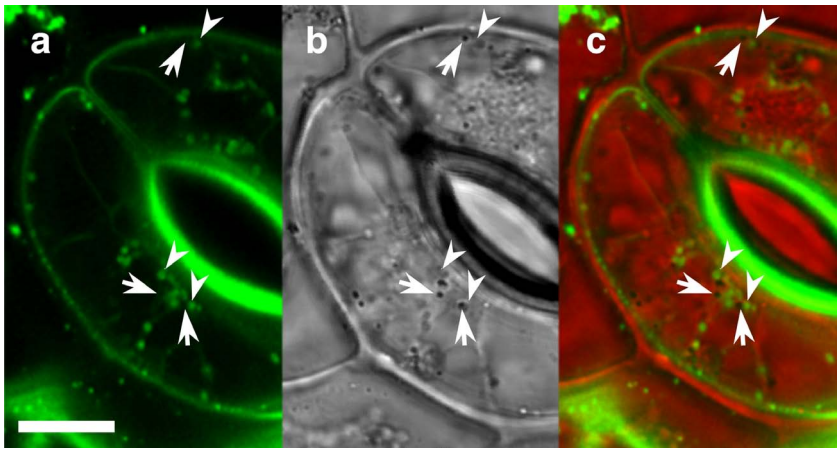

Figure 3.3: Lipid droplets are not labelled by FM2-10. Numerous structures, which are labelled by FM2-10 (a, arrowheads) after 2 h do not colocalise with Lipid droplets (b, arrows), which can be identified in DIC images by their contrast. In the merged image (c), a red color table was applied to the DIC image (b) for better contrast. Scale bar = 10 μm.

Mitochondria

FM-dyes have been developed from the related probe dimethyl-aminostyryl-methylpyridinium-iodine (DASPMI), a membrane-potential probe used to study mitochondria (Bereiter-Hahn 1976; Betz et al. 1992). To examine the possibility that the large FM-labelled structures in the guard cell cytoplasm are mitochondria cells were exposed to FM2-10 or FM1-43 and MitoTracker Red CMXRos. Overlays of both detection channels show that the MitoTracker colocalises with FM2-10 and FM1-43 (Fig. 3.4). In contrast to FM-dyes the MitoTracker neither labels the PM nor the small cortical structures of ∼300 nm (Fig. 3.1n, o, 3.4c, d). Note, however, that the MitoTracker accumulates in the lumen of the vacuolar compartment (Fig. 3.4, asterisks) whereas the tonoplast was never found to be stained by FM2-10 or FM1-43.

The size distribution histogram of structures stained with the MitoTracker is very similar to that of cells treated with FM1-43 and FM2-10, except that it lacks the peak at ∼300 nm (Fig. 3.1m). In addition to the most prominent peaks at ∼600 and ∼730 nm a minor peak at ∼470 nm is also present. Only few structures have sizes between 800 and 1200 nm and more. However, the size distribution for mitochondria obtained from electron micrographs in turn lacks the peak at ∼470 nm (Fig. 3.1p). Hence, only the peaks at ∼600 and ∼730 are caused by mitochondria. Since these organelles have an elongated shape, the applied measurement method reports two diameters (Eq. 2.2).

The colocalisation of the MitoTracker and FM2-10 and striking similarities of the size distributions for both markers strongly suggest that the large cytoplasmic structures stained with the styryl dyes FM2-10 and FM1-43 are mitochondria. On the other hand the intermediate structures with a diameter of ∼470 nm are obviously not mitochondria; the ability of the MitoTracker to stain them may point to a (pre)vacuolar nature of these compartments.

The ability of the cell-permeant MitoTracker to accumulate in active mitochondria after passively diffusing across the PM depends on the charging of the mitochondrial membranes (Haugland 2002). To examine whether labelling of mitochondria by FM-dyes occurs via the same pathway, the staining pattern in cells was monitored where the mitochondrial membrane potential had been depolarised by treatment with sodium azide. The results reported in Fig. 3.4g and h show that neither the MitoTracker nor FM2-10 reveal under this condition any appreciable staining of cytoplasmic structures. This implies that staining of the mitochondria by FM-dyes also depends on the mitochondrial membrane potential and is not associated with endocytic processes.

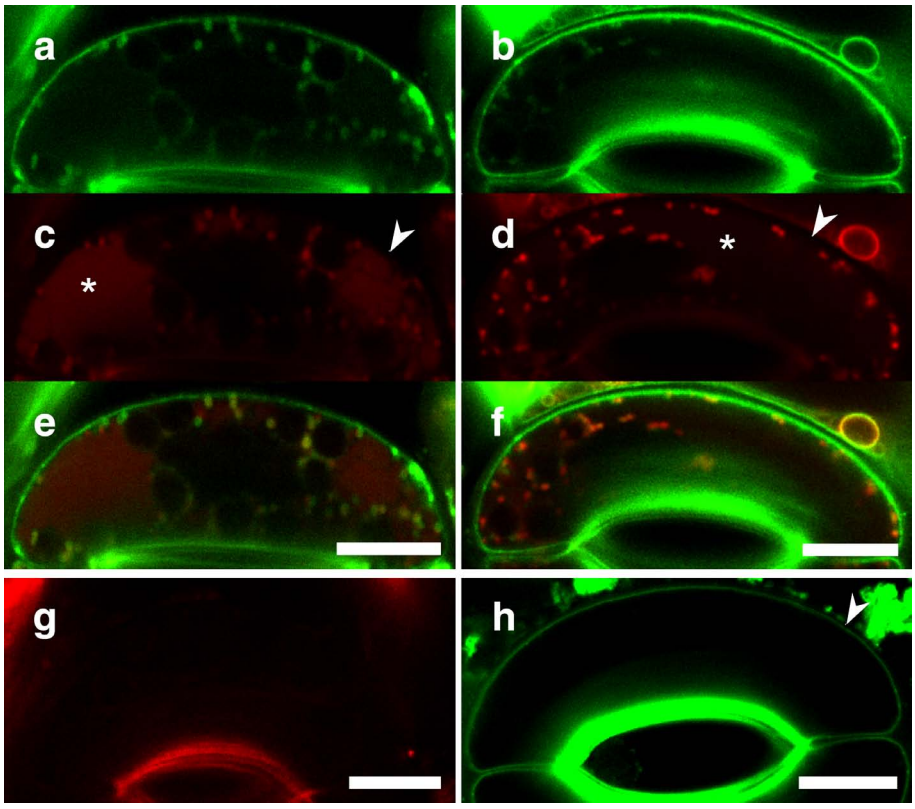

Figure 3.4: Colocalisation of the MitoTracker with FM2-10 and FM1-43 and the dependency of staining on membrane potential. Double labelling of guard cells with FM1-43 (a) or FM2-10 (b) and MitoTracker (c,d) reveal a clear colocalisation of each styryl dyes with the MitoTracker in the same cytoplasmic structures (e,f) but not in the PM, which is not stained by the MitoTracker (arrowheads). Note, that after more than 3 h of incubation, the MitoTracker also accumulates in the lumen of vacuolar compartments (asterisks). In intact guard cells pre-treated with 10 mM sodium azide for 10 min, neither the MitoTracker (g) nor FM2-10 (h) stains these structures. FM2-10 still brightly labels the PM (h, arrowhead). Scale bars = 10 μm.

Endocytic vesicles

The examination of staining with different FM-dyes implies that only the small structures of ~290/310 nm can be considered as a (primary) result of endocytosis. To further examine the possibility that these structures are indeed of endocytic origin a GFP chimera of the plant potassium inward rectifier (KAT1) was expressed in guard cells. Complementary electrophysiology studies on guard cell protoplasts demonstrate that this channel is inserted into the PM via exo- and retrieved by endocytosis during pressure-driven volume changes (Hurst et al. 2004).

Fig. 3.5a shows a typical image of a KAT1::GFP expressing guard cell (see also Ch. 3.3.1). Abundant green fluorescence can be detected at the cell periphery suggesting its PM localisation. This localisation is confirmed by a labelling of the PM of the same cell with FM4-64 dye (Fig. 3.5b), which colocalises with the GFP fluorescence (Fig. 3.5c). GFP labelling can also be detected in the form of small spherical structures inside the cytoplasm (Fig. 3.5d, arrowhead). An overlay of the images reveals for many of these structures a clear colocalisation of the GFP and FM4-64 signals (Fig. 3.5c and f, arrowheads). The obvious interpretation is that those structures, which carry both labels, are endocytic vesicles, which retrieve KAT1-channels from the PM.

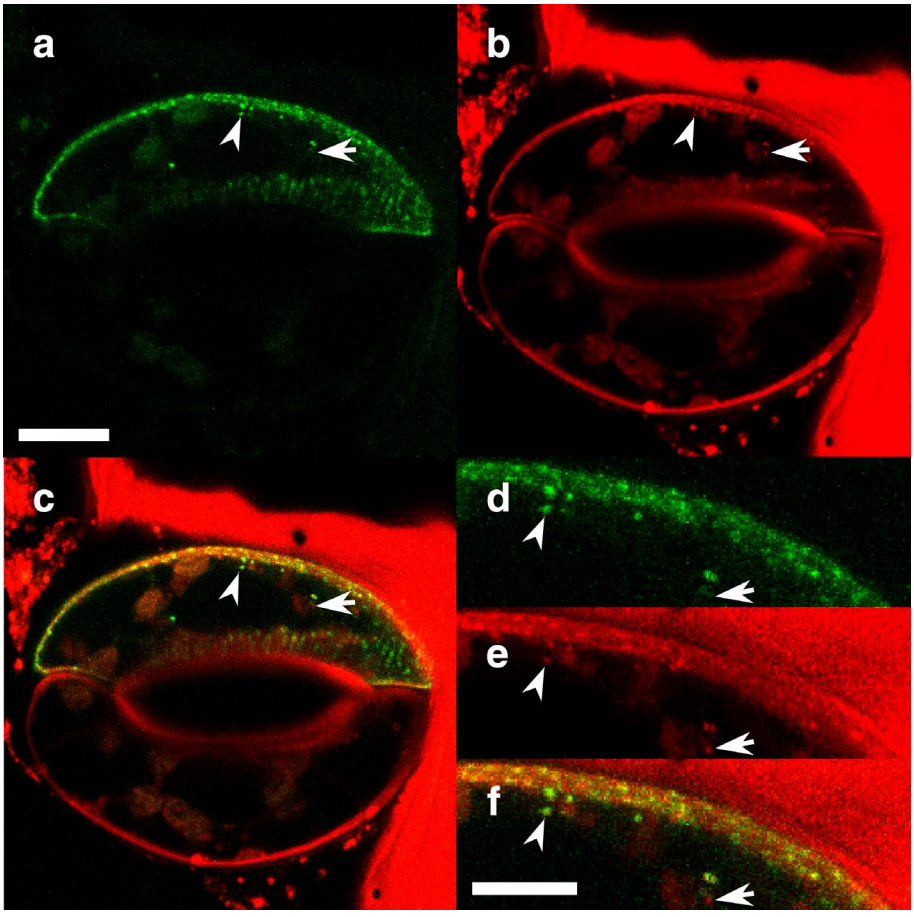

Figure 3.5: Colocalisation of FM4-64 and KAT1::GFP endocytic vesicles. A brightest-point-projection of seven consecutive sections of a guard cell expressing KAT1::GFP (a), additionally labelled with FM4-64 (b) reveals a colocalisation of both fluorescent signals in small cortical structures (arrowheads). Scale bar = 10 μm. The corresponding magnifications (d,e,f) show that these structures are distinct from the PM. Not all endocytosed vesicles carry GFP tagged KAT1 molecules (arrows). Scale bar = 5 μm.

A single cortical paradermal confocal section of a guard cell treated in the same way shows numerous structures of diffraction-limited sizes. While some structures are again labelled with both markers (Fig. 3.6, arrows), many structures carry only one of the markers (Fig. 3.6, arrowheads). Structures solely labelled by FM4-64 (Fig. 3.6, filled arrowheads) most likely represent endocytic vesicles, which do not carry a GFP labelled potassium channel. Structures labelled by the chimeric protein only (Fig. 3.6, outlined arrowhead) are most likely of exocytic origin and have yet to reach the PM.

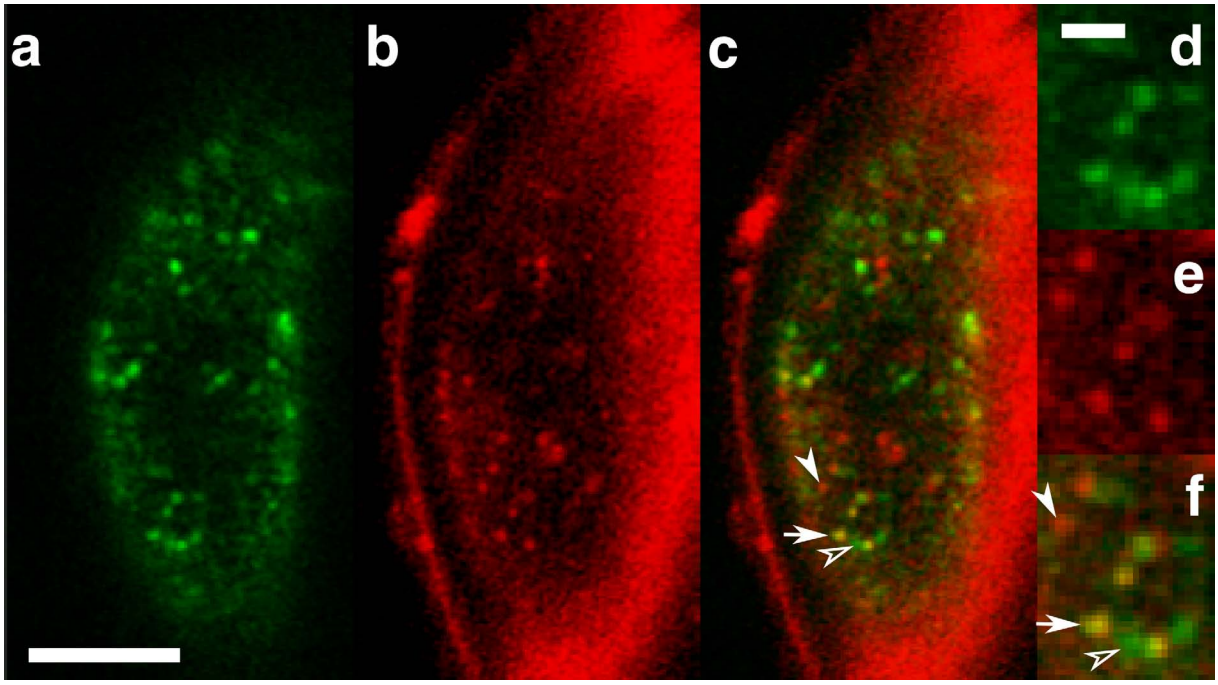

Figure 3.6: Endo- and exocytic vesicles. Cortical section of a guard cell expressing KAT1::GFP (a), additionally labelled with FM4-64 (b) reveal a colocalisation of both fluorescent signals only in some of the small cortical structures (c, arrows). Numerous structures are labelled only by KAT1::GFP (outlined arrowheads) or FM4-64 (filled arrowheads). Scale bar = 5 μm. Corresponding magnifications (d,e,f). Scale bar = 1 μm.

Previous electrophysiological measurements revealed that exo- and endocytosis of small vesicles accommodates for osmotically driven changes in surface area in guard cell protoplasts (Homann and Thiel 1999). It was therefore examined whether the small fluorescent structures labelled with FM4-64 and/or with KAT1::GFP have any relation to the sizes of single vesicles determined by the electrophysiological assay.

Fig. 3.7 illustrates a histogram for the size distributions of vesicles obtained from the fluorescent images and from the high resolution capacitance recordings. The data show that GFP and FM4-64 labelled structures as well as those from the electrophysiological assay have a very similar distribution. This is underlined by the values obtained from fitting the size distributions with the lognormal distribution (Tab. 3.2). The similarity of the size distributions is true not only for the peaks (x_c) but also for parameters defining the shape of the fitting functions (*A*, *w*).

The small difference between the peaks of GFP and FM4-64 labelled vesicles can be explained by the longer emission wavelength of FM4-64 (λ_{em} = 650 nm) with respect to GFP (λ_{em} = 510 nm).

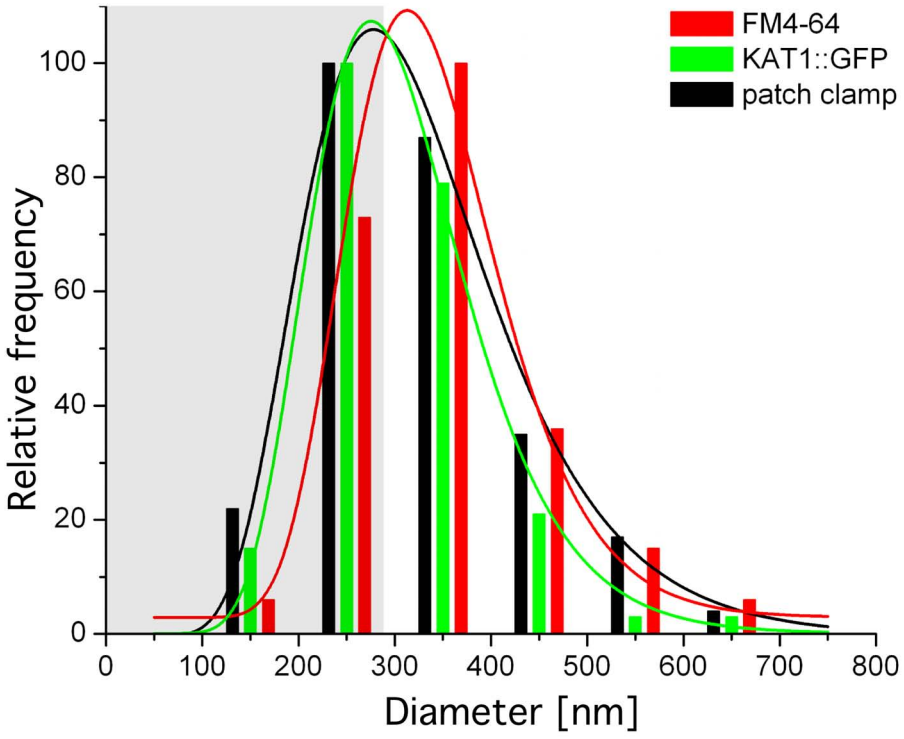

Figure 3.7: Size distribution histogram of vesicles measured with CLSM or the patch clamp technique. The size distribution histogram of structures labelled with KAT1::GFP, FM4-64 or endocytic steps recorded with the patch clamp technique (data from Fig 4a in: Homann and Thiel 1999) reveals a high similarity of the three different size measurements. The parameters of the lognormal fits are listed in Tab. 3.2.The grey box denotes the value range at which both methods are below resolution.

FM4-64	FM4-64	KAT1::GFP	patch clamp
x_c	312.79 ± 2.97	275.23 ± 4.01	277.59 ± 3.26
w	0.34 ± 0.02	0.41 ± 0.02	0.48 ± 0.02
A	106.80 ± 4.32	107.68 ± 3.79	106.48 ± 3.09

Table 3.2: Parameter values of size distribution fits from Fig. 3.7. Parameters of the lognormal functions, fitted to the size distribution histograms illustrated in Fig. 3.7. The center (x_c [nm]), width (w [nm]) and amplitude (A [abs. frequency.]) for each peak are given.

Both recording methods have their resolution limit at vesicle diameters of 250 nm or below (Fig. 3.7, grey box). In this value range, diffraction limits the microscopy technique. In contrast patch-clamp capacitance recordings are principally capable to achieve a much higher resolution (Thiel et al. 1998), but not in the special case of whole cell measurements on guard cell protoplasts. Nevertheless, even if the interpretation of the size distribution histogram is limited to the range beyond 250 nm, the high similarity among the size distribution of vesicles exceeding this limiting parameter is apparent. It indicates that with both methods the same type of endocytic vesicles were recorded.

3.1.4 Osmocytic vesicles

For microscopic investigations of stomatal movement guard cells are frequently closed by hyperosmotic treatment (Diekmann et al. 1993, Shope et al. 2003). In principle this treatment reflects the *in vivo* situation, in which K^+ serves as an osmoticum. However, osmotic changes in an experiment are usually applied in one or few steps, which does not reflect the *in vivo* situation. To examine this closing method the effect of such rapid osmotic changes on FM-dye uptake was investigated. First, the osmotic pressure of the bathing solution was evaluated which induced incipient plasmolysis, since plasmolysis was considered a rather artificial situation for guard cells. An osmolarity of 580 mosmol/kg was found to cause plasmolysis in less then 10% of the cells.

Guard cells were then pre-incubated with 10 μM FM4-64 for 10 min before the hyperosmotic treatment was administered in continuous presence of the dye. In Fig. 3.8 the broad range of observed structures after 20 min of hyperosmotic treatment is depicted in three examples. Some cells internalize the dye in large structures (> 1 μm, Fig. 3.8a), while most of the cells show a massive vesiculation (Fig. 3.8b) and even tubulation (Fig. 3.8c, arrowhead) of the PM.

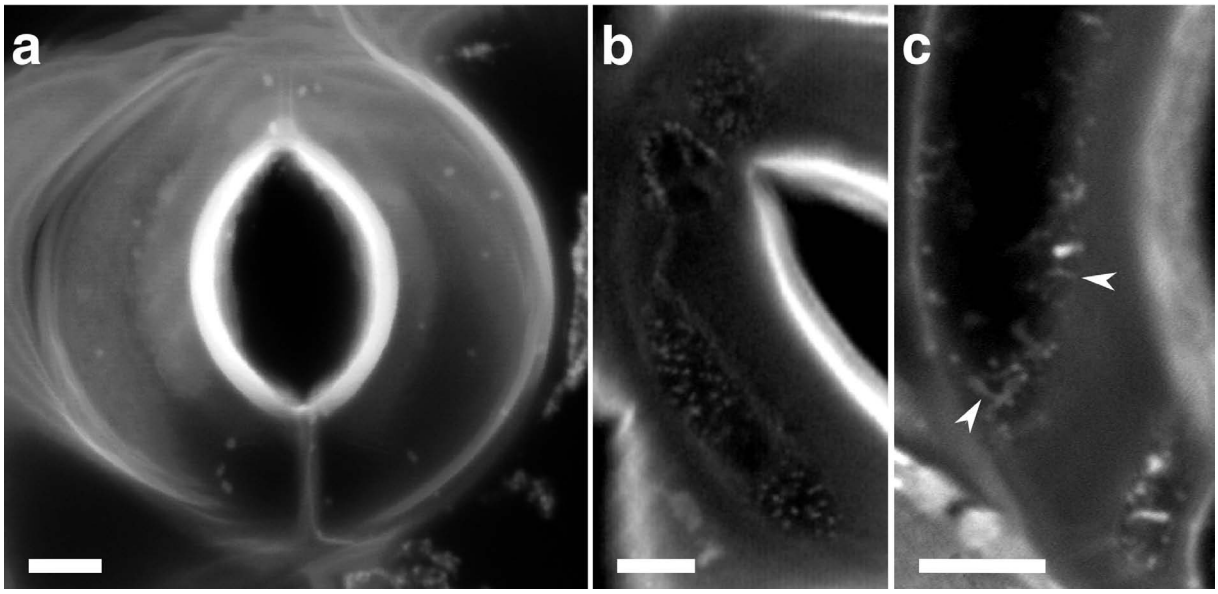

Figure 3.8: Osmocytic structures - uptake of FM4-64 after hyperosmotic treatment. Guard cells take up FM 4-64 into structures of broad size distribution if treated with hyperosmotic solutions. The sizes range from 1 μm (a) down to diffraction-limited (b). In most cases an increased uptake of punctuate and even filamentous (c, arrowheads) structures is observed. Scale bars = 5 μm

3.2 Fluid phase uptake

3.2.1 Theoretical considerations

Besides membrane proteins (KAT1::GFP) and membrane-affine FM-dyes a third marker was used to evaluate, whether intact guard cells perform endocytosis.

It is reasonable to assume that any endocytic process inevitably incorporates external fluid. Endocytosis should therefore be traceable by labelling the fluid phase surrounding the cells with a hydrophilic fluorescent dye. The uptake of such a fluid phase marker should label single endocytic vesicles or at least accumulate label in the target compartments to which they fuse.

This straightforward assumption however was not complied by former investigations. Using Lucifer Yellow as a marker, fluid phase uptake has so far only been shown in turgorless plant cell protoplasts (Wartenberg et al. 1992, Diekmann et al. 1993) or plant cells with a low turgor pressure (Oparka et al. 1991). However, in intact turgid guard cells - in contrast to the protoplasts of the same cell type - it was not possible to demonstrate uptake of the fluid phase (Diekmann et al. 1993). Diekmann and co-workers therefore suggested that vesicles sizes in intact guard cells were to small for detection with their setup. Hence, it remains to be shown, whether fluid phase uptake has so far only failed to be recorded or whether it does not occur in intact guard cells at all.

In the present study this problem was addressed by estimating the expected signal and adjusting it to the demands of the recording setup.

As noted in Ch. 2.3.3 a minimal number of fluorescent molecules are necessary in the focal spot of the confocal setup, in order to produce a recordable signal. To minimize this number the much brighter fluid phase marker Alexa 488 hydrazide was used instead of Lucifer Yellow (Haugland 2002). Especially when the 488 nm Ar-laser line is used for excitation, Alexa 488 hydrazide is superior to Lucifer Yellow having an extinction coefficient 100-times higher ($\varepsilon_{488\text{nm}}$= 71,000 cm^{-1} M^{-1}) than Lucifer Yellow. Around 200 molecules of this dye were estimated to be sufficient for detection with the setup used.

Next, the concentration of the applied Alexa 488 solution was adjusted to the expected vesicle size of 70 to 90 nm (Holstein 2002). Granted that the PM of vesicles has a thickness of 7 nm, a solution of 1.5 mM Alexa 488 is necessary to fill a vesicle with an outer diameter of 90 nm with 200 molecules. Thus the guard cells were incubated in solutions which had at least an Alexa 488 concentration of 1.5 mM.

To avoid any inconsistency with respect to the homogeneity and concentration of the dye solution, ready to use Alexa 488 hydrazide ”for microinjection” was purchased in a concentration of 10 mM dye solved in 200 mM KCl. The dye was further diluted in *standard* buffer.

3.2.2 Uptake of Alexa 488 hydrazide

After an incubation of 2 h in 1.5 mM Alexa 488, no uptake of the dye was found in cells with an apparently intact PM. Only some cells, which became leaky to the dye, were labelled heavily (Fig. 3.9a). In this case a leaky PM caused the infiltration of the dye, which is supported by the observation that these cells apparently lost turgor. This is indicated by the half aperture they contribute to the pore width and by their concave shaped tips. For cells which kept an intact PM, the long incubation provided evidence that the PM is impermeable for the dye and no autofluorescence signal emerged during incubation (Ch. 2.3.1).

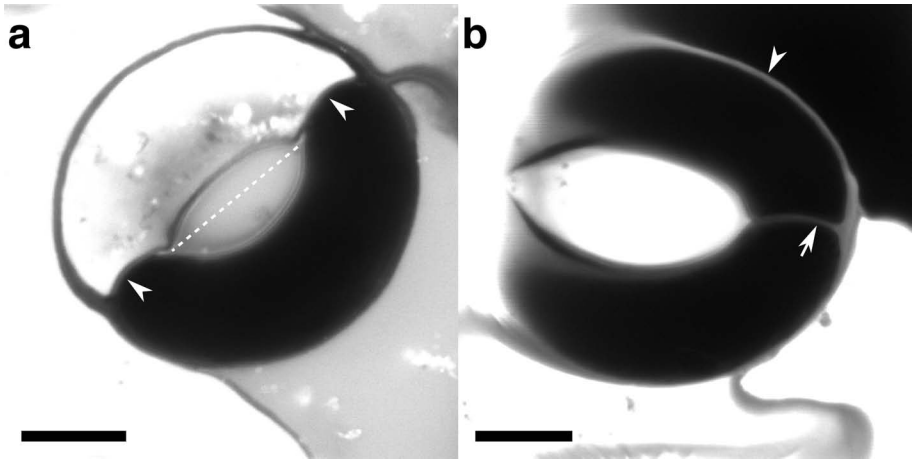

Figure 3.9: Membranes are impermeable for Alexa 488 hydrazides. The dye does not enter intact cells (a, right cell) but heavily labels cells, which became leaky.The half aperture (indicated by the dashed line) this cell contributes to the pore width and the concave shape of the tips (arrowheads) are additional signs for a turgorless, leaky cell (a, left cell). Alexa 488 brightly stains the fluid phase inside the cell walls between adjacent guard cells (b, arrow) and between guard cells and epidermal cells (b, arrowhead). Scale bars = 10 μm

After 2.5 h of continuous incubation still no discrete structures were observed (Fig. 3.10a). However, after 3 h suddenly all investigated cells had taken up Alexa 488 hydrazide (Fig. 3.10b). The stained structures - like those labelled with FM4-64 - were found in the cortical cytoplasm and had diffraction-limited diameters.

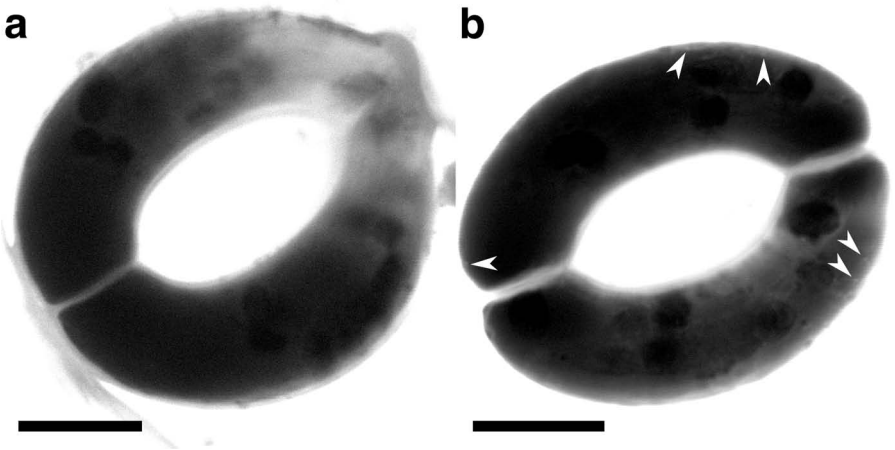

Figure 3.10: Instantaneous appearance of Alexa 488 labelled structures. After 2.5 h no uptake of Alexa 488 into discrete structures occurred (a). However, after an incubation of 3 h, labelled structures of diffraction limited size appeared in the cortical cytoplasm (b). Scale bars = 10 μm

Time series additionally reveal that the structures are mobile (Fig. 3.11). Thus, Alexa 488 apparently had been taken up by single vesicles after an incubation of 3 h.

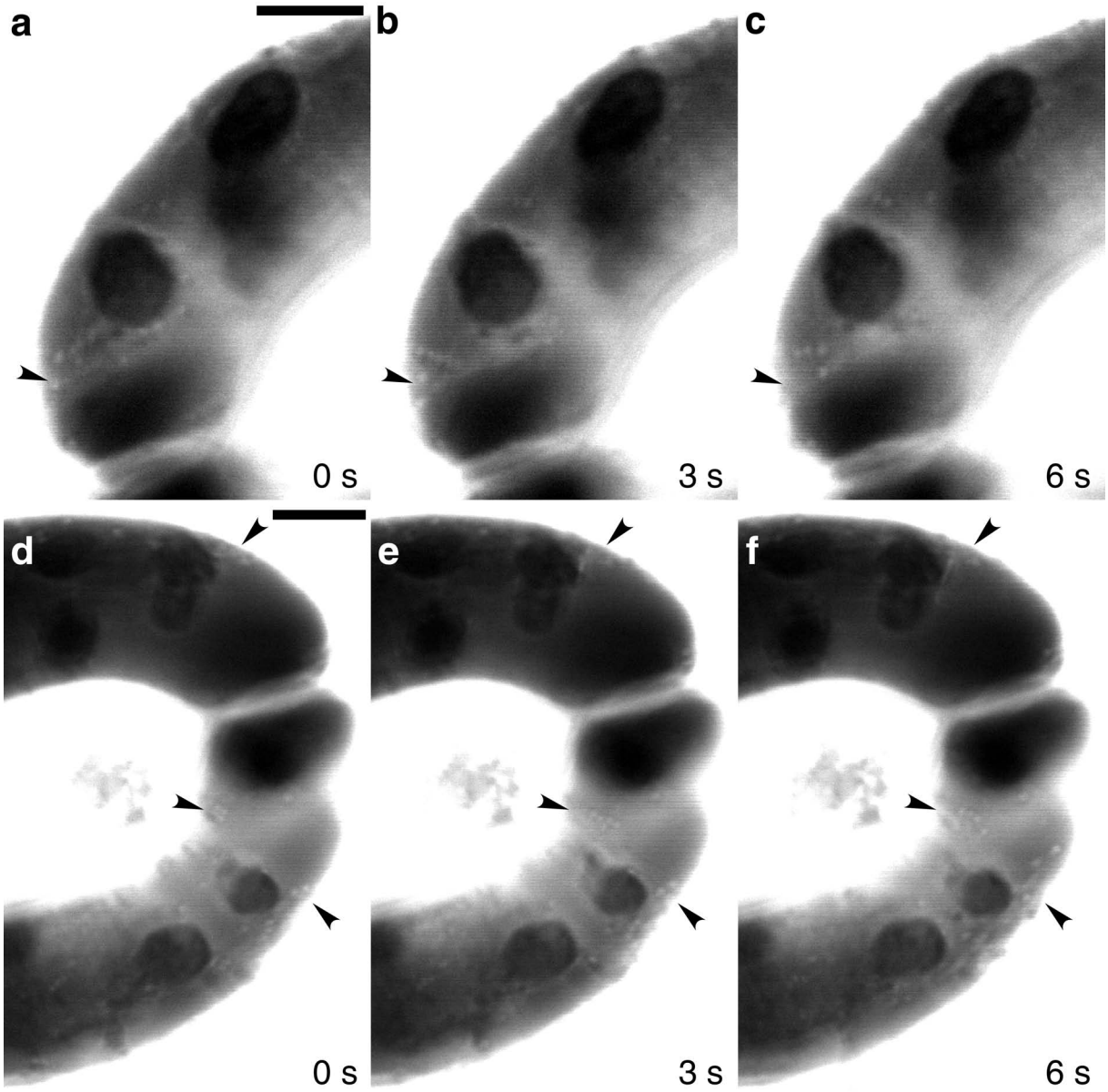

Figure 3.11: Time series of Alexa stained vesicles. Alexa 488 stained vesicles move between consecutive images, which have been recorded every 3 s with a capture speed of $\sim$1 frame/s. Arrowheads were placed at the same position in each slice of a time series to visualize the movement of the labelled structures (a-c and d-e). Scale bars = 5 μm.

An explanation for this delayed but instantaneous appearance is illustrated in Fig. 3.12. After 3 h of confocal investigation only one third of the initial buffer volume remained in the incubation chamber, while the rest had evaporated. The initial 1.5 mM Alexa solution therefore had been concentrated by a factor of 3, yielding a 4.5 mM solution. This concentration is sufficient to fill endocytic vesicles with 200 to 400 molecules, which have outer diameters between 66 to 80 nm, respectively.

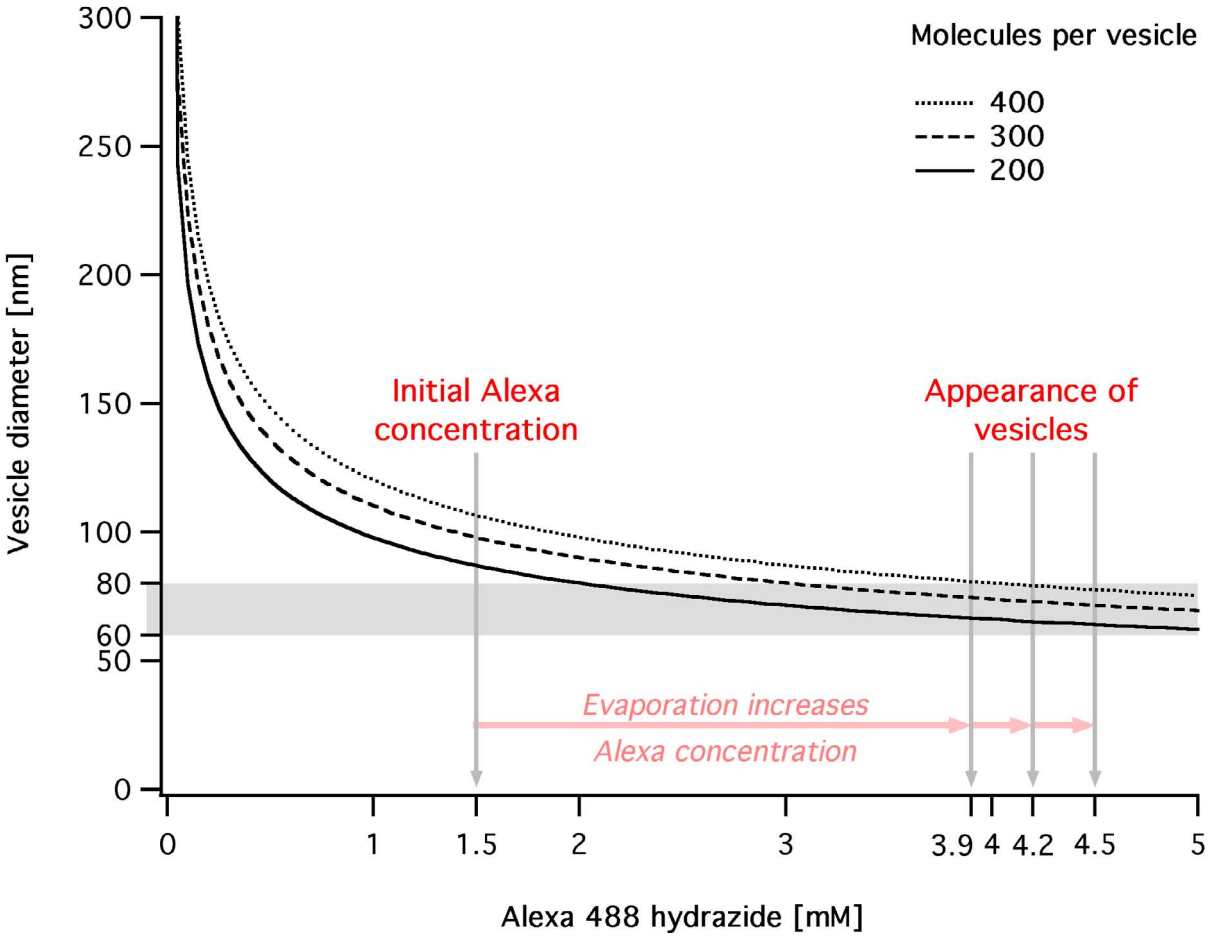

Figure 3.12: Fluid phase uptake in presence of concentrating Alexa 488 hydrazide. The outer vesicle diameter is plotted as a function of Alexa 488 concentration for the condition that a vesicle contains 200 (straight), 300 (dashed) or 400 dye molecules (dotted graph). At the beginning of the experiment, the dye concentration (1.5 mM) was not sufficient to fill vesicles with a size range of 60 to 80 nm (grey box) with 200 to 400 molecules. Only when the concentration increased to 4.5 mM the amount of dye required for detection was taken up by endocytic vesicles and they appeared as fluorescent objects of diffraction-limited size.

Thus, endocytic vesicles are at least smaller than 90 nm. Whether 200 molecules were sufficient for detection under these conditions or whether even twice the number was necessary, does not change this size prediction.

The same experiment was repeated two times. When the fluorescent structures appeared, the fluorescence intensity of the remaining bath solution was quantified in a fluorimeter. A comparison of the obtained values with the calibration curve (Fig. 2.14) then yielded the Alexa 488 concentration of the solution. The values (3.9 and 4.2 mM) correspond to vesicles with outer diameters of 69 to 83 and 67 to 81 nm, respectively, if they are considered to contain 200 to 400 molecules (Fig. 3.12).

When cells were incubated directly with 2.5 mM Alexa 488 no uptake was observed after 30 minutes, while a concentration of 5 mM led to vesicular detection after 15 min only.

An additional observation worth noting is that in about 20% of the cells, Alexa uptake was found mainly at the tips of the guard cells (Fig. 3.13).

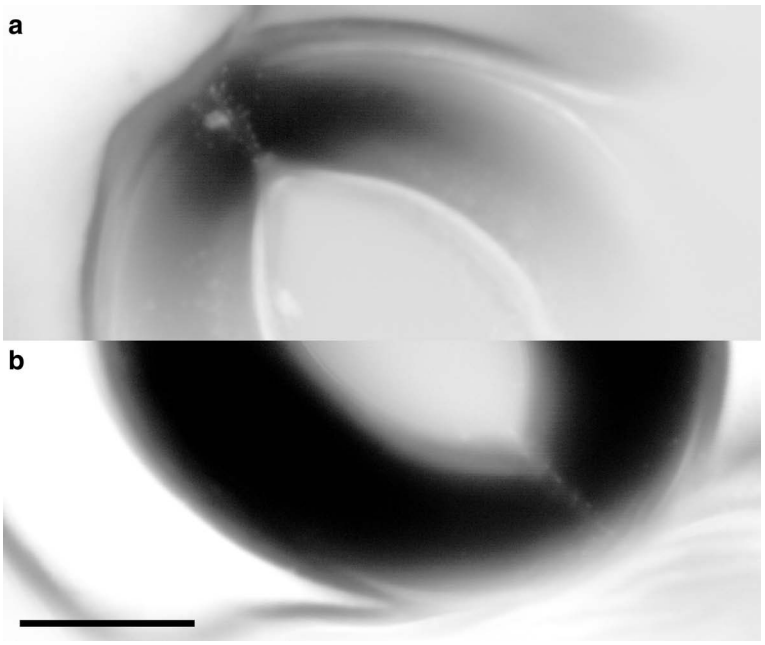

Figure 3.13: High vesicle turnover at the tips of guard cells. Separate sum-projections of consecutive slices of both tip regions (a and b) of the same stoma shows a significant higher abundance of stained vesicles compared to other areas of the cell. The different brightness of the images is a result of the different paradermal positions of the sections, which contribute to the projections. In (a) more cortical slices contribute to the projection, which results in a brighter projection. Scale bar = 10 μm

3.3 Membrane protein trafficking

Expression and endocytic retrieval from the PM of the chimeric protein KAT1::GFP has already been shown (Ch. 3.1.3). Here the overall cellular localisation of the protein is investigated and compared with other fluorescent chimeric proteins. This gives insight into the localisation and trafficking properties especially related to the potassium channel.

3.3.1 KAT1::GFP

Transiently expressed KAT1::GFP is mainly targeted to the PM in guard and epidermal cells (Fig. 3.14a, long arrow). Here it is organized in a radial symmetric pattern, which is composed of small punctuate structures (Fig. 3.14a and b, arrowheads) and stripes with a continuous fluorescent signal (arrows). This pattern is not found in epidermal cells or guard cell protoplasts (Fig. 3.14c and f, respectively). The radial symmetry mirrors the pattern found for both cortical cytoskeletons in guard cells, the actin (Hwang and Lee 2001) and microtubule cytoskeleton (Assmann and Baskin 1998).

In about 20 % of the investigated guard cells KAT1::GFP does not localize to the PM at all - or at least to an undetectable amount. In these cells, the chimeric protein is found in plate shaped structures, which concentrate at the nuclear envelope (Fig. 3.14d and f, arrowheads) and in the cortical cytoplasm (arrows). Structures of similar appearance and intracellular distribution have also been reported in guard cells of *N. tabaccum.* These structures, termed fusiform bodies, were found to reside in the lumen of the endoplasmatic reticulum (ER) and have been suggested to trap GFP-fusion proteins which follow the secretory pathway (Hawes et al. 2001).

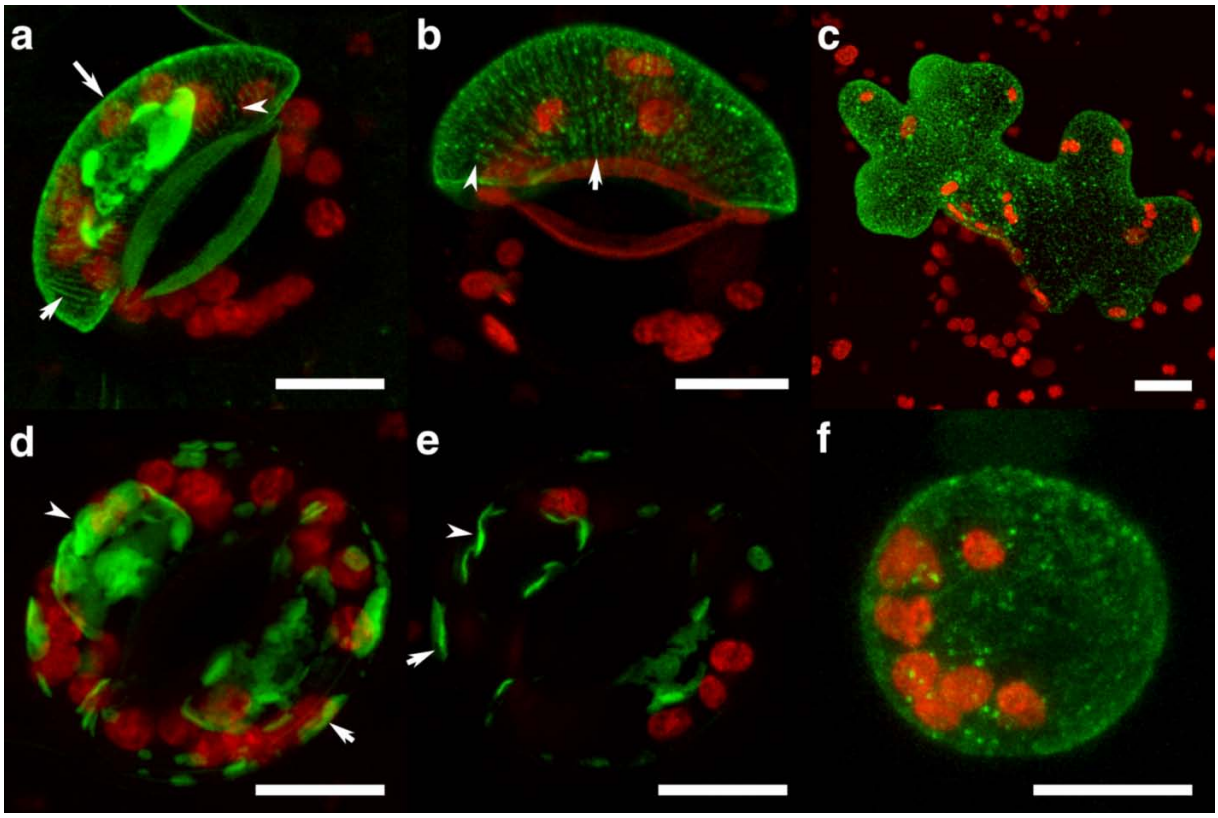

Figure 3.14: Transient expression of KAT1::GFP. KAT1::GFP transiently expressed in guard cells mainly localizes to the PM (a, long arrow). In the PM it is organized as a radial symmetric pattern, which resembles that of the cortical cytoskeleton in guard cells. The pattern consists of small punctuate structures (arrowheads) as well as of continuous stripes (arrows). This pattern is neither found in epidermal cells (c) nor guard cell protoplasts (f). In some guard cells, KAT1::GFP does not localize to the PM but to plate shaped structures, which concentrate around the nuclear envelope (d and e, arrowhead) and the cortical cytoplasm (e, arrows). Scale bars = 10 μm

Moreover the overall distribution of KAT1::GFP in the PM is not even. In the majority of cells, KAT1::GFP is absent from the PM behind the cuticular ledges. (Fig. 3.15, arrows). Due to the variable intensity of the autofluorescence in cuticular ledges, this absence was difficult to judge. However, a comparison with the distribution of GFP::TM23 (Ch. 3.3.4) allowed to draw this conclusion. In about 40% of the cells, a clearly enhanced signal of the protein is found at the tips of the cells (Fig. 3.15, arrowheads).

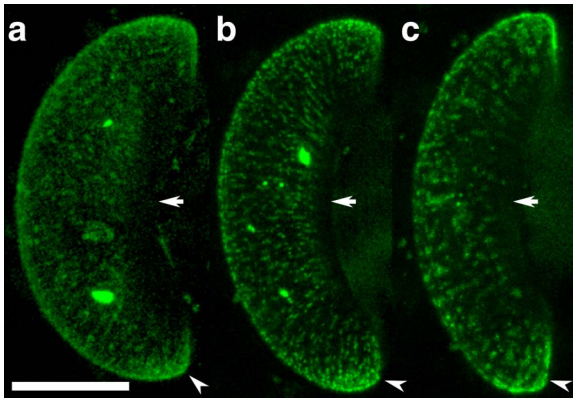

Figure 3.15: Enhanced localization of KAT1::GFP to guard cell tips. Brightest-point-projections of guard cells expressing KAT1::GFP reveal a enhanced localisation of the channel at the tips of guard cells (a-c). In turn, the channel is not found in the PM at the cuticular ledges (arrows). Scale bar = 10 μm

3.3.2 talin::YFP

To visualise the distribution of the actin cytoskeleton, guard and epidermal cells were transfected with talin::YFP. The talin domain in this construct originates from a mouse protein, which, in its native form, nucleates actin polymerisation. To deplete this function, the protein has been truncated by its catalytic domain. The remainder exhibits a high affinity to filamentous actin of plants (Kost et al. 1998).

Guard and epidermal cells show a meshwork of numerous fine filaments, when transfected with the construct. In epidermal cells, no specific orientation of the meshwork is found (Fig. 3.16a). Brightest-point-projections of guard cells also lack a specific orientation; only in most cortical paradermal confocal slices a radial symmetric pattern is found (Fig. 3.16b, upper and lower panel, respectively).

The actin cytoskeleton can be destroyed with latrunculin, a cell-permeable toxin from the Red Sea sponge *Latruncalia magnifica*. This toxin disrupts microfilament organization by the formation of 1:1 complex with monomeric G-actin (Ayscough et al. 1997). Incubating guard cells in presence of 10 μM latrunculin for 20 minutes is sufficient to destroy the filamentous meshwork (Fig. 3.16c and d). This demonstrates that the talin:YFP construct indeed labels the actin cytoskeleton.

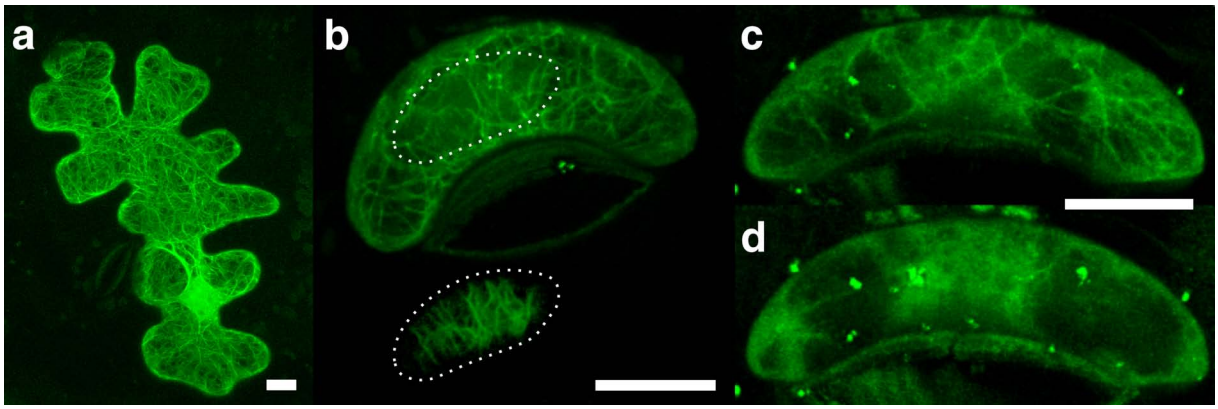

Figure 3.16: The actin cytoskeleton visualized by talin::YFP. In epidermal cells the actin cytoskeleton appears as a filamentous meshwork with no preferred orientation (a). In brightest-point-projections of guard cells, the same unoriented filamentous distribution is found (b, top panel). The expected radial symmetric orientation is only found in very cortical sections (b, bottom panel). The filamentous pattern (c) can effectively be destroyed within 20 min by 10 μM latrunculin (d). Scale bars = 10 μm.

3.3.3 HDEL::GFP

The ER in plant cells is known to appear as a network within the cytoplasmic strands (Saitat-Jeunemaitre et al. 1999). Since proteins with the leading amino acid sequence HDEL are retained in the ER (Denecke et al. 1992), the ER in guard and epidermal cells was visualized by the transient expression of HDEL::GFP.

The proper targeting of the construct to the ER was confirmed by its appearance in transfected epidermal cells. A fine meshwork, typical for the ER, was found in this cell type (Fig. 3.17a) . In guard cells, the construct brightly labelled the nuclear envelope (Fig. 3.17b and e, arrowheads), indicating its location in the ER. However, no meshwork within the cytoplasmic strands or the cortical cytoplasm was found (Fig. 3.17b, d and f, long and short arrows, respectively). Only in a very cortical section, a fine mesh was observed, which may reflect a reticulum (Fig. 3.17d, outlined arrowhead).

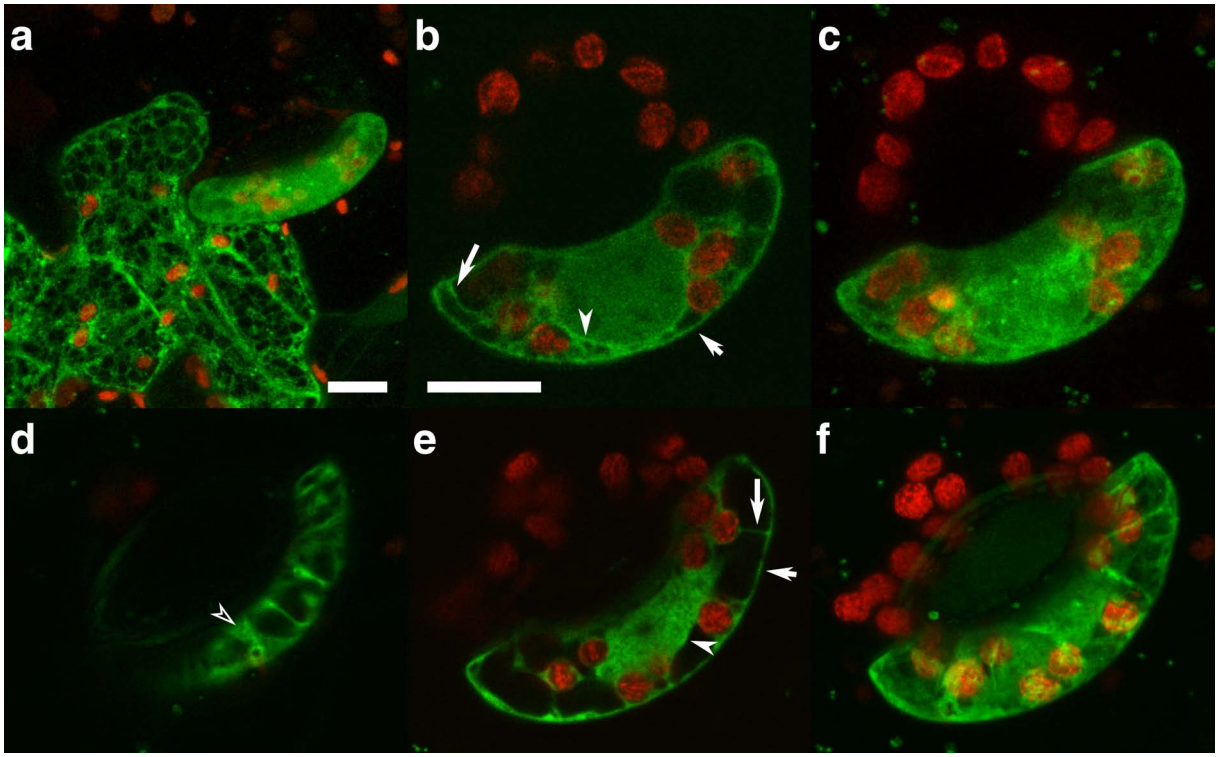

Figure 3.17: The ER visualized by HDEL::GFP. Unlike in epidermal cells (a, left cell) the distribution of the ER marker HDEL::GFP, was never found to have the typical reticulate appearance in guard cells. This becomes apparent in brightest-point projections (c, f). In corresponding aequatorial sections (b and e) the intense labeling of the nuclear envelope (arrowheads) and cytoplasmic strands (arrows) becomes obvious. Only in a very cortical section, a fine mesh may point to a reticulate distribution (d, outlined arrowhead). Scale bars = 10 μm.

3.3.4 GFP::TM23

To uncover, whether the localization of KAT1::GFP is related to the protein or rather represents the default for PM proteins in guard cells, the localisation of another protein was investigated for comparison. For the following reasons a fusionprotein of GFP followed by the 23 amino acid long transmembrane domain of the human lysosomal associated membrane protein (LAMP1) denominated GFP::TM23, was chosen for this purpose.

It has been shown that this protein is targeted to the PM in epidermal and guard cells of *N. tabaccum*, while shorter variations with transmembrane domains of 20 and 17 amino acids localise to the Golgi and the ER, respectively (Brandizzi et al. 2002). Thus, the targeting is based on the length of the transmembrane domain, rather than on an intrinsic signal (e.g. a sequence motif or a tertiary structure). It is therefore ideally suited to distinguish the specific features of KAT::GFP distribution, which are based on the channel, from those based on default targeting pathways in guard cells. To obtain even more information, guard cells expressing GFP::TM23 were co labelled with FM4-64 to investigate a possible overlap of the endocytic pathway with the distribution of the protein.

GFP::TM23 was targeted to the PM as confirmed by its colocalisation with FM4-64 (Fig. 3.18a-c, outline arrowheads). However, in contrast to the potassium channel, TM23 exhibited no radial symmetric pattern or any heterogeneity in distribution, at least on the scale of resolution (Fig. 3.18a, long arrow). GFP::TM23 distributed evenly over the entire PM of the guard cell, including the regions behind the cuticular ledges (Fig. 3.18g, long arrow). No enhanced signal was found at the tips.

TM23 and FM4-64 also clearly colocalised in numerous large structures with a diameter of around 600 nm (Fig. 3.18g-i, arrowheads). However, neither the nuclear envelope nor small and intermediate sized structures were labelled by both markers at the same time. While the former was weakly labelled by TM23 (Fig. 3.18g-i, outlined arrowheads) the latter were solely labelled by FM4-64 (Fig. 3.18d-f, arrowheads). These small and intermediate sized structures (vesicles and endosomes), were labelled by FM4-64 in advance of the large structures (data not shown).

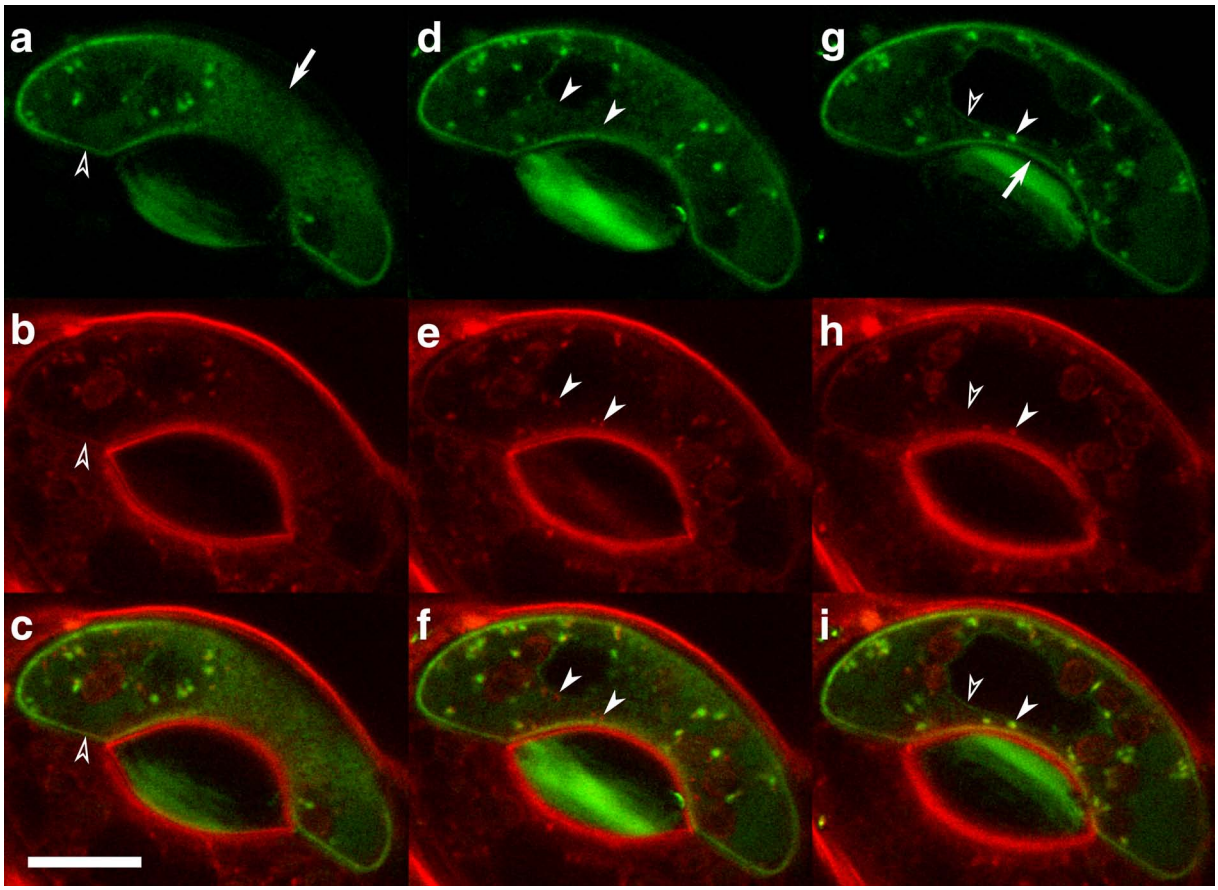

Figure 3.18: Colocalisation of GFP::TM23 and FM4-64. Three consecutive confocal sections of a guard cell transiently expressing GFP::TM23 (green) additionally labeled with FM4-64 (red) are shown, including the respective overlays (c, f, i). GFP::TM23 is evenly distributed in the PM and also targeted to the PM directly behind the cuticular ledges (long arrows, a and g, respectively). However its location is not restricted to the PM. The protein also localizes to numerous large structures and to the nuclear envelope (g-i, filled and outlined arrowheads, respectively). FM4-64, in turn, colocalizes with TM23 in the large structures, but not in the nuclear envelope. Small and intermediate sized structures are solely labelled by FM4-64 (d-f, arrowheads). Scale bar = 10 μm.

FM4-64 labelled the large structures but was absent from the nuclear envelope. The dye has recently been shown to colocalizes with a Golgi but not with an ER marker in tobacco BY-2 cells (Bolte et al. 2004b). Hence, it is reasonable to assume that the large structures observed in the present study are individual Golgi. TM23, in turn, localises to the PM and staining of the nuclear envelope clearly indicates that it is also found in the ER (Ch. 3.3.3). Since TM23 also labelled the large structures, the construct is detectable along the whole secretory pathway.

3.4 3D reconstruction of stomatal movement

3.4.1 Calculation of volume and surface area from 3D datasets

Guard cell movement is based on a volume in- and decrease, a process, which includes changes in 3D. Hence, CLSM is ideally suited to investigate these changes. While surface area and volume of guard cell protoplasts can be estimated from the protoplasts diameter or even precisely determined with patch-clamp capacitance measurements, these parameters are not easily obtained for intact guard cells. 3D image stacks were therefore recorded for 10 guard cells in open and closed states, respectively, as described in Ch. 2.3.4 and reconstructed in 3D (Fig. 3.19).

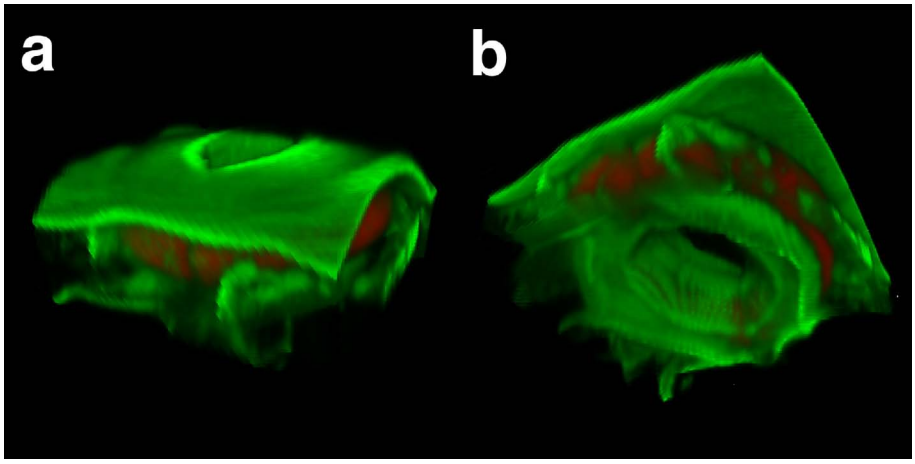

Figure 3.19: 3D reconstructions of stomata. Projections of the pre-processed image stacks show the same stomatal complex from an outer (a) and inner (b) periclinal view. The threshold pixels of the cells volume are shown in red, autofluorescence and FM2-10 labelling is pseudo-colored green.

The physiological relevant parameter which guard cells have to adjust is the conductance of the pore i.e. the area of the pore. Both, aperture and surface area of the pore were determined for each guard cell. The strong linear correlation of both parameters (Tab. 3.3) indicates that aperture is an excellent parameter to estimate stomatal conductance, as has been suggested by Raschke (1979).

To achieve a 50 % excursion in aperture, guard cells have to change their volume by 25 % and the surface area by 15 % (Tab. 3.3). Hence, excursion of the surface area during stomatal movement clearly exceeds the maximum elasticity of the PM, which is limited to about 2% (Wolfe and Steponkus 1983). Trafficking processes, which include and retrieve membrane material at the PM are therefore necessary to accommodate these changes.

CLOSED guard cells	**volume [μm^3]**		**surface area [μm^2]**		**aperture [μm]**	**pore area [μm^2]**
1	3700	4149	1677	1742	6.13	134.81
2	3757	3335	1642	1534	5.58	117.51
3	3535	3178	1592	1494	5.10	91.49
4	3458	3110	1621	1530	6.28	132.30
5	4648	3767	1891	1793	6.75	143.27
mean $\pm$ SD	3664 $\pm$ 464		1652 $\pm$ 126		5.97 $\pm$ 0.64	123.88 $\pm$ 20.53

OPEN guard cells	**volume [μm^3]**		**surface area [μm^2]**		**aperture [μm]**	**pore area [μm^2]**
1	4722	5131	1926	1976	12.85	266.50
2	4286	3855	1841	1700	11.64	279.33
3	4458	4087	1857	1756	12.75	256.19
4	4251	4185	1827	1818	12.40	246.70
5	5807	5255	2211	2081	13.08	262.00
mean $\pm$ SD	4604 $\pm$ 616		1899 $\pm$ 154		12.54 $\pm$ 0.56	262.14 $\pm$ 12.13

DELTA (open - closed)	**volume [μm^3]**		**surface area [μm^2]**		**aperture [%]**	**pore area [%]**
1	27.6	23.7	14.9	13.5	47.74	50.59
2	14.1	15.6	12.1	10.8	47.94	42.07
3	26.1	28.6	16.6	17.5	40.03	35.71
4	22.9	34.6	12.7	18.8	50.65	53.63
5	24.9	39.5	16.9	16.1	51.57	54.68
mean $\pm$ SD	**25.8 $\pm$ 7.7**		**15.0 $\pm$ 2.6**		**47.58 $\pm$ 4.54**	**47.34 $\pm$ 8.17**

Table 3.3: Quantifications on 3D guard cell objects. Values obtained from quantifications on 3D reconstructions of intact guard cells in closed and open states of 10 guard cells (5 stomata). A 3D reconstruction of stoma No. 3 is illustrated in Fig. 3.20.

Besides the quantification of volume and surface area the spatial distribution of the changes during stomatal movement was also investigated. This was visualized by overlaying open and closed stomata. The two 3D objects of guard cells in the closed state (Fig. 3.20a) were separated to match the aperture of the same complex in its open state (Fig. 3.20b and c). An overlay with the latter indicates that a significant volume change during stomatal movement occurs at the tips of guard cells (Fig. 3.20d and e). In addition, a volume change can also be attributed to a slight variation in the guard cell's cross section (Fig. 3.20f).

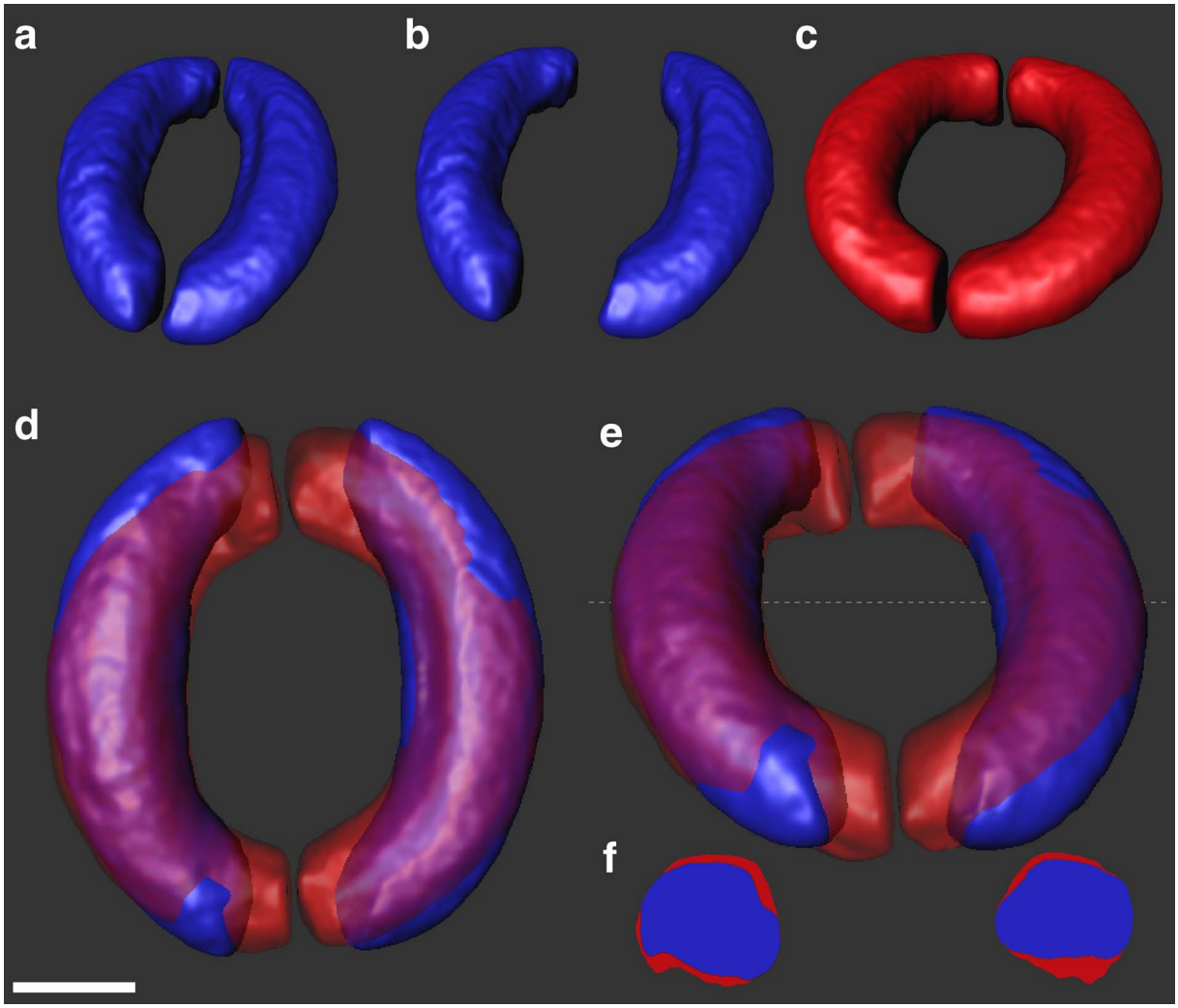

Figure 3.20: 3D reconstruction of a stomata. The isosurface of a single stomatal complex (No. 3, Tab.3.3) is shown in the closed (a) and open (c) position. 3D objects of guard cells of the closed reconstruction were separated to match the aperture of the open reconstruction (b) and subsequently overlaid (d and e). Prominent volume changes obviously occur at the tips of the guard cells. In addition, a volume change can also be attributed to a slight variation in the guard cell's cross section (f). The cross sections were obtained at the position marked with a dashed line in (e). Scale bar = 10 μm.

3.4.2 Model for 3D changes during stomatal movement

To distinguish, whether guard cell movement is indeed realized mainly by a volume increase and decrease at the tips or rather by an overall swelling and shrinking of the entire cell, the data obtained from 3D measurements was fitted to simplified 3D models for guard cells. At first approximation guard cells resemble a half torus:

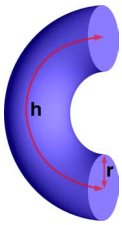

Figure 3.21: Half Torus. volume (V), surface area (A), radius (r), arc length (h) of a half torus

$$V = \pi r^2 h \tag{3.2}$$

$$A = 2\pi r(r + h) \tag{3.3}$$

Hence, the issue is now simplified to the question as to whether the radius or the length of the half torus changes. Since volume and surface area have been the only 3D values obtained for guard cells, volume is expressed as a function of surface area of a half torus. The two models predict different causal relations between volume (V) and the geometric parameters of the torus (h, r) as a function of surface area (A). They are described by Eq. 3.4 and 3.5:

elongating half torus

$$V(A) = \frac{Ar}{2} - \pi r^3 \tag{3.4}$$

thickening half torus

$$V(A) = \frac{h}{4\pi}\left(h\pi - \sqrt{2A\pi + h^2\pi^2}\right)^2 \tag{3.5}$$

The values for volume were plotted against the respective surface area values of individual guard cells and fitted to both models (Fig. 3.22). The whole dataset of guard cells of open and closed stomata is better described by the thickening model, as indicated by the residue plot (Fig. 3.22, upper panel) and the coefficients of determination (R^2, Tab. 3.4). Obviously, the 3D changes during stomatal movement are not well described by an elongating process, as otherwise expected from overlays of 3D reconstructions (Fig. 3.20).

In addition, separate fits to datasets of closed or open stomata were performed in order to yield the values for the length (h) and the radius (r). The remaining parameters, i.e the radius for the fit by the elongating and the length for the fit by the thickening model, were calculated by Eq. 3.2 and 3.3, by using the mean values for volume and surface area of the separate datasets (Tab.3.3). The results are summarized in Tab. 3.4.

It becomes evident that guard cells swell and elongate during the opening process. Moreover, the obtained parameters exactly fit to the changes visualised in Fig.3.20. Manual measurements of the arc lengths of this cell resulted in 48.32 μm and 50.57 μm for the closed and open states, respectively.

Thus, guard cells swell and elongate during stomatal opening, however the changes of volume and surface area are mainly determined by changes of the radius. Hence the movement is better described by a ”thickening” of a half torus.

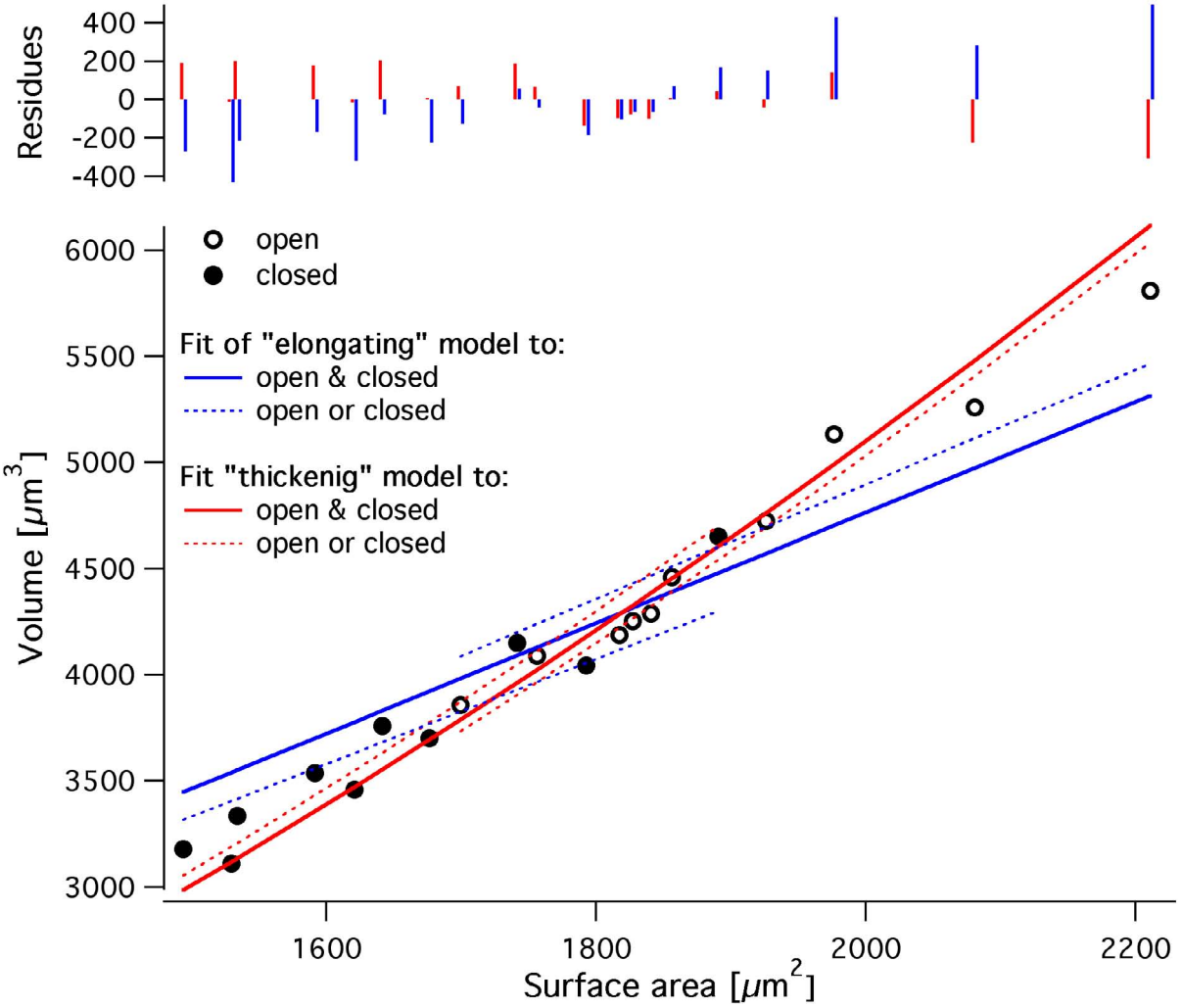

Figure 3.22: Torus models fitted to the 3D dataset. The volume of guard cells being part of closed (closed circles) and open (open circles) stomata is plotted against their surface area. Both torus models were fit to the whole dataset (cells of open and closed stomata, straight lines). Residues for these fits are shown in the top panel. In addition, the models were fit to datasets of closed and open stomata separately (dashed lines). Results of all fits are summarized in Tab. 3.4.

	linear			elongating			thickening		
	m	b	R^2	r [μm]	R^2	h* [μm]	h [μm]	R^2	r* [μm]
closed	3.67 $\pm$ 0.32	-2380 $\pm$ 521	0.97	4.95 $\pm$ 0.12	0.84	48.18	48.85 $\pm$ 0.79	0.93	4.89
open	3.94 $\pm$ 0.22	-2888 $\pm$ 413	0.98	5.39 $\pm$ 0.11	0.87	50.73	51.55 $\pm$ 0.71	0.95	5.33
open&closed	3.77 $\pm$ 0.13	-2539 $\pm$ 233	0.95	5.21 $\pm$ 0.09	0.88	49.21	50.45 $\pm$ 0.59	0.96	5.11
Shope et al.	4.03 $\pm$ 0.28	-2709 $\pm$ 287	1.00	6.29 $\pm$ 0.19	0.89	48.6	49.69 $\pm$ 1.57	0.95	6.16

Table 3.4: Results of fits to the 3D datasets of guard cell volume and surface area. Values of parameters marked with a asterisk were calculated as described in the text.

3.4.3 Comparison to published data

In a similar analysis on 3D changes of stomatal movement (Shope et al. 2003), the authors arrived at a different result. In their study, an absolute linear relationship between volume and surface was found. This was, however, not the case in the present study which is at first indicated by the slightly different slope of linear fits to the separate datasets (Tab. 3.4).

To further evaluate this, the dataset of the present study together with the dataset published by Shope et al. (2003) was fitted to the different models. For a better visualisation, especially of the nonlinearity of the thickening models, the fits were extrapolated to value ranges beyond those of the datasets (Fig. 3.23).

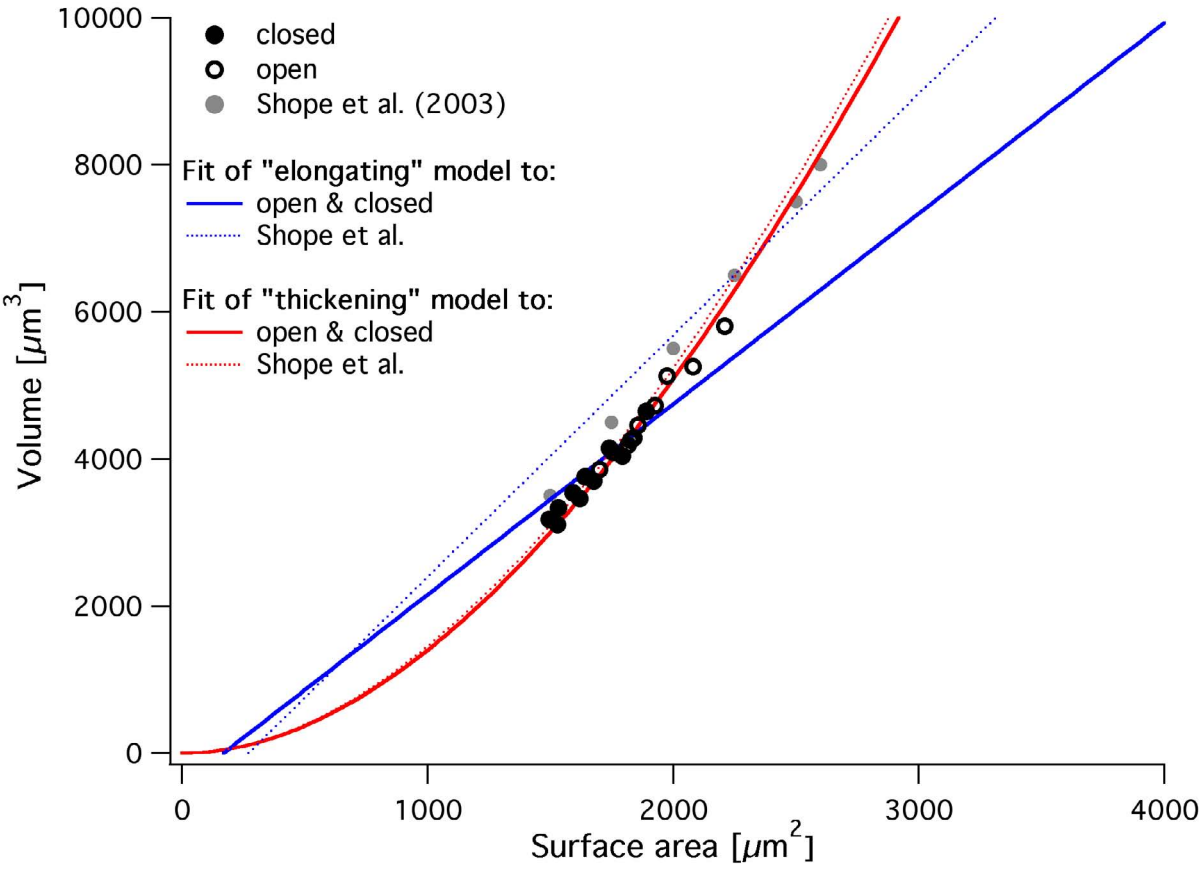

Figure 3.23: Extrapolations of the torus models fits. Both models were fit to the combined dataset of open and closed stomata of the present study and to the data from Shope et al (2003). The fits are extrapolated to values beyond those of the datasets to visualize the (non)linearity. Results of the fits are summarized in Tab. 3.4.

The slope of the linear elongating model does not describe the almost linear relationship between volume and surface area of guard cells of both datasets. In contrast, the nonlinear thickening yields a good fit to the present and also the data of Shope et al. (2003). Even more important, however, is the fact that the fit to the dataset of the present study predicts the values of Shope et al. and vice versa.

Hence, the nonlinear thickening model describes and even predicts the relation between volume and surface area during stomatal movement.

Chapter 4

Discussion

Endocytosis has so far only been demonstrated in plant cells with a relatively low internal pressure (Emans et al. 2002, Baluska et al. 2002, Parton et al. 2001); the entire process was even questioned to be possible against a high turgor on the basis of energetic considerations (Gradmann and Robinson 1989). However, every eukaryotic cell is likely to perform exo- and endocytosis to permit a general turnover of PM proteins and to maintain the PMs integrity.

The question whether endocytosis is indeed not possible against high turgor was therefore readressed in an investigation using guard cells. The pressure values reached by this cell type are among the highest found in the plant kingdom (4.5 MPa); even cells in closed stomata have pressures in the range of 1 MPa (Franks et al. 2001). But more important, the general problem of membrane turnover is brought into particular focus with this cell type, due to the considerable and repetitive variations in the surface area of the guard cells PM during stomatal movements.

The endocytic pathway was investigated by following the uptake and fate of different fluorescent markers. Besides the membrane-affine styryl dyes and the fluid phase marker Alexa 488 hydrazide, also fusion proteins were imaged by CLSM. Namely a potassium inward rectifying channel (KAT1) and a 23 amino acid long transmembrane domain (TM23) were fused to the green fluorescent protein (GFP), respectively. Furthermore, the general demand for membrane trafficking processes caused by the volume changes during stomatal movement was evaluated. Quantifications of volume and surface area on 3D reconstructions of intact guard cells yielded the characteristic relation between both values during stomatal movement.

4.1 Endocytosis against high turgor

Small fluorescent structures of diffraction-limited sizes were found in the cortical cytoplasm of intact guard cells, which were incubated in the presence of FM-dyes or Alexa 488 or transiently expressed KAT1::GFP. Evidence is presented that these structures are endocytic vesicles.

4.1.1 Endocytosis of FM4-64 and KAT1::GFP

The small fluorescent structures which were found most prominently in the cortical regions of cells can for the following reasons be identified as endocytic vesicles:

First, they colocalise with structures carrying KAT1::GFP proteins. KAT1 is a PM K^+-channel. The activity of the KAT1::GFP chimera can be measured with electrophysiological methods in the PM of transfected guard cell protoplasts. Furthermore, it has been shown that this chimera can be retrieved from the PM via endocytosis (Hurst et al. 2004). Hence, it is reasonable to assume that structures which are colabelled with KAT1::GFP and FM4-64 are endocytic vesicles, and have retrieved the K^+-channel protein from the PM via endocytosis.

Second, previous capacitance recordings have resolved endocytosis of single vesicles in guard cell protoplasts (Homann and Thiel 1999). They revealed an estimate for the size of the expected endocytic vesicles and thereby offer a reference point for the interpretation of the present data. These authors note that vesicles with a subresolution diameter contributed to the recorded signal but could not be resolved as single endocytic steps and thus did not contribute to the observed size distribution. The size distribution histograms of vesicles for both methods are therefore truncated at their respective resolution limits: the patch-clamp technique by the SNR and confocal microscopy by diffraction and by SNR. The latter is in this case mainly determined by the amount of dye present in the vesicle. Hence, it is only reasonable to compare the size distributions of vesicles monitored for both methods in their well resolved range (e.g. above $\sim$250 nm). But also in this range the close similarity between both methods implies that the same endocytic vesicles have been measured.

Previous experiments with *V. faba* guard cell protoplasts have collected a body of evidence for a dynamic nature of the PM. It was found that an excursion in the size of the PM surface area, which occurs during moderate and slow swelling and shrinking, is accomplished by an exo- and endocytic incorporation and retrieval of membrane into and from the PM (Homann and Thiel 1999). Together with the vesicular membrane also K^+-channel proteins are delivered or retrieved via exo- and endocytosis (Homann and Thiel 2002, Hurst et al. 2004). The present data now show that this system can be extrapolated to turgid guard cells. The fact that endocytic vesicles carrying the GFP tagged K^+-channel KAT1 were identified in turgid cells shows that endocytosis is possible against high turgor pressure. Since all intact guard cells were investigated under constant hypoosmotic conditions, i.e. under a natural osmotic gradient, controlled endovesiculation rather than vesiculation of the PM upon an osmotic shock (i.e. osmocytosis; Ch. 4.4.1) led to the observed endocytic vesicles. Notably these double labelled vesicles have only been observed in the cortical cytoplasm. This might point to a reserve or recycling pool of vesicles carrying K^+-channels, which may be retrieved from and inserted into the PM during the closing and opening cycles of guard cells. Such a pool has already been suggested by Hurst et al. (2004) based on the observation that K^+-channels are inserted into the PM immediately after applying a swelling stimulus to a patch-clamped protoplast.

4.1.2 Endocytosis of Alexa 488 hydrazide

Investigations with the fluid phase marker Alexa 488 hydrazide further support the view that endocytosis is feasible against high turgor pressure and occurs in intact guard cells. The similarity between structures labelled by Alexa 488 to those labelled by FM4-64 suggests that the fluid phase marker also stains endocytic vesicles. The similarity holds true for the diffraction-limited size as well as for the location of the structures in the cortical cytosol. Moreover, if an Alexa 488 solution of sufficient concentration was used, the first endocytic structures were recordable after a delay similar to that which was observed by FM4-64 stainings. For both dyes the first labelled structures appeared after about 10 to 15 min.

In addition to their appearance as diffraction-limited structures in confocal recordings, the mean size of Alexa stained vesicles was also calculated. This calculation was based on

- the *measurement* of the molarity an Alexa 488 solution with progressing concentration had right in the moment when the first diffraction-limited structures appeared in the cortical cytoplasm.
- the *estimation* of the signal demand of the confocal setup used to detect the structures. Based on comparison with similar setups, it was estimated that at least 200 molecules are necessary in order to produce a detectable signal above noise.
- the *assumption* that endocytic vesicles do not have a ”matrix”, as reported for exocytic vesicles (Reigada et al. 2003). If this assumption is wrong, the dye molecules do not have access to the whole volume of forming vesicles. This would result in an underestimation of the vesicle size to an unknown extent.

Because no information is available to support the last assumption, the calculated sizes have to be dealt with some care. However, the calculated range of 66 to 83 nm is in good agreement to sizes reported for clathrin-coated vesicles in plants (70 - 90 nm; Barth and Holstein 2004, Low and Chandra 1994).

Additional evidence that the diffraction-limited structures are single vesicles rather than small endosomes is provided by the manner in which they appeared. In the same context the similar brightness argues for a vesicular nature.

All structures labelled in presence of a continuously concentrating Alexa solution appeared in a all-or-none fashion, i.e. no structure was recordable until the Alexa solution reached the molarity, at which each structure was labelled with the number of dye molecules sufficient for detection. Because only structures with diffraction-limited size were observed, the vesicles apparently have a narrow size distribution, which explains their similar brightness. Such a scenario is only expected for structures which are in direct contact to the dye reservoir, i.e. the external solution. This only holds true for endocytic vesicles, forming at the PM. In contrast,

this scenario is not expected from a continuous accumulation of Alexa molecules in endosomes, which are filled with dye by insufficiently labelled and hence invisible vesicles. In this case, a constant increase in brightness should have been observed for individual endosomes. Also a broad distribution in brightness should have been expected for numerous endosomes.

As an additional piece of evidence for an endocytic uptake it now remains to be shown, whether the vesicles labelled by the fluid phase marker are fusion competent, as it is expected of every type of endocytosis (Robinson et al. 1991). Final discharge of the fluorescent marker into the vacuole as evidence for the fusion competence of the first endocytosed structures has so far only been shown for FM4-64.

To summarize, it is evident that the fluid phase marker Alexa 488 hydrazide is taken up only into structures of diffraction-limited size whose calculated diameters are similar to those of clathrin-coated vesicles. This is in accordance with the findings of Diekmann et al. (1993) who were not able to demonstrate fluid phase uptake in intact turgid guard cells of *V. faba* using Lucifer Yellow. Since Lucifer Yellow is inferior to Alexa 488 with respect to brightness whenever fluorescein optics are used (Haugland 2002) the authors made the right conclusion in suggesting a size for the vesicles to small to be detected with their setup. Obviously, only endocytic processes which produce larger structures are traceable with this fluid phase marker.

Recent success to trace fluid phase uptake with Lucifer Yellow in the inner cortex of maize root apices (Baluska et al. 2004) supports that view. In this work a F-actin-dependent uptake was described to occur into tubulo-vesicular compartments invaginating from the PM at actomyosin-enriched pit-fields. This closely resembles a likewise actin-dependent pathway in mammalian cells, known as macropinocytosis, which is mechanically unrelated to all the other endocytic routes and produces vesicles with diameters of up to 1 μm (Conner and Schmidt 2003). It is a main route for the uptake of nutrients in mammalian cells and may have the same function in root cells. But more important for the current context is that macropinosomes are likely to take up enough Lucifer Yellow to be detected.

This leads to the conclusion that intact guard cells do not perform pinocytosis. They rather use small structures for endocytosis in order to minimize the uptake of unwanted, soluble molecules. For cells at the outermost cell layer of the plant, this is a sensible approach. Since small structures have a high surface to volume ration, uptake of the membranous relative to the fluid phase is maximized.

4.2 Endocytic mechanisms

Evidence has been presented here that FM4-64, KAT1::GFP and Alexa 488 hydrazide are reliable markers to demonstrate endocytosis in intact turgid guard cells. This allows to evaluate details about the endocytic mechanism underlying the uptake of each marker. Moreover, it allows to propose a general mechanism for endocytosis capable to operate against high turgor.

4.2.1 Uptake characteristics indicate differences in the endocytic mechanisms

Based on the fact that all markers are detectable in endocytic vesicles of diffraction-limited dimensions it can be assumed that at least 200 molecules of each marker have to be present in a vesicle. This allows to draw conclusions on the respective uptake mechanism of each marker. Molecules can become endocytosed in two ways: First, if they are trapped with the fluid phase, which inevitably gets enclosed in every endocytic vesicles. Second, if they are bound to the membrane. In both cases, a specific concentration of fluorescent molecules is necessary to label the endocytic vesicles for detection.

The first case has been demonstrated in detail for Alexa 488 hydrazide. Since the dye molecules were not bound to the membrane, they could not be concentrated by the endocytic machinery. This required relatively high concentrations of $\sim$4 mM of Alexa 488 to label a 90 nm vesicle with at least 200 molecules.

Uptake of the membrane-affine FM-dyes is an example for the second case. These dyes have been used in concentrations one order of magnitude lower than Alexa 488. Thus the question arises whether a concentrating mechanism of the endocytic machinery contributed to the uptake of these membrane bound dyes to permit their detection in single vesicles. On average, a single lipid occupies an area of 0.61 nm^2 in a membrane bilayer (Berger et al. 1997). The inner leaflet (40% of the lipids) of a vesicle with a diameter of 90 nm then contains $\sim$15,000 lipids. Schote and Seelig (1998) have quantified that if a 5 μM FM1-43 solution is in equilibrium with a biomembrane, about every 12^{th} lipid is replaced by a FM1-43 molecule. This would correspond to $\sim$1250 FM1-43 molecules per vesicle. Thus a concentrating mechanism is not necessary for detection of FM labelled vesicles.

Uptake of KAT1::GFP is also an example for the second case, since it is a membrane protein. If no concentrating mechanism prior to endocytic uptake is assumed, the channel density in an endocytic vesicle and the PM should be equal. With 200 fluorophores necessary for detection, each recordable vesicle then contains at least 50 KAT1 channels, since the tetrameric protein is tagged by four GFPs. For a 90 nm vesicle, this results in a channel density corresponding to about 1,000,000 KAT1 channels in the PM of a single guard cell. In contrast, only a current equivalent to 3000 channels was measured in guard cells protoplasts (Hurst et al. 2004). This illustrates that a concentrating mechanism has facilitated confocal detection of vesicles labelled with KAT1::GFP. As K^+-channels are know to form clusters in the PM (Ehrhardt et al. 1997), the concentrating is most likely a result of the endocytosis of pre-clustered KAT1 from the PM (Hurst et al. 2004).

The GFP::TM23, in turn, does not follow either of the aforementioned mechanisms, although it is also a PM bound protein. For a transmembrane molecule at least a passive endocytic

uptake along with the membranous phase had been expected, as it has been observed for the FM-dyes. However, no endocytic uptake of the protein was found, because GFP::TM23 does not colocalise in endocytic vesicles labelled by FM4-64. Apparently, the protein is actively excluded from endocytic uptake.

The best explanation for this behavior lies in the complete lack of any recognizable motif in GFP::TM23 to be recognized by the endocytic machinery. It is known that the cytoplasmic tails of many surface receptors and non-receptor proteins, which undergo endocytosis, contain motifs that are recognized by components of the coated pits. Mutations in these mainly tyrosine- and leucine-based motifs inhibit endocytosis of these proteins (Mousavi et al. 2004). Most importantly, GFP::TM23, the transmembrane domain of which stems from the human lysosome-associated membrane protein LAMP1 (Brandizzi et al. 2002), lacks the Tyr-386, which is the major determinant that mediates internalization of the LAMP1 (Fig. 4.1). By deleting the c-terminal region of LAMP1 (DL381), endocytosis was abolished completely (Williams and Fukuda, 1990). GFP::TM23, which lacks any of these motifs, may therefore not be recognized for endocytosis even in guard cells of *V. faba*. Apparently lack of an endocytic signal maintains the protein in the PM.

```
TM23     0 -GFPSTIEGREAEALIPIAVGGALAGLVLIVLIAYLVGRKRS-------
LAMP1  341 FGSVEECLLDENSTLIPIAVGGALAGLVLIVLIAYLVGRKRSHAGYQTI
Dl381  341 FGSVEECLLDENSTLIPIAVGGALAGLVLIVLIAYLVGRKR--------
```

Figure 4.1: C-termini of GFP::TM23, wt-LAMP1, and DL381. Both GFP::TM23 and DL381 lack the C-terminal Tyr-386 (red) of LAMP1, which was found to be required and sufficient to target LAMP1 to lysosmes (Williams and Fukuda 1990). Transmembrane domains are underlined.

It may be that imaging of the endocytic retrieval of GFP::TM23 has failed due to insufficient signal. However, the signal intensity of GFP::TM23 and FM4-64 in the PM was comparable. Moreover, GFP::TM23 was also not found in endosomes, stained by FM4-64. Both observations favor the view that GFP::TM23 was indeed not endocytosed.

4.2.2 Possible mechanism of endocytosis against high turgor

The debate about the occurrence of endocytosis in intact plant cells (Cram 1980, Gradmann and Robinson 1989, Hawes et al. 1995, Robinson and Hedrich 1991, Robinson and Hillmer 1990, Robinson et al. 1991, Oparka et al. 1993, Saxton and Breidenbach 1988) may be closed. A wealth of information about endocytic processes different from the simple osmocytic uptake has emerged during the last 10 years. These do not only include information about the molecular components and architecture of the process (Barth and Holstein, 2004; Holstein, 2002; Lam et al., 2001), but also show the relevance for physiological processes. Some of them are even specific to plants, such as the recycling and polar localisation of PIN1 at the PM, a candidate transporter for the plant hormone auxin (Geldner et al. 2003).

Nevertheless, the hurdle of turgor pressure for endocytosis in guard cells is more pronounced than in other plant cells investigated. Uptake of extra cellular markers has so far only been shown in intact plant cells with a relatively low turgor pressure such as tobacco BY-2 cells (Emans et al. 2002), root apices of *Zea mays* (Baluska et al. 2002) and pollen tubes of *Lilium longiflorum* (Parton et al. 2001). No uptake of the fluid phase marker Lucifer Yellow could be detected in intact guard cells but in protoplasts (Diekmann et al. 1993). In this context it is also not possible to a priori extrapolate the data on endocytic activity in guard cell protoplasts to intact guard cells. The available data rather appeared to assign high turgor a virtually preventive role. In a recent publication Shope et al. (2003) were able to show an uptake of the endocytic marker FM4-64 in osmotically shrinking guard cells. However, no direct evidence for the formation of endocytic vesicles was found. The authors even note that no constitutive uptake in absence of osmotic treatment was observed.

Considering the findings observed in this study, it is reasonable to review the influence of high turgor on endocytic processes and to propose a possible mechanism. It is of special importance to reconsider the amount of energy which is necessary for the process with clathrin in the first place. Endocytosis in plants has in particular been questioned on the basis that the energy provided by clathrin self-assembly into polyhedral structures is not sufficient to drive endocytosis against high turgor (Gradmann and Robinson, 1989). Recent data show that clathrin is not sufficient to drive membrane budding even in mammalian systems lacking any turgor pressure (Nossal 2002) and thus is not a limiting factor for the process at all. Gradmann and Robinson (1989) therefore arrived at the right conclusion regarding the contribution of clathrin. However, the authors have gone too far in ruling out the entire process of endocytosis against high turgor.

The current picture of endocytosis includes two driving forces for the formation of vesicles. The first is provided by the polymerisation of proteins like clathrin, caveolin, dynamin, amphiphysin and endophilin onto the cytoplasmic phospholipid leaflet. These proteins act in a more or less concerted manner to locally force the curvature of the membrane (Huttner and Schmidt 2002, Mousavi et al. 2004). For mammalian and yeast cells there is also growing evidence that actin plays an important role in endocytic events. Numerous proteins have been identified that functionally link actin with the endocytic machinery and at the same time regulate actin filament dynamics. Thus, these proteins could also harness forces produced during actin polymerisation to facilitate steps in the endocytic process. (Engqvist-Goldstein and Drubin 2003). The second force is provided by the active generation of a molecular asymmetry between the two monolayers of the PM. The following discussion will focus on the latter.

An increase of the number of phospholipids in the inner leaflet compared to the outer was found to cause vesicularisation in living cells (Farge et al. 1999) and even in giant unilamellar vesicles in the absence of any protein involvement (Farge and Devaux 1992). Hence, changes in the surface area asymmetry of the membrane induced by an asymmetric transmembrane distri-

bution of phospholipids is sufficient to generate the driving force for vesicle generation during endocytosis. Moreover, an increase of the phospholipid number in the inner layer also increased a bulk-flow endocytosis of membrane proteins, whereas an increase in the phospholipid number of the outer layer decreased their uptake rate. Rauch and Farge (2000) extended the evaluation on the budding forces introduced solely by the surface area asymmetry by additionally looking at the influence of pressure asymmetry (i.e. osmotic pressure) between the inner and outer volume. Hypoosmotic constrains were found to be a strong inhibitor of endocytosis. However, it was possible to abolish this effect by increasing the surface area asymmetry. Obviously there is a competition between the two antagonistic forces applied to the budding membrane: the volumic asymmetry force that opposes the vesiculation, and the membrane surface area asymmetry, the driving force of the budding.

From these findings important conclusions can be drawn for the endocytosis against high turgor in guard cells: First, high turgor pressure is indeed a strong inhibitor of endocytosis and could in principle prevent the whole process. But since this inhibitory effect can be overcome by increasing the surface area asymmetry, guard cells are likely to generate a degree of steady-state membrane surface area asymmetry which is sufficient to promote vesiculation under the current turgor. Such a steady-state asymmetry is known to be important for normal cell function, since it vanishes as an early sign of apoptosis (Schlegel and Williamson 2001). Lipid composition of the PM can change within minutes (Helmut Quader, personal communication) and is therefore not a limiting step to adjust the asymmetry to different turgor pressures. It will be of great interest, whether plants make use of such forces to promote endocytosis against high turgor.

These findings also point to a methodical claim to fame: The intercalation of molecules into the outer leaflet of the PM, which cannot flip to the inner leaflet, has been demonstrated to have an inhibitory effect on endocytosis. Since FM-dyes are believed to share exactly these properties, the endocytic markers might, at least to some degree, inhibit the process which they are supposed to trace.

In this context, epsin, a protein which localises early to endocytic spots, has been shown recently to make use of this principle: it influences the surface area asymmetry to provide the mechanical force to bend a flat membrane into an emerging bud. The n-terminal domain of Epsin intercalates an amphiphatic α-helix which is exposed upon binding the head group of phosphatidyl-innositole-4,5-bisphosphate (PtdIns(4,5)P2) into the cytosolic membrane leaflet and subsequently recruits clathrin to the membrane (Ford et al., 2002; Staehlin et al. 2003). Even its ENTH-domain (epsin n-terminal homology) alone was able to bend membranes, while the ANTH-domain (AP180 n-terminal homology) failed. Recently an AP180 which contains the ANTH-domain has been found in *A. thaliana* (Barth and Holstein 2004). However, a protein which contains the specific ENTH-domain still awaits discovery in the plant kingdom. Nevertheless such a protein is very likely to exist, since it would produce exactly the driving force for endocytosis against high turgor.

4.3 Endocytic pathways

Besides the small cortical structures, which have been identified as endocytic vesicles, the FM-dyes also labelled structures of intermediate and large sizes. Their possible identification will be evaluated in this chapter.

The quantum yield of styryl dyes increases by more than two orders of magnitude upon partitioning into a lipid environment and they are thought to be membrane impermeable (Cochilla et al. 1999, Henkel et al. 1996). Because of these properties FM-dyes are frequently used for monitoring endocytosis in living cells. The appearance of fluorescent label inside cells is generally taken as evidence for endocytic activity and the respective fluorescent structures are interpreted in the context of compartments along the endocytic pathway. The present study now shows that different styryl dyes are able to label three distinct populations of cytoplasmic structures in intact guard cells. These structures can be distinguished on the basis of their diameter and their affinity to the three dyes tested. An analysis of the fluorescent images reveals that the small cortical structures, but not all labelled structures inside a cell, can be interpreted in the context of endocytosis (see Ch. 4.3).

4.3.1 Intermediate structures are compartments of the endocytic pathway

The size distribution histograms of all fluorescent markers reveal a clear peak at $\sim$470 nm. The fact that this peak occurs with all FM-dyes suggests that it reflects a real structure, which is discernable from the small endocytic vesicles. Circumstantial evidence suggests that they are prevacuolar or endosomal-like compartments. They will be further referred to as endosomes.

An argument in support of this hypothesis is the finding that FM4-64 reveals the highest relative number of these intermediate sized structures. This dye is also the only among the FM-dyes which stains the tonoplast after long incubation. In addition, structures around that size can be shown distant from the PM e.g. in cytoplasmic strands. These findings suggests that the intermediate sized structures are compartments in the endocytic pathway from the PM to the tonoplast. This is in agreement with the observation that FM4-64 colocalises with Rab5 homologs Ara7 and Ara6 in early endosomes in *Arabidopsis thaliana* protoplasts (Ueda et al. 2001). On early endosome - Ara7 or Ara6 - might be identical to the PCR (Holstein 2002).

Notably, structures of the very intermediate size are also detected in cells treated with the MitoTracker, a dye designed to label mitochondria. Since this dye also gives a well detectable signal in vacuoles, it is reasonable to assume that this membrane-permeable dye can also label endosomes. This is supported by the fact, that the size distribution histogram of guard cell

mitochondria, measured in electron micrographs, lacks a peak at ∼470 nm. Moreover, the manufacturer states that MitoTrackers tend to stain other cellular structures when used at higher concentrations. Such concentrations have been used in this study in order to get a well detectable signal during the colocalisation with FM2-10.

4.3.2 Large structures are not part of the endocytic pathway

FM4-64 labels the Golgi

The nuclear envelope as well as the PM are both labelled by GFP::TM23. It is therefore likely that the large structures found in guard cells expressing this protein are single Golgi stacks. It can therefore be concluded that FM4-64, which colocalised with GFP::TM23 in these structures, also stains the Golgi. This is also supported by the staining kinetics. FM4-64 has recently been shown to label the Golgi about 30 min after it labels endocytic structures (Bolte et al. 2004b), as it was the case in this study.

FM1-43 and FM2-10 also label mitochondria

It is a significant observation that in particular the FM1-43 and FM2-10 also labelled large cytoplasmic structures with a mean diameter of ∼600/730 nm. For two reasons these structures are likely to be mitochondria. First, the structures had the expected size of guard cell mitochondria, according to size distribution histograms from CLSM images of guard cells labelled with the MitoTracker Red and measurements from electron micrographs. In addition both histograms confirm the double peak which is caused by the elongated shape of mitochondria. Second, they were colabelled with MitoTracker, a specific fluorescent label for mitochondria. FM1-43 and FM4-64 have also been reported to stain mitochondria of *Neurospora crassa* hyphae, even though the latter only after prolonged incubation (Fischer-Parton et al. 2000). Thus, the ability to stain mitochondria applies to all three FM-dyes. The intensity and kinetics, however, are dependent on the amount of dye present in the cytosol (see below). Collectively, this indicates that the large FM-labelled structures in guard cells are mitochondria.

Styryl dyes where developed as membrane potential sensors (Fluhler et al. 1985, Grinvald et al. 1988) and as membrane potential sensitive probe they were used to study mitochondria (Bereiter-Hahn 1976). In this context it is interesting to note that a preincubation of guard cells with sodium azide abolished the appearance of cytoplasmic label with FM and MitoTracker-dyes in guard and epidermal cells. Hence, the absence of label in azide-treated cells is most likely due to the inability of the dyes to label the depolarised mitochondria. Differential labelling with a putative endocytic marker in the presence versus absence of a metabolic inhibitor is thus not necessarily a proof of an endocytic uptake of the marker, as it is used frequently (Fischer-Parton et al. 2000).

4.3.3 FM-dyes can penetrate a phospholipid bilayer

The ability of FM-dyes to stain mitochondria in living intact guard cells questions the general view, that these dyes cannot penetrate bilayers.

The MitoTracker used in this study does not enter cells via an endocytic pathway but is cell-permeant. It is reported to passively diffuse across the PM and accumulate in active mitochondria (Haugland 2002). Accordingly, staining of endocytic vesicles was never observed with this dye. The conclusion is that this MitoTracker directly enters the cytosol from where it stains three compartments: mitochondria, endosomes, and vacuoles. Since the mitochondrial staining can be effectively prevented by sodium azide, the membrane potential of these organelles must play a crucial role in order to be labelled by this dye.

The same behavior was found for FM2-10. While a vesicular pathway between the PM and mitochondria has so far not been observed, this dye is also likely to directly enter the cytosol from where it stains active mitochondria. Since FM-dyes were developed from a membrane potential sensitive dye used to label mitochondria (Bereiter-Hahn 1976), this assumption is reasonable. However, if these dyes can enter the cytosol, they must be able to cross a membrane. This may happen via any of the following mechanisms:

Stretch-activated channels

It has been reported that stretch-activated channels of Chinese hamster ovary cells can transport FM1-43 across the PM. This in turn led to FM-labelled mitochondria (Nishikawa and Sasaki 1996, Gale et al. 2001). In view of the fact that stretch-activated channels have been described in guard cells of *V. faba* (Cosgrove and Hedrich 1991) these channels may be a possible route for FM-dyes to enter the cytosol. Uptake via a stretch-activated channel has not been observed for larger dyes such as FM3-25 (Meyers et al. 2003). Since FM2-10 in turn is smaller then FM1-43, it might enter the cytosol more easily via this pathway. This would explain the more intense and rapid staining of mitochondria with FM2-10.

Moreover, Cosgrove and Hedrich summarize that the stretch-activated channels in guard cells generally appear more similar to those in animal cells (Morris 1990) with respect to conductance, open times and ion selectivity, than to stretch-activated channels in other cell types such as yeast (Gustin et al. 1988) or tobacco suspension cells (Falke et al. 1988). This could explain, why mitochondrial staining by FM-dyes has not been reported in investigations on BY-2 cells of *N. tabaccum* (Bolte et al. 2004a, 2004b) or roots of *A. thaliana* (Geldner et al. 2003). In accordance neither stretch-activated channels nor unspecific uptake of FM-dyes have ever been reported for neurons (Meyers et al. 2003).

Photodestruction

Uptake of dyes may also result from local damage of labelled PM and endocytosed membrane. Illumination of fluorescent dyes inevitably produces hyper oxide radicals by an energy transfer from their triplet state to molecular oxygen (Betz et al. 1992). This may directly, or via lipid peroxidation, lead to membrane damage. This effect is used by a technique called photochemical internalization to deliver membrane impermeable macromolecules into the cytosol (Selboa et al. 2002). In this technique, macromolecules, which can not penetrate a membrane, are applied to cells together with photosensitisers molecules. Once a cell incorporates both molecules by endocytosis, illumination of the photosensitiser damages the vesicular or endosomal membrane and the macromolecule is released into the cytosol.

The unspecific uptake of FM-dyes via photochemical internalisation is in agreement with the observation that guard cells more often became leaky at the PM, in correlation with factors promoting the production of ROS: illumination intensity, duration of incubation, and concentration and extinction coefficient of the dye (Piston 1999). The behavior is reflected in the observed toxicity of the dyes. If the PM becomes leaky the result is a complete loss of turgor in parallel with an intense overall staining of all membranous compartments. This toxic effect was observed more frequently for FM1-43 than for FM2-10 and for the latter in a dose and incubation-time dependent manner, as it is typical for toxic effects. On average the dye leaked into the turgorless cells after incubation for 2h in 5 μM FM1-43, 6h in 100μM and after 12 h in 20 μM FM2-10 containing buffers. This is in accordance with the results of an early study on FM-dye uptake on tobacco BY-2 cells (Emans et al. 2002), although the authors did not consider any unspecific uptake despite the use of extremely high FM1-43 concentration (20 μM) in combination with intense illumination protocols (4D-imaging). However, a bright staining of the entire endomembrane system reported in this publication raises doubts about the significance of the observations and points to a labelling via leakage rather than endocytosis.

Lipid peroxidation depends on the presence of unsaturated fatty acids, which are more abundant in the plant kingdom. This might explain why FM1-43 has been used very successfully in investigations on animal cells without apparent negative side effects. In the present study, evidence for a leakage of FM1-43 through the PM has been presented. Photodestructive effects therefore render this dye almost useless for long-term investigations of membrane trafficking, at least in guard cells. In contrast, mitochondrial labelling with FM2-10 was observed in fully turgescent cells. Unspecific diffusion through a leaky membrane, as suggested by Horobin (2002), is therefore unlikely to be the pathway for this dye.

At least two different pathways may contribute to membrane permeability of FM1-43 and FM2-10. FM4-64 performed best as an endocytic marker. An effect like PCI might be limited by its large stokes shift and hence its longer emission wavelength while uptake via stretch activated channels might be limited by its unsaturated chain which results in a larger size.

4.3.4 FM-dyes get sorted due to differences in their hydrophobicity

It is apparent that FM4-64 passes through the entire endocytic pathway up to the vacuole but does not stain mitochondria. This is consistent with previous investigations showing that FM4-64 is staining the tonoplast of various cell types from a broad origin such as pollen tubes of *Lilium longiflorum* (Parton et al. 2001), protoplasts of *A. thaliana* (Ueda et al. 2001), *Saccharomyces cerevisiae* (Vida and Emr 1995), numerous fungal hyphae (Fischer-Parton et al. 2000), and *Dictyostelium* (Heuser et al. 1993).

However, according to the present data, it appears that all FM-dyes also stain early structures in the endocytic pathway such as endocytic vesicles and presumably endosomes. Hence, the fact that FM2-10 does not label the tonoplast either implies that this dye escapes at early stages from the endocytic pathway into the cytosol (from where it can label mitochondria), or that it recycles back to the PM, while FM4-64 remains in the pathway to the vacuole or Golgi. Since the three dyes mainly differ in their hydrophobicity, it can be reasoned that this parameter is a major cause for their differential behavior.

In mammalian cells all endocytic vesicles fuse with the tubovesicular sorting endosome, regardless from which endocytic process they evolve. This primary target compartment is the first site at which molecules get sorted into different pathways. Using fluorescent analogues it has been shown that this sorting is based primarily on two properties of these molecules (Mukherjee et al. 1997, 1999; Hao and Maxfield, 2000): First, fluorescent lipid analogues distribute between the membrane and the aequous phase according to their hydrophobicity, which can be quantitatively expressed as a partitioning coefficient. Hydrophilic molecules have a lower affinity to membranes and thus lower partitioning coefficients. Second, membrane-bound lipid analogues distribute between membrane domains of high and low fluidity and curvature according to their shape and hydrophobicity. The latter are determined mainly by the degree of saturation and chain length, respectively.

The sorting endosome then delivers fluid phase molecules and hydrophilic molecules, which in part partition into the fluid phase, to late endosomes and lysosomes (lytic pathway). A closer inspection of membrane-bound molecules in turn revealed that lipid analogues with two long saturated 16-carbon tails are sorted by the sorting endosome to late endosomes (lytic pathway). Analogues with either short saturated 12-carbon or unsaturated 18-carbon acyl chains are delivered to the endocytic recycling compartment (ERC) and are targeted back to the PM (recycling pathway).

All in all, molecules with an affinity to the fluid phase and rigid membranes mainly enter the lytic pathway, whereas those with an affinity to fluid or highly curved membrane domains are recycled via the ERC back to the PM (Fig. 4.2).
Although a sorting endosome in plants has not been identified so far, this picture of sorting processes is mirrored by investigations on guard cells with FM-dyes.

In this scenario the behavior of FM4-64 can mainly be described as a membrane-bound

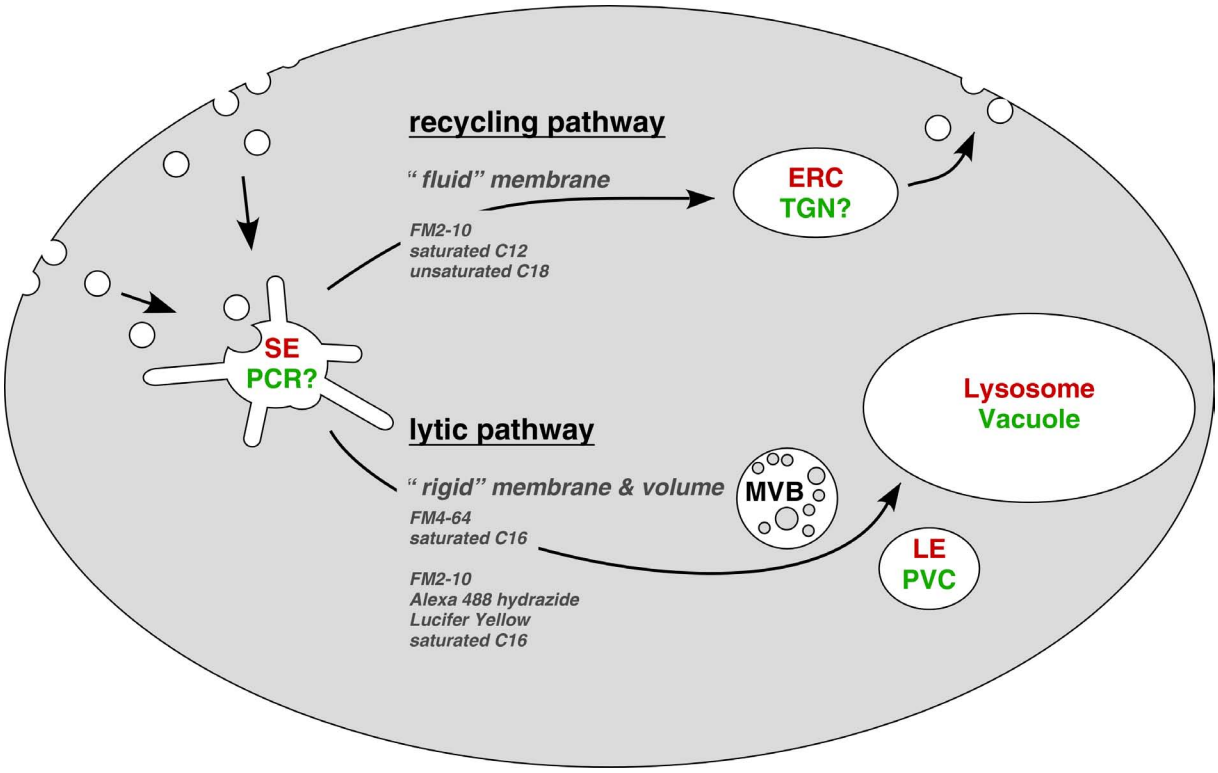

Figure 4.2: Sorting of endocytosed molecules into different pathways. Endocytic vesicles deliver molecules to the tubovesicular sorting endosome (SE). This organell sorts molecules according to their chemical properties into the recycling or lytic pathway. Naming in red is according to conventions in animal literature, suggested plant counterparts are labelled green: sorting endosome (SE), endocytic recycling compartment (ERC), trans golgi network (TGN), multi vesicular bodies (MVB), pre-vacuolar compartment (PVC).

probe with high affinity to membrane domains with low curvature and fluidity. In fact the intramembrane part of this molecule has a length comparable to an aliphatic 16-carbon chain. FM2-10 in turn, with a taillength similar to a 12-carbon chain, is likely to have a preference for fluid membrane domains of high curvature.

A hypothetic sorting scenario can now be described in the following way:

Membrane-affine dyes (FM4-64, FM2-10) and fluid phase markers (Alexa 488 hydrazide) enter in vesicles, which fuse with a compartment capable of sorting. Based on its tubovesicular appearance, the partly coated reticulum (PCR) might resemble the mammalian sorting endosome. However, for the time being this assumption is solely based on morphological similarity (Fowke et al. 1991, Tanchak et al. 1988). In the sorting organelle molecules bound to rigid membranes (e.g. FM4-64) or solved in the fluid phase (e.g. Alexa 488) are targeted to the lytic pathway. This pathway has recently been shown to lead via multivesicular bodies (MVB) and the prevacuolar compartment (PVC) eventually to the vacuole (Tse et al. 2004). Molecules bound to fluid membranes (e.g. FM2-10 and possibly some FM4-64 (due to its unsaturated nature) are sorted into the recycling pathway leading via a plant counterpart of the ERC. This could be the trans golgi network (Holstein 2002).

Whether FM4-64 enters an additional pathway to the Golgi is not finally answered. Evidence has been provided in this study and by Bolte et al. (2004), whereas Tse et al. (2004) have not seen any evidence. Whether this pathway is similar to the recycling pathway is also not known. Since staining of the Golgi is observed before tonoplast labelling, the dye may also reach vacuoles via the Golgi. In this sense these dyes may behave like storage proteins (Neumann et al. 2003).

Lack of appropriate markers for endosomal compartments in plant cells - especially those for live cell investigations - and the similar sizes of the involved organelles in EM studies (Low and Chandra, 1994) leaves us with the speculation that any of the described plant endosomal compartments (i.e. PCR, MVB, PVC, TGN) may have caused the signals corresponding to the 470 nm sized structures. Granted that sorting of different FM-dyes does occur, it may be speculated that those labelled by FM2-10 are mainly PCR and TGN whereas those labelled by FM4-64 are MVB and PCV (Fig. 4.2).

It is also worth noting that in addition to their preference for membranes with a specific fluidity FM-dyes also distribute between membranes and the aqueous phase according to their partition coefficients. Since the solubility of FM-dyes in the lipid environment is favored by longer tails and more double bonds (Betz et al. 1996), a higher fraction of the less hydrophobic probes FM2-10, is released from the membrane (Hao and Maxfield 2000). This could in principle target FM2-10 also to the lytic pathway. However, since this dye has not been found to label the tonoplast, the amount of FM2-10 in the fluid phase is likely to be very small.

To sum up, the chemical difference of the dyes causes a different affinity to membranes and as a consequence, the dyes may be sorted into different endocytic pathways. However, not all fluorescent structures labelled with FM-dyes can be interpreted in the context of endocytic activity. Unspecific uptake of dye or leakage from endocytic compartments may deliver dye to the cytosol and lead to a staining of compartments such as the mitochondria, not involved in endocytosis. FM4-64, the dye with the highest hydrophobicity, turns out to be the most suitable tool for monitoring endocytosis in guard cells. This dye not only marks endocytic vesicles in turgid guard cells but FM4-64 passes through the entire endocytic pathway up to the vacuole. Apparently it does not stain mitochondria.

4.4 Stomatal movement

4.4.1 Membrane traffic during stomatal movement

The postulation that endo- and exocytosis need to be feasible in turgid guard cells was mainly substantiated by their demand for frequent surface area changes. Since biomembranes have a limited elasticity of around 2 % (Wolfe and Steponkus 1983), the observed surface area change in the order of 15 % favors claim for membrane trafficking processes, which add and retrieve

new membrane material at the PM during stomatal movement.

As a consequence, a high amount of internalized membrane was postulated to be present in a closed guard cell - likely in the form of a pool of vesicles - which was thought to be reused during a subsequent swelling of the guard cell. However, such a pool has never been found in EM studies on closed stomata or experimentally shrunken protoplasts.

Another approach to verify the existence of such a membrane pool is to follow the uptake of fluorescent endocytic markers and to correlate the internalized fluorescence with the surface area decrease. A number of reasons will be discussed, why this approach is error-prone, if not senseless in the case of investigations on intact guard cells.

In the present study, a constitutive endocytic uptake was observed for all markers used. This uptake occurred under hypoosmotic conditions and in absence of any visible changes of cell size and stomatal aperture and therefore changes in the surface area of the PM. Therefore, the uptake was most likely caused by endocytic events counterbalanced by an equal number of exocytic events, indicating a dynamic equilibrium. Hence it is not possible to directly correlate endocytically internalized fluorescence with a decrease in surface area of the PM. This becomes especially important for investigations on the closing process of intact guard cells. Since stomata close within about 30-60 min, depending on the applied stimulus (i.e. biotic stimuli like ABA, darkness, or high ambient CO_2), constitutive endocytic uptake hampers the correlation of internalised fluorescence with the decrease in PM surface area.

But even more important the constitutive endocytosis traffic is likely to be sufficient to realise the surface area changes, especially on the time scale guard cells need for closing. Low and Chandra (1994) calculated that the complete PM of plant cells exchanges within 10-180 min due to constitutive membrane traffic. Thus the observed 15 % change in surface area during stomatal movement could be accomplished within at least 25 min. In accordance, a calculation based on the endocytic frequency measured in protoplasts of *Zea mays* L. coleoptiles (0.25 events $min^{-1}\mu m^{-2}$; Thiel et al. 1998) yields 30 min for the same 15 % change. These calculations show that a slight imbalance of constitutive traffic towards exo- or endocytic events would be sufficient to achieve the necessary surface area changes on the time scale of stomatal opening or closing.

Collectively, a continuous exchange of membrane rather than a pool of vesicles is more likely to facilitate the surface area changes of the PM during stomatal movement. This would also explain why such a pool has never been found in EM studies on closed guard cells.

In principle, closing of stomata can in experimental situations be accelerated by osmotic treatment. This would reduce the relative contribution of constitutive endocytosis to the amount of fluorescence, which is internalized in consequence of the surface area decrease. However, for the following reasons, this approach is not favorable for the quantification of endocytosis during stomatal closure.

Superficially this treatment reflects the *in vivo* situation, in which K^+ serves as an osmoticum. However, in contrast to the natural continuous and slow accumulation of K^+, osmotic changes in an experiment are usually applied in one or few steps. The findings in the present study are in agreement with the literature, that such treatment causes an uptake of fluorescent markers into structures of a broad size distribution ranging from 0.5 to 2.5 μm (Diekmann et al. 1993, Kubitscheck et al. 2000, Oparka et al. 1991, Wartenberg et al. 1992). Reassessment of published data demonstrates that sizes of such "osmocytic" structures correlate with the applied step in osmolarity (R^2 = 0.93). Even giant unilammelar vesicles show the same endovesiculation under hyperosmotic treatment (Claessens 2003). But most important, no fusion, neither with the endomembrane system nor with the PM upon reswelling or deplasmolysis, has ever been observed for osmocytic structures (Oparka et al. 1996). The observation that these internalized membranes are smooth (Gordon-Kamm and Steponkus 1984) adds further support to the view that osmocytic structures are generally fusion-incompetent. These observations indicate that osmocytic vesiculation is an intrinsic property of membranes under hyperosmotic stress. It has been termed osmocytosis in order to distinguish this phenomenon from endocytosis in which vesicle internalization is always followed by coordinated fusion with other subcellular compartments (Robinson et al. 1991).

Since plant cells undergo osmocytosis when they plasmolyse under stress conditions (i.e. drought or cold shock; Oparka at al. 1996), this process is not truly artificial. But it is not likely that stomatal movement relys on it. If guard cells would internalize membrane into fusion-incompetent structures, they would gradually accumulate them in the course of repetitive open and closing cycles. Hence experimental conditions, which favor osmocytosis, were prevented throughout the present study.

4.4.2 3D changes during stomatal movement

Analysis of the relation between volume and surface area of intact guard cells during stomatal movement revealed that the changes are mainly determined by the swelling of the cells, i.e. by an increase of their cross section.

Although the relation between volume and surface area is well described by a straight line, the likewise linear model of an elongating half torus fails to do so. In contrast, the alternative nonlinear thickening model is sufficient to describe the whole range of changes from closed to open stomata. This was true for both the present and the data of Shope et al (2003), even though the changes of the radius are not enough to produce a marked nonlinearity in the datasets. Moreover, the fit to the dataset of the present study predicts the dimensions of guard cells observed by Shope et al. (2003) and vice versa. Hence, the thickening model is sufficient to describe the bulk 3D characteristics of stomatal movement. This is, however, in contrast to finding that a clear elongation ($\sim$2.25 μm) of the guard cells can be measured in 3D reconstructions. The conclusion is that the 3D shape of guard cells is more complex than a half tours.

Fits to separate datasets of closed and open stomata also show that guard cells swell and elongate. While the radius changes by 0.44 μm (8.9 %) the cells elongate by 2.63 μm (5.4 %). This is in contrast to the findings of Shope and co-workers, who found an identical change for both values of $\sim$40 %. It explains why their data fit well to a straight line, while the slight difference in the slopes between linear fits to datasets from closed and open cells of the present study points to a nonlinear relation. The larger the change in radius relative to the change in length, the more pronounced the nonlinearity of the relation between volume and surface area will be. These differences between the present and the data from Shope et al. are most likely explained on the basis of different methods used to induce stomatal movement. Since the osmolarity of the ambient solution does not change *in vivo* (Willmer and Fricker 1996), stomata in the present study were opened by the fungal toxin fusicoccin under isoosmotic conditions. In contrast, Shope et al. changed the osmotic potential of the incubation buffer.

Raschke (1979) suggested that the radial orientation of cellulose microfibrills in the cell walls of guard cells (Ziegenspeck 1938) allow the crossectional shape but not its area to change. However, this has not been observed in the present study. The area of the cross sections differs by 20 %, hence the cell wall needs to have a limited elasticity. The observed elongations, in turn, are in well agreement with the scenario presented by Raschke (1979) namely that ”guard cells push each other apart when they inflate”.

The observed changes are also consistent with another model for guard cell movement, which evaluated pressure and volume data on the basis of the theory of polymer elasticity (Sharpe et al. 1987). When guard cells begin to open, they show an isotropic expansion until their pressure reaches a level above the pressures in the neighboring cells. After that the anisotropic expansion (i.e. elongation) begins, when the radial walls have reached the limits of their elasticity. These phases have already been proposed by Ståfelt (1927), who termed them ”Spannungsphase” (tension phase) and ”Motorische Phase” (motor phase).

In the present study the 3D features of guard cells were determined with high precision. Even details down to the folds, which form in the polar parts of the closed guard cells (Raschke 1979), were determined with high precision. Together with pressure data (Franks et al. 2001) this would allow to obtain a spatial distribution of the cell walls’ elastic modulus, which in turn would allow to model the 3D changes during stomatal movement in detail.

4.5 Different characteristics of polarity

4.5.1 Growth polarity

The swelling of a cell does not require any polarity for the traffic of membrane. The surface area of the PM can be adjusted by vesicular processes anywhere in order to prevent a rupture of the PM, as it is probably the case in a swelling protoplast. But is there any demand for polarity in a ”growing” guard cell? Are there special sides of exo- and endocytosis during stomatal movement?

In the plant kingdom two different types of cell growth are found. Pollen tubes and and root hairs show a directional or polarized growth: they only grow at one end of the cell, as do all eukaryotic cells of the remaining kingdoms. This type of growth is characterized by targeting of exocytic vesicles towards actin-enriched discrete domains, while the rest of the cell does not grow at all (Belanger and Quantrano 2000). It is also characterized by compensatory endocytosis at domains different from the growing zone (Parton et al. 2001). The majority of plant cells, however, exhibit an unidirectional elongation. This type of growth results from the establishment of non-growing domains, which are actively maintained at the opposite end-poles of the cell. It is driven by turgor, and the elongation is mainly a result of the differential ability of the cell walls to expand. While nothing is known about the targeting of exocytic vesicles, the non-growing domains are again sites of enhanced endocytosis (Baluska et al. 2003).

The majority of the findings in the present study favors the second ”growth” type as a mechanism underlying stomatal movement. Guard cells show a turgor driven and unidirectional elongation and no accumulation of actin has been found at the tips. Moreover, the enhanced amount of KAT1 signal and Alexa 488 uptake at the tips of guard cells points to an elevated endocytic rate in this region. This elevated endocytic rate could serve to maintain the size of the membranes between adjacent guard cells and thereby define them as non-growing domains. Note that in this scenario only endocytosis but not exocytosis needs to be ”polarized”.

4.5.2 Distribution polarity of KAT1::GFP

Another phenomenon which showed marked polarity was the distribution of KAT1, an important protein for guard cell movement.

First, KAT1::GFP was rarely found in the ventral PM which faces the cuticular ledges. Besides its enhanced localisation at the guard cells’ tips it mainly localized to dorsal areas of the guard cell. In contrast, GFP::TM23 was evenly distributed in the PM. The ventral cell wall in kidney-shaped guard cells is known to be heavily thickened and cuticularised, while the dorsal wall, facing the adjacent epidermal cells, is thin and not cuticularised at all (Willmer and Fricker 1996). Hence, the distribution of KAT1 but not TM23 mirrors the areas, where bulk ion fluxes are supposed to occur during stomatal movement. Interestingly, immunolocalisation of PM H^+-ATPase in minor veins of *V. faba* also showed a non-homogeneous distribution in

transfer cells. This pump was more concentrated in the regions adjacent to the bundle sheath, phloem parenchyma and xylem vessels (Bouché-Pillon et al. 1994)

Second, the channel was distributed in the PM in a radial symmetric pattern composed of small punctuate structures and stripes with a continuous fluorescence. The radial symmetry mirrors the orientation of the actin cytoskeleton in guard cells (Hwang and Lee 2001). In view of the finding that the actin filaments modulate the activities of inward rectifying potassium channels (K^+_{in}) in guard cells of *V. faba* (Hwang et al. 1997), this may point to a connection of KAT1 to actin filaments and/or a role of actin in the trafficking of KAT1. Moreover, the density of KAT1 in endocytic vesicles is reported to be higher than it is in the PM (Hurst et al. 2004). Strong evidence for the endocytosis of KAT1 into diffraction-limited structures has been presented in the present study. It is therefore reasonable to speculate that the stripes, due to their lower fluorescence intensity, resemble KAT1 in the PM tethered to actin, whereas the bright point like structures are a result of an accumulation due to endocytosis. This view is further supported by the literature:

There is growing evidence that actin plays a direct role in endocytosis (Engqvist-Goldstein and Drubin 2003). In particular it has been shown that other K^+_{in}, namely Kir 1.1 (Sterling et al. 2002) and Kv 1.2 are endocytosed upon phosphorylation of a tyrosine. This disrupted the binding to the actin-binding protein cortactin, which in turn led to dynamin- and clathrin-dependent endocytosis (Nesti et al. 2004). The authors posit that tethering to F-actin maintains the channel at the cell surface and the disruption of that interaction frees the channel to undergo endocytosis. Worth remembering in this context is that also GFP::TM23 was maintained in the PM, presumably because it lacks a specific tyrosine.

Phosphorylation also synchronously affects K^+_{in} and the actin cytoskeleton in guard cells. Ocadaic acid, a specific inhibitor of type 1 an 2A serine/threonine phophatases, has been demonstrated to inhibit the transporters for in- and outward rectified K^+ currents (Thiel and Blatt 1994). Both currents were inhibited in a parallel manner and the kinetics of the voltage-dependent currents were not affected. Both observations point to a decrease in the number of channels and therefore to an inactivation involving endocytosis. The same inhibitor also induces the depolymerisation of actin and promotes stomatal closure (Hwang and Lee 2001). The Phosphatase activity is shown to be necessary for both maintaining long actin filaments and open stomata, while disintegration of actin is necessary to close stomata. Finally, the protein kinase which phosphorylates KAT1 in *V. faba* is ABA-responsive (Mori et al. 2000) and has a high homology to a serine/threonine kinase from Arabidopsis (Assmann 2003).

Taken together, the posit made by Nesti et al. (2004) may also hold true for regulation of KAT1 during stomatal movement in guard cells of *V. faba*.

While the specific signals controlling the endocytosis of KAT1 clearly remain to be investigated, exo- and endocytosis can be considered key elements for the regulation of stomatal movement besides their role in crude membrane traffic for surface area adjustments.

References

Abbé E (1873) Beiträge zu Theorie des Mikroskops und der mikroskopischen Wahrnehmung. *M. Schultze's Arch. Microsc. Anat.* 9:413-468

Assmann SM (2003) OPEN STOMATA1 opens the door to ABA signaling in *Arabidopsis* guard cells. *TIPS* 8(4):151-153

Assmann SM and Baskin TI (1998) The function of guard cells does not require an intact array of cortical microtubules *J. Exp. Bot.* 49:163-170

Ayscough KR, Stryker J, Pokala N, Sanders M, Crews P, and Drubin DG (1997) High rates of actin filament turnover in budding yeast and roles for actin in establishment and maintenance of cell polarity revealed using the actin inhibitor latrunculin-A. *J. Cell Biol.* 137:399-416.

Baluska F, Wojtaszek P, Volkmann D, and Barlow P (2003) The architecture of polarized cell growth: the unique status of elongating plant cells. *BioEssays* 25:569-576

Baluska F, Samaj J, Hlavacha A, Kendrick-Jones J, and Volkmann D (2004) Actin-dependent fluid phase endocytosis in inner cortex cells of maize root apices. *J. Exp. Bot.* 55(396):463-473

Baluska F, Hlavacka A, Samaj J, Palme K, Robinson DG, Matoh T, McCurdy DW, Menzel D, and Volkmann D (2002) F-Actin-Dependent Endocytosis of Cell Wall Pectins in Meristematic Root Cells. Insights from Brefeldin A-Induced compartments. *Plant Physiol.* 130:422-431

Baron-Epel O, Gharyal PK, and Schindler M (1988) Pectins as mediators of wall porosity in soybean cells. *Planta* 175:389-395

Barth M and Holstein SE (2004) Identification and functional characterization of *Arabidopsis* AP180, a binding partner of plant alphaC-adaptin. *J. Cell Sci.* 15(117):2051-2062

Battey NH, James, NC, Greenland AJ, and Brownlee C (1999) Exocytosis and Endocytosis. *Plant Cell* 11:643-659

Belanger KD and Quatrano RS (2000) Polarity: the role of localized secretion. *Curr. opin. Plant Biol.* 3:67-72

Bereiter-Hahn J (1976) Dimethylaminostyrylmethylpyridiniumiodine (daspmi) as a fluorescent probe for mithochondria in situ. *Biochim. Biophys. Acta* 423:1-14.

Berger O, Edholm O, and Jähnig F (1997) Molecular dynamics simulations of a fluid bilayer of dipalmitoylphosphatidylcholine at full hydration, constant pressure, and constant temperature. *Biophys. J.* 72:2002-2013

Betz W J, Mao F, and Smith CB (1996) Imaging exocytosis and endocytosis. *Curr Opin Neurobiol*. 6:365-371

Betz WJ, Mao F, and Bewick GS (1992) Aktivity dependent fluorescent staining and destaining of living vertebrate motor nerve terminals. *J. Neurosci*. 12:363-375

Blancaflor EB and Gilroy S (2000) Plant cell biology in the new millennium: new tools and new insights. *Am. J. Bot.* 87(11):1547-1560

Bolte S, Spencer B, and Satiat-Jeunemaitre B (2004a) The N-myristoylated Rab-GTPase m-Rabmc is involved in post-Golgi trafficking events to the lytic vacuole in plant cells. *J. Cell Sci.* 117:943-954

Bolte S, Talbot C, Boutte Y, Catrice O, Read ND, and Satiat-Jeunemaitre B (2004b) FM-dyes as experimental probes for dissecting vesicle trafficking in living plant cells. *J. Microscopy* 214:159-173

Bouch-Pillon S, Fleurat-Lessard P, Fromont JC, Serrano R, and Bonnemain JL (1994) Immunolocalization of the Plasma Membrane H^+ -ATPase in Minor Veins of Vicia faba in Relation to Phloem Loading. *Plant Physiol.* 105(2): 691-697

Brandizzi F, Frangne N, Marc-Martin S, Hawes C, Neuhaus JM, and Paris N (2002) The Destination for Single-Pass Membrane Proteins Is Influenced Markedly by the Length of the Hydrophobic Domain. *Plant Cell* 14:1077-1092

Carroll AD, Moyen C, Van Kesteren P, Tooke F, Battey NH, and Brownlee C (1998) Ca^{2+}, Annexins, and GTP Modulate Exocytosis from Maize Root Cap Protoplasts. *Plant Cell* 10:1267-1276

Chaloner WG (1970) The rise of the first land plants. *Biol. Rev. Camebridge Phil. Soc.* 45:353-377

Charpilienne A, Nejmeddine M, Berois M, Parez N, Neumann E, Hewat E, Trugnan G, and Cohen J (2001) Individual Rotavirus-like Particles Containing 120 Molecules of Fluorescent Protein Are Visible in Living Cells. *J. Biol. Chem.* 276(31):29361-29367

Claessens MMAE (2002) Size Regulation and Stability of Charged Lipid Vesicles. PhD-thesis, Wageningen University, The Netherlands, ISBN 90-5808-927-4

Cochilla AJ, Angleson JK and Betz WJ (1999) Monitoring secretory membrane with FM1-43 fluorescence. *Annu. Rev. Neurosci.* 22:1-10

Conner SD and Schmid S (2003) Regulated portals of entry into the cell. *Nature* 422:37-44

Cosgrove DJ and Hedrich R (1991) Stretch-activated chloride, potassium, and calcium channels coexisting in plasma membranes of guard cells of *Vicia faba* L. *Planta.* 186:143-153

Cram WJ (1980) Pinocytosis in plants. *New Phytol.* 84:1-17

Denecke J, De Rycke R, and Botterman J (1992) Plant and mammalian sorting signals for protein retention in the endoplasmic reticulum contain a conserved epitope. *EMBO J.* 11:2345-2355

Denk W, Piston D, and Webb W (1995) Two-photon molecular excitation in laser-scanning microscopy. In: *Handbook of Biological Confocal Microscopy* (Pawley J, ed) Plenum Press, New York, pp. 445-458

Denk W, Strickler JH, and Webb WW (1990) Two-photon laser scanning fluorescence microscopy. *Science* 248(4951):73-76

Diekmann W, Hedrich R, Raschke K, and Robinson DG (1993) Osmocytosis and Vacuolar Fragmentation in Guard Cell Protoplasts: Their Relevance to Osmotically-Induced Volume Changes in Gurad Cells. *J. Exp. Bot.* 44(267):1569-1577

Ehrhardt T, Zimmermann S, and Müller-Röber B (1997) Association of plant K+(in) channels is mediated by conserved C-termini and does not affect subunit assembly. *FEBS Lett.* 409:166-170

Emans N, Zimmermann S, and Fischer R (2002) Uptake of a Fluorescent Marker in Plant Cells Is Sensitive to Brefeldin A and Wortmannin. *Plant Cell* 14:71-86

Engqvist-Goldstein AE and Drubin DG (2003) Actin assembly and endocytosis: from yeast to mammals. *Annu. Rev. Cell. Dev. Biol.* 19:287-332

Falke LC, Edwards KL, Pickard BG, and Misler S (1988) A stretch-activated anion channel in tobacco protoplasts. *FEBS Lett.* 237(1-2):141-144

Farge E and Devaux PF (1992) Shape changes of giant liposomes induced by an asymmetric transmembrane distribution of phospholipids. *Biophys. J.* 61:347-357

Farge E, Ojcius DM, Subtil A, and Dautry-Varsat A (1999) Enhancement of endocytosis due to aminophospholipid transport across the plasmamembrane of living cells. *Am. J. Physiol.* 276 (Cell Physiol. 45):725-733

Fischer-Parton S, Parton RM, Hickey PC, Dijksterhuis J, Atkinson HA, and Read ND (2000) Confocal microscopy of FM4-64 as a tool for analysing endocytosis and vesicle trafficking in living fungal hyphae. *J. Microscopy.* 198(3):246-259.

Fluhler E, Burnham VG, and Loew LM (1985) Spectra, membrane binding, and potentiaometric responses of new charge shift probes. *Biochemistry* 24:5749-5755.

Ford MGJ, Mills IG, Peter BJ, Vallis Y, Praefcke GJK, Evans PR, and McMahon HT (2002) Curvature of clathrin-coated pits driven by epsin. *Nature* 419:361-366

Fowke LC, Tanchak MA, and Galway ME (1991) Ultrastructural cytology of the endocytic pathway in plants. In: *Endocytosis, Exocytosis and Vesicle Trafffic in Plants* (Hawes CR, Coleman JOD, Evans DE, eds.) Soc. Exp. Biol. Sem. Ser. 45:15-40

Franks PJ, Buckley TN, Shope JC, and Mott KA (2001) Guard Cell Volume and Pressure Measured Concurrently by Confocal Microscopy and the Cell Pressure Probe. *Plant Phyiol.* 125:1577-1584

Gale JE, Marcotti W, Kennedy HJ, Kros CJ, and Richardson GP (2001) FM1-43 Dye Behaves as a Permeant Blocker of the Hair-Cell Mechanotransducer Channel. *J. Neurosci.* 21(18):7013-7025

Geldner N, Anders N, Wolters H, Keicher J, Kornberger W, Muller P, Delbarre A, Ueda T, Nakano A, and Jurgens G (2003) The Arabidopsis GNOM ARF-GEF mediates endosomal recycling, auxin transport, and auxin-dependent plant growth. *Cell* 112(2):219-30

Girkin JM and Wokosin DL (2002) Resolution and Contrast in Confocal and Two-Photon Microscopy. In: *Confocal and Two-Photon Microscopy: Foundations, Applications and Advances* (Diaspro A, ed) New York, Wiley-Liss, pp. 221

Gordon-Kamm WJ and Steponkus PL (1984) The behaviour of the plasma membrane following osmotic contraction os isolated protoplasts. *Protoplasma* 123:161-173

Gradmann D and Robinson DG (1989) Does turgor prevent endocytosis in plant cells? *Plant Cell Environ.* 12, 151-154

Grinvald A, Frostig RD, Lieke E, and Hildesheim R (1988) Optical imaging of neuronal activity. *Physiol Rev.* 68:1285-1366

Gustin MC, Zhou XL, Martinac B, and Kung C (1988) A mechanosensitive ion channel in the yeast plasma membrane. *Science* 242:762

Göppert-Mayer M (1931) Über Elementarakte mit zwei Quantenspüngen. *Ann. Physik* 9:273-294

Hamann S, Folke Kiilgaard J, Litman T, Alvarez-Leefmans FJ, Winther BR, and Zeuthen T (2002) Measurement of Cell Volume Changes by Fluorescence Self-Quenching. *Journal of Fluorescence* 12(2):139-145

Hao M and Maxfield FR (2000) Characterization of Rapid Membrane Internalization and Recycling. *J. Biol. Chem.* 275(20):15279-15286

Haseloff J (1999) GFP Variants for Multispectral Imaging of Living Cells. *Methods in Cell Biology* 58:139-151

Haseloff J, Siemering KR, Prasher DC, and Hodge S (1997) Removal of a cryptic intron and subcellular localisation of green fluorescent protein are required to mark transgenic *Arabidopsis* plants brightly. *Proc. Natl. Acad. Sci. USA* 94:2122-2127

Haugland RP (2002) Handbook of Fluorescent Probes and Research Products, 9th edn., Molecular Probes, Inc., Eugene, Oregon, USA

Hawes CR, Crooks K, Coleman J, and Saitat-Jeunemaitre B (1995) Endocytosis in plants: fact or artefact? *Plant Cell Environ.* 18:1245-1252

Hawes CR, Saint-Jore C, Martin B, and Zheng HQ (2001) ER confirmed as the location of mystery organelles in Arabidopsis plants expressing GFP! *TIPS* 6:245-246

Heim R, Prasher DC, and Tsien RY (1994) Wavelength mutations and posttranslational autoxidation of green fluorescent protein. *Proc. Nat. Acad. Sci. USA* 91:12501-12504

Henkel AW, Lübke J, and Betz WJ (1996) FM1-43 ultrastructural localization in and release from frog motor nerve terminals. *Proc Natl Acad Sci USA* 93:1918-1923

Heuser J, Zhu Q, and Clarke M (1993) Proton pumps populate the contractile vacuoles of *Dictyostelium* amoebae. J. Cell. Biol. 121:1311-1327

Hillmer S, Hedrich R, Robert-Nicoud M, and Robinson DG (1990) Uptake of Lucifer Yellow CH in leaves of *Cammelia communis* is mediated by endocytosis. *Protoplasma* 158:142-148

Holstein SEH (2002) Clathrin and Plant Endocytosis. *Traffic* 3:614-620

Homann U (1998) Fusion and fission of plasma-membrane material accommodates for osmotically induced changes in the surface area of guard cell protoplasts. *Planta* 206:329-333

Homann U and Thiel G (1999) Unitary exocytic and endocytic events in guard-cell protoplasts during osmotically driven volume changes. *FEBS Lett.* 460:495-499

Homann U and Thiel G (2002) The number of K^+ channels in the plasma membrane of guard cell protoplasts changes in parallel with the surface area. *Proc. Natl. Acad. Sci. USA* 99(15):10215-10220

Horobin RW (2002) Polymethine dyes - 2. Styryls, Styryls, thiazoles, coumarins and flavonoids. In: *CONN's Biological Stains - A Handbook of Dyes, Stains and Fluorochromes for Use in Biology and Medicine* (Horobin RW and Kiernan JA, eds.) 10th edn. BIOS Scientific Publishers, Oxford UK, pp. 349-366

Hurst AC, Meckel T, Homann U and Thiel G (2004) Trafficking of the plant potassium inward rectifier KAT1 in guard cell protoplasts of *Vicia faba*. *Plant J.* 37(3):391-397

Huttner WB and Schmidt AA (2002) Membrane curvature: a case of endofeelin?... *Trends in Cell Biol.* 12:155-158

Hwang JU and Lee Y (2001) Abscisic Acid-Induced Actin Reorganization in Guard Cells of Dayflower Is Mediated by Cytosolic Calcium Levels and by Protein Kinase and Protein Phosphatase Activities. *Plant. Phys.* 125:2120-2128

Hwang JU, Suh S, Yi H, Kim J, and Lee Y (1997) Actin Filaments Modulate Both Stomatal Opening and Inward K^+-Channel Activities in Guard Cells of *Vicia faba* L. *Plant Physiol.* 115(2):335-342

Inoué S and Spring K (1997) Video Microscopy, Plenum Press, New York

Jonkman JEN and Stelzer EHK (2002) Resolution and Contrast in Confocal and Two-Photon Microscopy. In *Confocal and Two-Photon Microscopy: Foundations, Applications and Advances* (Diaspro A, ed) New York, Wiley-Liss, pp. 109

Kost B, Spielhofer P, and Chua NH (1998) A GFP-mouse talin fusion protein labels plant actin filaments in vivo and visualizes the actin cytoskeleton in growing pollen tubes. *Plant J.* 16(3):393-401

Kubitscheck U, Wedekind P, Zeidler O, Grote M, and Peters R (1996) Single nuclear pores visualized by confocal microscopy and image processing. *Biophys J.* 70(5):2067-2077

Kubitscheck U, Homann U, and Thiel G (2000) Osmotically evoked shrinking of guard-cell protoplasts causes vesicular retrieval of plasma membrane into the cytoplasm. *Planta* 210:423-431

Lam BC, Sage TL, Bianchi F, and Blumwald E (2001) Role of SH3-domain containing proteins in clathrin-mediated vesicle trafficking in Arabidopsis. *Plant Cell* 13: 2499-2512

Lichtman JW (1994) Confocal microscopy. *Scientific American* 271:40-45

Low PS and Chandra S (1994) Endocytosis in Plants. *Annu. Rev. Plant Phys. Mo. Biol.* 45:609-631

Meckel T, Hurst AC, Thiel G, and Homann U (2004) Endocytosis against high turgor: Guard cells of *Vicia faba* constitutively endocytose fluorescently labelled plasma membrane and GFP tagged K^+-channel KAT1. *Plant J.* 39(2):182-193

Meyers JR, MacDonald RB, Duggan A, Lenzi D, Standaert DG, Corwin JT, and Corey DP (2003) Lighting up the Senses: FM1-43 Loading of Sensory Cells through Nonselective Ion Channels. *J. Neurosci.* 23(10):4054-4065

Mori IC, Uozumi N and Muto S (2000) Phosphorylation of the inward-rectifying potassium channel KAT1 by ABR kinase in Vicia guard cells. *Plant Cell Physiol.* 41(7):850-6

Morris CE (1990) Mechanosensitive ion channels. *J. Membrane Biol.* 113:93-107

Mousavi SA, Malerod L, Berg T, and Kjeken R (2004) Clathrin-dependent endocytosis. *Biochem. J.* 377:1-16

Mukherjee S, Soe TT, and Maxfield FR (1999) Endocytic Sorting of Lipid Analogues Differing Soley in the Chemistry of Their Hydrophobic Tails. *J Cell Biol.* 44(6):1271-1284

Murashige T and Skoog F (1962). A revised medium for rapid growth and bioassays with tobacco tissue culture. *Physiol. Plant.* 15:473-497

Nesti E, Everill B, and Morielli AD (2004) Endocytosis as a Mechanism for Tyrosine Kinase-dependent Suppression of a Voltage-gated Potassium Channel. *Mol Biol Cell.* 15(9):4073-4088

Neumann U, Brandizzi F, and Hawes C (2003) Protein Transport in Plant Cells: In and Out of the Golgi. *Ann. Bot.* (Lond.) 92:167-180

Nishikawa S and Sasaki F (1996) Internalization of styryl dye FM1-43 in the hair cells of lateral line organs in *Xenophus* larvae. *J. Histochem Cytochem.* 44(7):733-741

Nossal R (2001) Energetics of Clathrin Basket Assembly. *Traffic* 2:138-147

Oparka KJ, Cole L, Wright KM, Coleman, JOD, Hawes CR, and Evans DE (1991) Fluid-phase endocytosis and intracelllular compartmentation of fluorescent probes. In: *Endocytosis, Exocytosis and Vesicle Traffic in Plants.* SEB Seminar Series. Cambridge: Cambridge University Press, pp. 81-102

Oparka KJ, Wright KM, Murant EA, and Allan EJ (1993) Fluid-phase endocytosis: do plants need it? *J. Exp. Bot.* 44:247-255

Oparka KJ, Prior DAM, and Crawford JW (1996) Membrane conservation during plasmolysis. In: *Membranes: Specialized Functions in Plants* (Smakwood M, Knox JP, Bowles DJ, eds.) BIOS Scientific Publishers Ltd. pp. 39-56

Ormö M, Cubitt AB, Kallio K, Gross LA, Tsien RY, and Remington SJ (1996) Crystal structure of the *Aequorea victoria* green fluorescent protein. *Science* 273:1392-1395

Parton RM, Fischer-Parton S, Watahiki MK, and Trewavas AJ (2001) Dynamics of the apical vesicle accumulation and the rate of growth are related in individual pollen tubes. *J. Cell Sci.* 114:2685-2695

Patterson GH and Piston WP (2000) Photobleaching in Two-Photon Excitation Microscopy. *Biophys. J.* 78:2159-2162

Piston DW (1999) Imagig living cells and tissues by two-photon excitation microscopy. *Trends in Cell. Biol.* 9:66-69

Raschke K (1979) Movements of Stomata. In: *Encyclopedia of Plant Physiology, Vol. 7, Physiology of Movements* (Haupt W and Feinleb ME, eds.), Springer, Berlin, pp. 382-441

Rauch C and Farge E (2000) Endocytosis switch controlled by transmembrane osmotic pressure and phospholipid number asymmetry. *Biophys J.* 78(6):3036-3047

Rayleigh, Lord (1896) On the theory of optical images, with special reference to the microscope. *Phil. Mag.* 54(5):167-195

Reigada D, Dez-Prez IE, Gorostiza P, Verdaguer A, Gmez de Aranda I, Pineda O, Vilarrasa J, Marsal J, Blasi J, Aleu J, and Solsona C (2003) Control of neurotransmitter release by an internal gel matrix in synaptic vesicles. *Proc. Natl. Acad. Sci. USA* 100(6):3485-3490

Robinson DG, Hedrich R, Herkt B, Diekmann W, and Robert-Nicoud M (1991) Endocytosis in plants: problems and perspectives. In: *Endocytosis.* NATO ASI Series H62. Berlin, Springer-Verlag pp. 459-466

Robinson DG and Hedrich R (1991) Vacuolar Lucifer Yellow uptake in plants: endocytosis or anion transport; a critical opinion. *Bot. Acta* 104:257-264

Robinson DG and Hillmer S (1990) Endocytosis in Plants. *Physiol. Plant.* 79:96-104

Sandison DR and Webb WW (1994) Background rejection and signal-to-noise optimization in confocal and alternative fluorescence microscopes. *Appl. Optics.* 33:603-615

Saxton MJ and Breidenbach RW (1988) Receptor-mediated endocytosis in plants is energetically possible. *Plant Physiol.* 86:993-995

Schlegel RA and Williamson P (2001). Phosphatidylserine, a death knell. *Cell Death and Differentiation* 8:551-563

Schote U and Seelig J (1998) Interaction of the neuronal marker dye FM1-43 with lipid membranes. Thermodynamics and lipid ordering. *Biochim Biophys Acta.* 9;1415(1):135-46.

Selboa PK, Hogset A, Prasmickaitea L, and Berg K (2002) Photochemical Internalisation: A Novel Drug Delivery System. *Tumor Biol.* 23:103-112

Sharpe PJH, Wu H, and Spence RD (1987) Stomatal mechanics. In: *Stomatal Function.* (E Zeiger, GD Farquhar, IR Cowan, eds) Stanford University Press, Stanford, CA, pp. 91-114

Shope JC, DeWald DB, and Mott KA (2003) Changes in Surface Area of Intact Guard Cells Are Correlated with Membrane Internalization. *Plant Physiol.* 133:1-8

Siegel MS and Isacoff EY (1997) A genetically encoded optical probe of membrane voltage. *Neuron* 19:735-741

Staehlin RV, Long F, Peter BJ, Murray D, De Camilli P, McMahon HT, and Cho W (2003) Contrasting Membrane Interaction Mechanisms of AP180 N-terminal Homology (ANTH) and Epsin N-terminal Homology (ENTH) Domains. *J. Biol. Chem.* 278(31):28993-28999

Stelzer EHK (1998) Contrast, resolution, pixelation, dynamic range and signal-to-noise ratio: fundamental limits to resolution in fluorescence light microscopy. *J. Microscopy* 189:15-24

Sterling H, Lin DH, Gu RM, Dong K, Hebert, SC, and Wang WH (2002). Inhibition of Protein-tyrosine Phosphatase Stimulates the Dynamin-dependent Endocytosis of ROMK1. *J. Biol. Chem.* 277:4317-4323

Ståfelt MG (1927) Die photischen Reaktionen im Spaltffnungsmechanismus. *Flora* 121:236-272

Tanchak MA, Rennie PJ, and Fowke LC (1988) Ultrastructure of the partly coated reticulum and dictyososmes during endocytosis by soybean protoplasts. *Planta* 175:433-441

Thiel G, Kreft M, and Zorec R (1998) Unitary exocytotic and endocytotic events in *Zea mays* L. coleoptile protoplasts. *Plant J.* 13(1):117-120

Thiel G and Blatt MR (1994) Phosphatase antagonist okadaic acid inhibits steady-state K^+ currents in guard cells of *Vicia faba*. *Plant J.* 5: 727-733

Tse YC, Mo B, Hillmer S, Zhao M, Lo SW, Robinson DG, and Jiang L (2004) Identification of multivesicular bodies as prevacuolar compartments in *Nicotiana tabacum* BY-2 cells. *Plant Cell* 16(3):672-693

Tsien RY (1998) The green fluorescent protein. *Annu. Rev. Biochem.* 67:509-544

Ueda T, Yamaguchi M, Uchimiya H, and Nakano A (2001) Ara6, a plant-unique novel type Rab GTPase, functions in the endocytic pathway of *Arabidopsis thaliana*. *EMBO J.* 17:4730-4741

Vida TA and Emr SD (1995) A new vital stain for visualizing vacuolar membrane dynamics and endocytosis in yeast. *J. Cell Biol.* 128(5):779-92

Wahl M, Koberling F, Patting M, Rahn H, and Erdmann R (2004) Time-resolved confocal fluorescence imaging and spectrocopy system with single molecule sensitivity and sub-micrometer resolution. *Curr Pharm Biotechnol.* 5(3):299-308.

Wartenberg M, Hamann J, Pratsch I, and Donath E (1992) Osmotically induced fluid-phase uptake of fluorescent markers by protoplasts of Chenopodium album. *Protoplasma* 166:61-66

Webb RH (1999) Theoretical basis of confocal microscopy. *Methods in Enzymology* 307:3-20.

White NS, Errington RJ, Fricker MD, and Wood JL (1996) Aberration control in quantitative imaging of botanical specimens by multidimensional fluorescence microscopy. *J Microscopy* 181:99-116

Williams MA and Fukuda M (1990) Accumulation of membrane glycoproteins in lysosomes requires a tyrosine residue at a particular position in the cytoplasmic tail. *J. Cell Biol.* 111:955-966

Willmer CM and Fricker M (1996) Stomata 2nd edn. Chapmann and Hall

Wolfe J and Steponkus PL (1983) Mechanical properties of the plasma membrane of isolated plant protoplasts. *Plant Physiol.* 71:276-285

Xu C, Zipfel W, Shear JB, Williams RM, and Webb WW (1996) Multiphoton fluorescence excitation: New spectral windows for biological nonlinear microscopy. *Proc. Natl. Acad. Sci.* USA 93:10763-10768

Ziegenspeck H (1938) Die Micellierung der Turgeszenzmechanismen. Teil I: Die Spaltöffnungen (mit physiologischen Ausblicken) *Bot. Archiv.* 39:268-372

Acknowledgements

I would like to thank my thesis supervisors, Gerhard Thiel and Ulrike Homann. They were always a source of motivation and never lost patience when listening to the very first versions of my scientific ideas. Thanks for always waiting for the subsequent versions ...
Next, I have to express my deepest gratitude to Ulrich Kubitscheck. He gave this work the essential impulses and unceasingly tried to undersand my emails.
I am much obliged to Thomas W. Holstein for providing the three most important pieces of equipment for my work: a microscope, a fast computer, and a gun. Without his support this thesis would probably deal with something different. I also keep in mind who gave me the very first introduction to the ”confocal thing”: Thank you, Ulrike Engel.
Special thanks to Annette Hurst and Gisela Marx who made all the molecular biology (and so much more) work. Without them, not a single ”banana” would have glowed in green color.
Many thanks also to Marc-Thorsten Hütt and Manuel Dehnert for their help with numbers and curves, Steffen Noe and Jan Lentfer for ”X” support, and to Karl Schuller, Udo Pelger and the rest of their excellent crew for transmuting fancy dreams into usable hardware.
Of course, I will not forget my colleagues Mario Mehmel and Hans Henrick von Rosenberg-Lipinsky, who often gave me the feeling not to be at work. We should have a beer right now.
All remaining members of the group are acknowledged for providing me with the warm feeling that there is always someone who listens to my sometimes verbose thoughts ;-)
Im am grateful to my parents who always gave me all support I needed. Thanks a million.
My most special thank you goes to Doro. She provided me with love and support, shared all the ups and downs during this work, and all to often had to put my head back into place.

Curriculum Vitae

Personal data

	Tobias Meckel born on Febuary 25th in Stuttgart, Germany unmarried

Education

2000 - 2004	PhD-student at Darmstadt University of Technology in the group of Prof. Dr. Gerhard Thiel Title of the thesis: "Endocytosis against high the high turgor of guard cells." Disputation with distinction (*summa cum laude*)
2000	Graduation (’Diplom’) April, 20th with distinction (mark: 1.0)
1999 - 2000	Diploma thesis at Darmstadt University of Technology on the "Development of a PAGE-based enzyme activity assay for reactive oxygen scavenging enzymes”
1994 - 1999	Study of biology at Darmstadt University of Technology. Subjects: plant physiology, biochemistry, pharmacology, organic chemistry
1993 - 1994	Ambulance officer at the German Red Cross, Wiesbaden
1992 - 1993	Civil service as medical assistant and paramedic in a live-saving organization. Examination as an ambulance officer.
1982 - 1992	Secondary school (”Gymnasium”) in Idstein. Representative position (’Schülersprecher’) during the last year. Examination (”Abitur”) May 1992 (mark: 2.0).
1979 - 1982	Elementary school in Wallrabenstein.

scientific activity in foreign countries

1998	Half year studies at the Research School of Biological Science (RSBS), Australian National University, Canberra, Australia
1994	Practical trainings at Ethosha National Park, Okaukuejo, Namibia and Krüger National Park, Skukuza, South Africa

teaching

	Annual graduate course "Electrophysiology of *Chara carolina*"
	Annual graduate course ”Confocal Laser Scanning Microscopy”
	Frequent lecture substitute ”Exo- and Endocytosis in plants”

additional qualifications

Languages	German and English, fluent
Computer	Responsible for network administration and web design in the group of Prof. Gerhard Thiel.
	Extended experience with MacOS, Windows and Linux
	Experience with scientific software i.e. Huygens, Imaris, ImageJ, Photoshop, Mathematica, IGOR, SigmaPlot
	Basic programming experience
Further education	Seminar on ”Arguing and Negotiating - the Harvard Concept”, Darmstadt University of Technology